Enhanced Engine Efficiency Through Subsystem Lubricant Viscosity Investigations
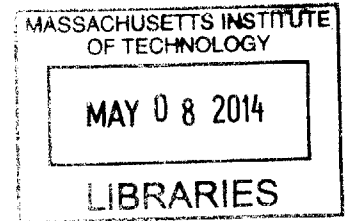
by

Tomas Vianna Martins

B.S., Mechanical Engineering
Massachusetts Institute of Technology, 2012

Submitted to the Department of Mechanical Engineering
in partial fulfillment of the requirements for the degree of

Master of Science in Mechanical Engineering

at the

MASSACHUSETTS INSTITUTE OF TECHNOLOGY

February 2014

© Massachusetts Institute of Technology 2014. All rights reserved.

Author...
Department of Mechanical Engineering
January 23, 2014

Certified by........
Victor W. Wong
Principal Research Scientist
Thesis Supervisor

Accepted by...
David Hardt, Professor of Mechanical Engineering
Chairman, Department Committee on Graduate Theses

Enhanced Engine Efficiency Through Subsystem Lubricant Viscosity Investigations

by

Tomas Vianna Martins

Submitted to the Department of Mechanical Engineering
on January 23, 2014, in partial fulfillment of the
requirements for the degree of
Master of Science in Mechanical Engineering

Abstract

This study initiates a three-year project to investigate the potential benefits in fuel efficiency, engine emissions, lubricant longevity, and engine durability. Two experimental testing platforms were designed and implemented to empirically study the effects of lubricant formulations on the internal combustion engine's frictional losses. A motored cylinder head enables the characterization of valvetrain lubrication regimes and friction contributions. A Kohler KDW-702 engine was also instrumented with pressure and torque measuring instrumentation, in addition to being modified to have two separate lubrication circuits - one to lubrication the valvetrain system, and one for the crankcase system. Using a novel split lubrication strategy, the full engine experimental setup was used to investigate the effect of lubricant viscosity on subsystem friction as well as demonstrate the efficiency gains possible by optimizing lubricant formulations on a subsystem basis.

The Kohler KDW-702 test engine was shown to experience significant boundary contact within its valvetrain system, contrasting the predominantly hydrodynamic nature of the crankshaft bearings and piston assembly. A split lubrication configuration addressed this, using a 15W-40 oil in the cylinder head, and a 10W-30 oil in the crankcase, yielding 6% lower overall friction and 3% higher mechanical efficiency over the stock recommended full 15W-40 lubrication configuration. While significant frictional gains have been demonstrated through the use of a split lubrication system and optimized lubricant viscosity classifications, the project will continue to demonstrate benefits in engine emissions, lubricant degradation, and engine component wear.

Thesis Supervisor: Victor W. Wong
Title: Principal Research Scientist

Acknowledgments

Contents

List of Figures

11

List of Tables

Chapter 1

Introduction and Background

The work performed and detailed here, under the project title "*Lubricant Formulations to Enhance Engine Efficiency in Modern Internal Combustion Engines*", was funded by the United States Department of Energy under cooperative agreement #DE-EE0005445. It discusses the initial stages of development and research for an original approach to improving internal combustion engine efficiency through subsystem specific lubricant formulation optimization.

1.1   Internal Combustion Engine Fundamentals

The internal combustion (IC) engine radically changed human transportation by enabling the high power conversion of chemical energy stored in organic fuels to mechanical work useful for powering planes, trains, automobiles, and any other vehicle [1]. Just three years ago did the total number of automobiles in operation around the world surpass the one billion unit mark[2]. While the IC engine has successfully provided the means for high speed transportation, there are environmental and sustainability detriments that must be considered and mitigated, such as high pollution and the limited supply of organic hydrocarbon based fuels.

As shown in figure 1-1, the conventional IC, reciprocating piston engine generates mechanical work by igniting a mixture of fuel and air within a cylinder and using a piston to transmit the pressure of combustion to a spinning crankshaft. At the begin-

Four-stroke cycle
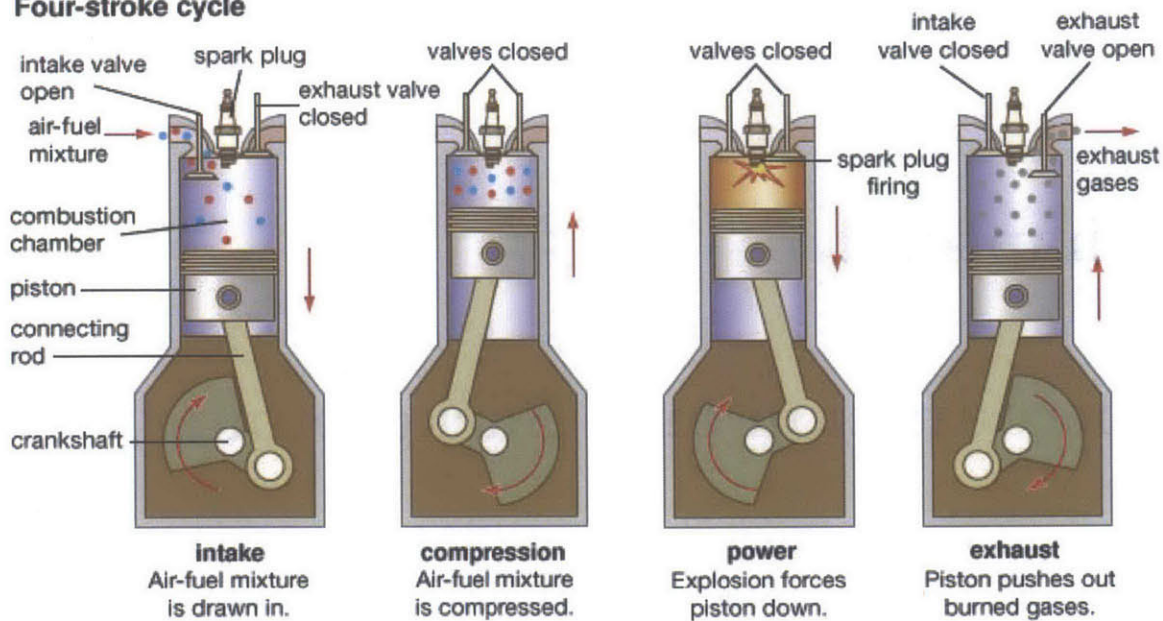
Figure 1-1: The four strokes of an IC, reciprocating piston engine - intake, compression, power, exhaust.

ning of the intake stroke, the intake valve opens as the piston is traveling downward, letting a mixture of air and fuel rush into the cylinder. Once the piston reaches the bottom dead center (BDC) position, it turns around and travels upward and compresses the fuel and air mixture to the small clearance volume between the cylinder head surface and the piston.

Close to the piston's top dead center (TDC) position, combustion of the fuel and air mixture initiates and continues through the power stroke as the piston travels downward. Finally after combustion, the exhaust valve opens and the piston travels up, pushing the spent mixture charge out, and the entire cycle begins again. Every cycle of a four stroke engine is comprised to two revolutions of the crankshaft, one revolution of the camshaft. The crankshaft travels 720 "crank angle" degrees accordingly throughout one cycle.

It is the responsibility of the valvetrain system to open and close the intake and exhaust valve at the appropriate times within the engine cycle. To accomplish this, the engine crankshaft turns a smaller camshaft at half its speed to synchronize one

full revolution of the camshaft with one full cycle of the engine. The camshaft will possess various intake and exhaust cam lobes that protrude and rotate with the shaft. A particular cam lobe will actuate the opening and closing of the valve it controls at the correct timing.
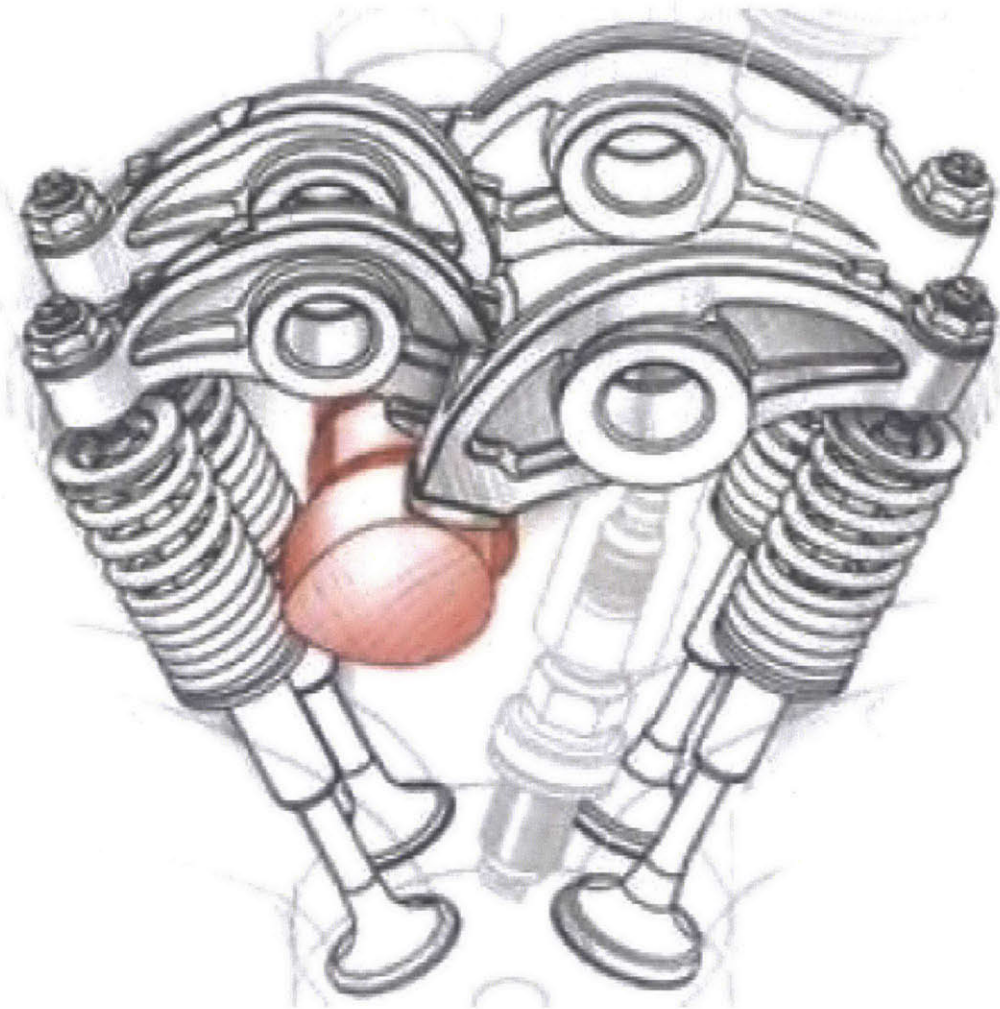
Figure 1-2: Single overhead cam valvetrain (SOHC) configuration with rocker arms.

Throughout engine testing, it is important to determine a qualitative and comparative measure of engine load that is independent of engine size. Clearly, a one liter engine and a three liter engine can produce the same torque and power output, but they will do so at different engine loads. Consequently, engine mean effective pressure (MEP) was formed to characterize how hard a particular engine is working at a time. Mean effective pressure is equal to the total work produce per cycle, W_{cycle} divided

by an engine's displacement volume,V_d as follows:

$$MEP = \frac{W_{cycle}}{V_d} \tag{1.1}$$

The total amount of mechanical work the piston extracts from the combustion of fuel divided by the engine displacement is called the *Gross Indicated Mean Effective Pressure* or GIMEP. The piston also performs work on the combustion gases to pull in a fresh charge of air and expel out the previous combusted mixture. Normalizing this pumping work with the engine displacement, we can calculate the *Pumping Mean Effective Pressure* or PMEP. Therefore, the net positive work that piston extracts is represented by the gross work minus the pumping work. If we normalize this as well, we find the *Net Indicated Mean Effective Pressure*, where:

$$GIMEP = NIMEP + PMEP \tag{1.2}$$
$$NIMEP = GIMEP - PMEP \tag{1.3}$$

Once the piston and crankshaft extract the net indicated work from the combustion gases, it is transferred to the flywheel and out the engine to drive whatever load is connected to the engine, such as a generator, dynamometer, or transmission. The many moving components around the engine such as the piston and crankshaft experience sliding friction during the engine cycle, and not all of the net extracted work is transferred to the flywheel. The frictional losses and the brake work seen at the flywheel can both be normalized as well by the engine displacement and represented by a *Friction Mean Effective Pressure* (FMEP) and *Brake Mean Effective Power* (BMEP). The distribution of engine mean effective pressure and the calculation of friction pressure can be represented by:

$$GIMEP = PMEP + FMEP + BMEP \tag{1.4}$$
$$NIMEP = FMEP + BMEP \tag{1.5}$$
$$FMEP = NIMEP - BMEP \tag{1.6}$$

16

1.1.1 Diesel Engine Operation

The diesel engine was developed in the late 1800's separately by English inventor Herbert Akroyd Stuart and Rudolf Diesel, whose name the engine bears. Unlike the common spark ignition(SI) engine which fires a spark plug to ignite a compressed homogeneous air and fuel mixture, the diesel engine initiates combustion by injecting diesel fuel into high temperature compressed intake air. The diesel engine is used for a large variety of applications, both personal and commercial, driving over 700,000 of the vehicles in the United States[3]. By utilizing high compression ratios to heat up the gas temperature sufficient to initiate combustion, the diesel engine is also more efficient than the conventional SI engine.

Chemically, it is important for all IC engines to combust fuel with a proper ratio of supply air. Since the SI engine uses a spark to initiate a hemispherical combustion flame that travels across the combustion chamber, it is important that the a stoichoimetric ratio of fuel to air is provided in the intake charge. Consequently, the SI engine controls its output load and speed by controlling the amount of air that enters the engine through a throttle. At idling conditions, the throttle is almost closed, letting in a relatively small amount of air that can be mixed with a small amount of fuel, keeping the output engine work low. At full load, the SI engine's throttle is fully open, allowing in as much air as it can to maximize the amount of fuel burned and work extracted.

The diesel engine contrasts this method of control by fundamentally burning its fuel very differently. About 20° before TDC, diesel is injected into the combustion chamber. After a short delay period, the fuel autoignites spontaneous and commences diffusion flame combustion. This flame has a rich core that continuously supplies a mixing and combustion region with fuel to burn. Figure 1-3 illustrates the distribution of fuel and air around a quasi-steady diesel combustion plume[4]. Combustion occurs at the edge of the flame and is fed by the rich fuel mixture within the flame and the lean air mixture outside of the flame.

The nature of the flame fuel and air dynamics results in stoichiometric combustion

17

on average. As such, the diesel engine does not need an active control of its intake air mass flow rate to control engine load. Mechanical energy production is only controlled by the fuel injection system - primarily fuel injection timing and duration. Older engines accomplish this fuel injection control mechanically with pumps driven by the camshaft, or timing belt. Mechanical fuel injectors commence injection of fuel when the contained fuel reaches a particular pressure. Mechanical fuel injection pumps intermittently pump high pressure to individual injectors to initiate combustion.
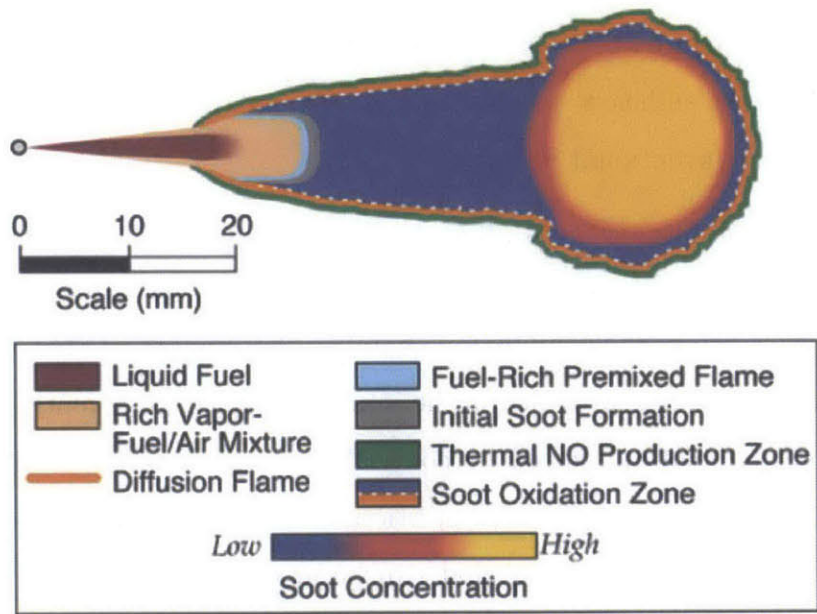
Figure 1-3: Quasi-steady diesel combustion plume[4]

Newer engines have transitioned to electronically controlled and actuated fuel injectors. Extremely high pressure fuel rails supply up to 2,500 bar fuel to electromechanical injectors that atomize their fuel spray as best as possible to improve mixing and combustion.

1.1.2 Diesel Engine Advantages and Disadvantages

The nature of diesel combustion inherently presents a variety of advantages and disadvantages when compared to other IC engine technologies. Benefits such as higher efficiency and torque as well as detriments like higher noise and particulate emissions

18

is observed when comparing the diesel engine to the spark ignition engine[5]. Altogether the case for the diesel engine is extremely compelling, enabling key services for millions of people around the globe.

In order to withstand high compression ratios and combustion pressures of around 60 bar, diesel engines are manufactured to be much more robust and reliable. Engine lifespans of a million miles is not uncommon for diesel technology [6]. Furthermore, higher compression ratios translate to higher efficiency and lower emissions. Diesel engines have about 20-40% higher fuel economy and 20% lower carbon dioxide emissions than spark ignition gasoline engines. Diesel engines produce more torque at lower speeds due to their inherent resistance to engine knock, or uncontrolled detonation that spark ignition engines have to protect against by retarding spark timing and decreasing efficiency[6].

While the added durability and reliability from robust diesel engine blocks is enjoyed, it comes at the cost of weight. Traditional diesel engines yield lower specific power densities than their SI counterparts. Modern diesel engines have greatly evolved and use technologies such as sophisticated forced induction to reach volume specific power densities of over 80 kW/L. Although lower greenhouse and hydrocarbon emissions can be achieved with diesel engine technology, higher nitrous oxide and particulate matter emissions added high aftertreatment costs to diesel engine manufacturing [5].

1.2 Project Motivation

Since the early twentieth century, the internal combustion engine has been constantly evolving. Large efficiency, torque, or power gains were seen with the introduction of transformational technologies such as turbocharging, electronic fuel injection, electronic ignition, and the three way catalytic converter among many others. As the negative environmental impact of its widespread use became increasingly evident in the late 1960's, the US government began to progressively create regulations intended to decrease engine exhaust emissions.

While many emissions reduction technologies have been implemented to resolve the problem, one popular solution has been to decrease engine emissions by decreasing the amount of fuel needed to travel the same distance. One can say that this approach certainly considered double-green. The increase in engine efficiency and fuel economy allows us to both improve our utilization of nonrenewable fossil fuels as well as release less greenhouse gases and hydrocarbon emissions per mile traveled. This project focuses on increasing fuel efficiency by reducing frictional losses within an engine through better lubrication.

Both spark ignition and compression ignition engines share the same geometrical configurations with a primary crankshaft driven by connecting rods and pistons. They also both have valvetrains responsible for the actuation of the intake and exhaust valves. As such, lubrication is accomplished similarly for both engine types - with a bottom oil sump and a crankshaft driven oil pump that circulates pressurized lubricant to the crankshaft, cylinder, and valvetrain components. Therefore, our project research is directly applicable to both spark ignition and compression ignition technologies making its potential impact far-reaching.

1.2.1 Emissions Regulations

The emission of greenhouse gases have increased exponentially throughout the twentieth century. Carbon dioxide emissions have increased sixteenfold from 2,500 teragrams in 1900 to 32,000 teragrams in 2008 [7]. The United States alone emitted 6,700 million metric tons of CO_2 equivalent in 2011, of which 28% came from the transportation industry.
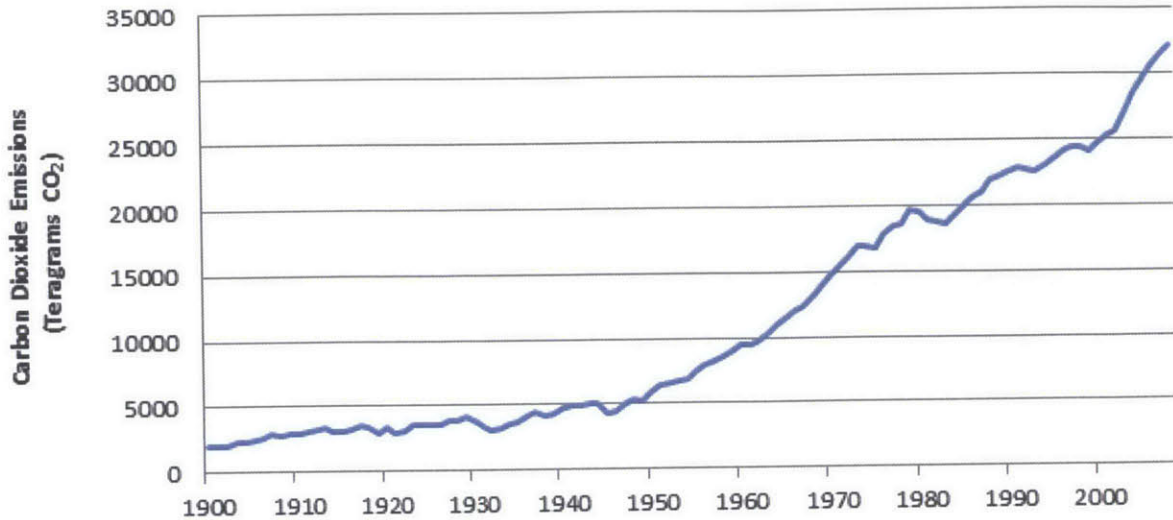
Figure 1-4: Global carbon dioxide emissions from 1900 to 2008[8].

Increasing government regulation has attempted to resolve the automotive greenhouse gas emissions problem by setting emission limit standards vehicles must adhere to. In 2013, the United States Enviromental Protection Agency (EPA) tightened standards federal automotive, drastically decreasing allowable emitted concentrations of carbon dioxide, carbon monoxide, hydrocarbons, and nitrous oxides [9]. New Tier 3 EPA standards limit carbon monoxide emissions to one gram per mile, a dramatic decrease from the Tier 2 four grams per mile limit released in 2000[10]. In August of 2012, the Department of Transportation and the Environment Protection Agency finalized a fuel economy standards implementation plan that increases fuel economy to the equivalent of 54.5 miles per gallon (MPG) for cars and light-duty trucks by 2025[11]

1.2.2 Lubricant Optimization for Enhanced Fuel Economy

Mechanical energy conversion efficiency quantifies the amount of output engine work produced as a percentage of indicated mechanical work produced by the pistons, or rather what percentage of produced mechanical energy is not lost to friction and accessories. Modern IC engines experience maximum mechanical efficiencies of around 90%, utilizing almost all extracted work for engine output. Frictional losses from

sliding surfaces and lubricant shear rob the engine of a significant amount of the mechanical work that it extracted from the combustion charge. It is the duty of engine oil to mitigate this problem by lubricating and protecting sliding surfaces, and in turn minimizing engine friction and maximizing durability as much as possible.

Modern IC engines use one dedicated lubricant to lubricate the entire engine, leading lubricant manufacturers to consider different lubrication regimes, conditions, and functional requirements present all over the engine. Furthermore, contamination of the lubricant from crankcase blow-by (when combustion gases bypass the piston rings and enter the crankcase) leads to the convection of detrimental particles to other cleaner systems in the engine.

By acknowledging that the lubricant serves different purposes in different parts of the engine, we can attempt to eliminate formulation trade offs by separating the lubrication circuit into multiple regions and allowing the use of different lubricants. If multiple lubrication circuits are implemented within an engine, a lubricant manufacturer may formulate a particular oil exclusively for use within a particular engine subsystem without consideration for engine lubrication elsewhere.

For this project, two main systems were identified for the separation of the lubrication circuit - the valvetrain system and the crankcase system. The valvetrain system is a very clean system that experiences lower temperatures, and based on the application, predominantly metal-on-metal sliding component contact. The crankcase lubricant on the other hand experiences higher temperatures, contamination and dilution from blow-by gases, and predominantly lubricant separated sliding contact. These fundamentally different considerations demand different functional lubricant requirements.

The individual design of unique subsystem specific lubricants may achieve lower overall frictional losses when compared to a conventional single oil system. Each lubricant is optimized to minimize the friction within its respective subsystem, yielding overall mechanical efficiency gains not possible with one engine lubricant.

1.3   Project Objectives

This project seeks to demonstrate the efficiency benefit of enhanced subsystem specific lubricant formulations through empirical investigations of a split lubrication engine combined with comprehensive lubrication modeling. No such lubrication strategy has been implemented in the literature and the original nature of the concept holds great educational value.

This work initiates the experimental side of the project, with the fabrication and operation of two experimental setups, capable of characterizing subsystem specific frictional losses as well as running a split lubrication configuration. A test matrix containing four candidate lubricants was developed and carried out to characterize the effect of lubricant viscosity on subsystem friction. Furthermore, the optimization of the lubricant base stock on a subsystem basis for our experimental engine will be discussed. Finally, base stock viscosity recommendations will be made for the valvetrain and crankcase regions of our particular engine model.

Chapter 2

Internal Combustion Engine Lubrication

Lubrication is defined as the interposition of a substance between two sliding surfaces in order to prevent surface wear. The IC engine has many sliding surfaces and without engine oil to act as a lubricant between them, the engine would quickly seize and lock up. The engine lubrication system is responsible for providing each and every necessary component with an appropriate supply of engine oil during operation.

The engine oil pump is generally driven by the crankshaft and pumps pressurized oil through passages, shown in figure 2-1, to key components that need lubrication. For a normal IC engine, these components include the crankshaft, the cylinder liner, the camshaft, and the valvetrain cam lobes and followers. Once the lubricant participates in local component lubrication, it will fall down, sometimes through large passages, to the main sump in the crankcase.

Although many components are continuously supplied with lubricant, local differences in component temperature, pressure, and relative surface speed will greatly affect what regimes dominates lubrication. Some surfaces are completely separated by a fluid film of lubricant while others still exhibit significant metal-to-metal surface contact. Understanding the mechanisms that influence both friction and wear at sliding surfaces is important when attempting to design lubricants for low friction operation.

Camshaft

Oil Pressure Regulator

Oil Pump

Crankshaft

Oil Filter
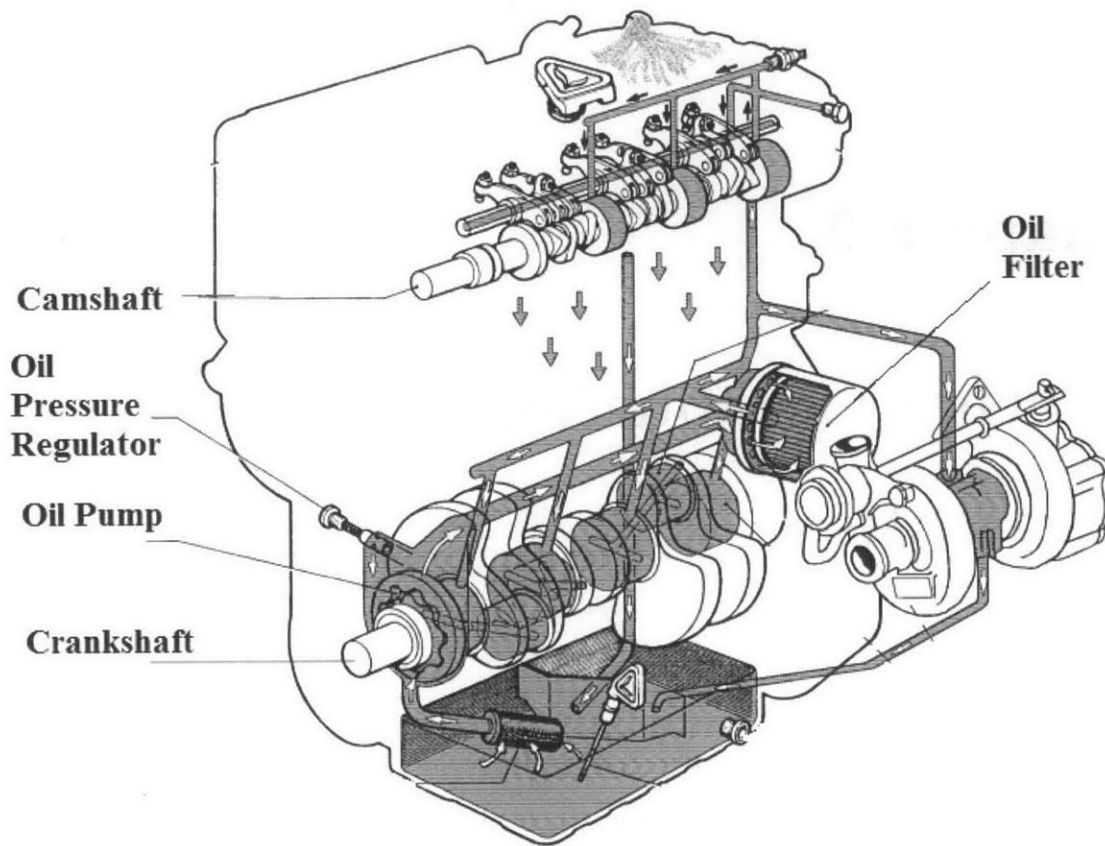
Figure 2-1: Kohler engine lubrication circuit.

2.1 Lubrication Regimes

Lubricated sliding surfaces will experience one of three predominant lubrication film behaviors - boundary lubrication, hydrodynamic lubrication, and mixed lubrication. Boundary lubrication occurs when the pressure between the two surfaces are high enough for surface asperities to contact and support the interfacial load. Hydrodynamic lubrication occurs when the relative sliding motion creates a thin lubricant film between two surfaces that supports the pressure and prevents any contact between the two surfaces. Mixed lubrication occurs when some surface asperities contact, causing both the fluid film and asperities to support the load.

The Navier-Stokes equation shown below is a conservation equation for momentum within a fluid. It determines the velocity field within a fluid as it is flows influenced

26

by forces from pressure gradients, viscous shear, and gravity.

$$\rho \frac{D\mathbf{v}}{Dt} = -\nabla p + \mu \nabla^2 \mathbf{v} + \rho \mathbf{g} \qquad (2.1)$$

The lubrication approximation states that at very small relative length scales, such that a very thin fluid film is established, viscous effects dominate the characteristic flow within a fluid, simplifying equation 2.1 to:

$$\frac{\partial p}{\partial x} = \mu \frac{\partial^2 u}{\partial y^2} \qquad (2.2)$$

Engine components experience oil films that are on the order of microns thick, making this approximation valid[12]. If we perform a simple scaling of equation 2.2, we can see how the local oil film thickness, H, changes with pressure, P, viscosity, μ, and sliding speed, U.

$$\frac{P}{L} \sim \frac{\mu U}{H^2} \qquad (2.3)$$

$$H \sim \frac{\sqrt{\mu U L}}{P} \qquad (2.4)$$

The length of an oil film, L, at steady state operation will not change locally, indicating that local lubricant film thickness, H, scales with the square root of the oil viscosity and the relative surface speed, and inversely scales with the square root of the hydrodynamic oil pressure.

Engine components experience high sliding velocities and low pressures establish large oil films while low sliding velocities and high pressures experience metal-to-metal surface contact. Equation 2.4 also illustrates the impact lubricant viscosity can have on determining local lubrication regime. If normal operating conditions cause two sliding surfaces to rub, a mere increase in lubricant viscosity may be enough to induce the formation of a larger film, and consequently decreasing component wear and friction coefficient.

An increase in lubricant viscosity is not, however, the final solution to component

durability and low friction. Once a full film of lubricant is established between two surfaces preventing any contact, friction work is generated by purely viscous shear, which increases with lubricant viscosity.
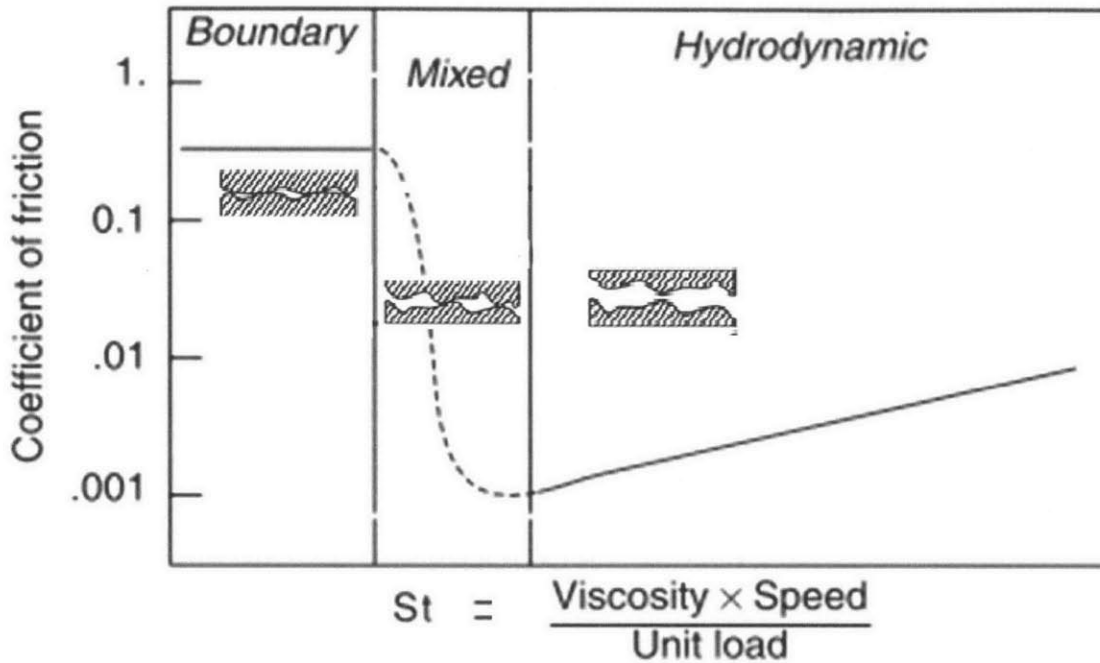
Figure 2-2: The Stribeck curve illustrates the relationship between coefficient of friction and lubrication regimes.

Figure 2-2 illustrates the friction behavior during this . On the vertical axis is the characteristic sliding coefficient of friction between the two surfaces. On the horizontal axis is a nondimensional number, the Stribeck number, that compares viscous forces to contact forces.

The Stribeck number is defined as the lubricant viscosity times the sliding speed over the pressure. Like the Stribeck number, the intermediary lubricant film thickness increases with viscosity and sliding speed, but decreases with pressure, as illustrated by equation 2.4. Consequently, although the shape of the hydrodynamic friction coefficient region would be slightly different, the Stribeck curve would look very similar with the lubricant film thickness as the independent, x-axis variable. The three regions illustrate the level of contact typical for its lubrication regime.

28

The left region of the graph represents boundary friction with surface on surface contact. This metal-to-metal contact is associated with fluid independent sliding friction coefficients and nonzero surface deformation and wear[13]. The chemical and mechanical interactions between the surface asperities lead to wear and high friction coefficients of 0.1 - 0.5. The coefficient of friction in this region is constant and independent of the sliding Stribeck number.

As mentioned, when sliding speeds are fast enough and pressures are low enough, a lubricant film is developed between the two surfaces as shown in figure 2-3, preventing contact. Therefore, when hydrodynamic lubrication is preserved, no wear is experienced on the component surfaces. On the right portion of the graph, both sliding surfaces are fully separated by the oil film and the coefficient of friction grows as the Stribeck number grows.
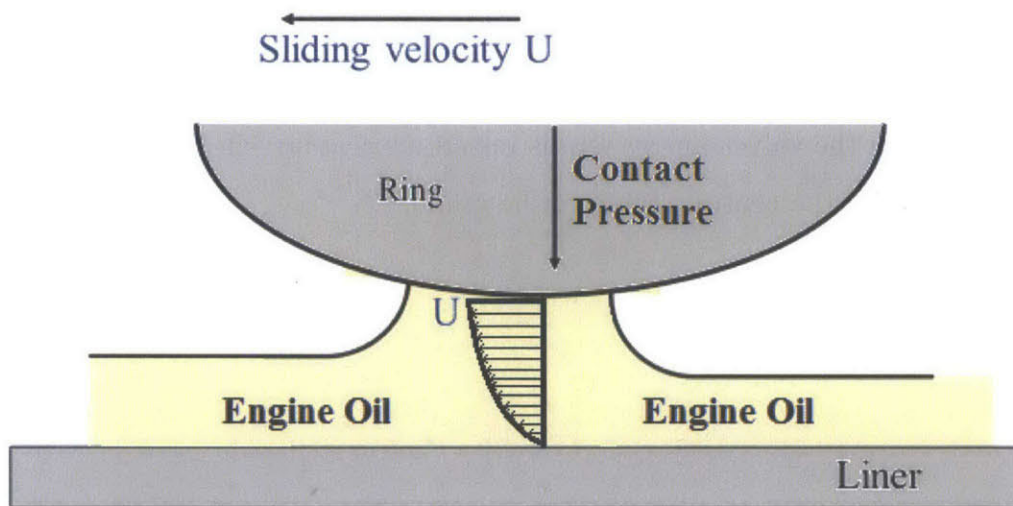
Figure 2-3: Simplified piston compression ring and liner lubrication film.

The transition from boundary to hydrodynamic friction can be seen in the middle in the mixed lubrication regime. Here, the coefficient of friction drops as more and more surface asperities lose contact with one another, until no asperities touch anymore, the oil film thickness is relatively thin, and we see a global minimum in friction

coefficient.

This minimum is the ideal lubrication operating point for sliding surfaces. Since both surfaces have completely separated from one another, wear and surface deformation is no longer an issue. Furthermore, the thin oil film yields the lowest friction coefficient possible for the surfaces. Naturally, while some surfaces on the engine may locally or instantaneously operate at this minimum, greatly varying and changing operating conditions yield sliding behaviors throughout the engine that operate at many different points along this curve.

Therefore, with the objective of subsystem friction reduction by lubricant formulation optimization, we can say that a group of sliding surfaces, that perform friction work within a subsystem, altogether operate with an effective Stribeck number that places the subsystem lubrication at a particular point on the Stribeck curve. For example, it will be shown that the engine valvetrain system exhibits monotonically decreasing friction as camshaft speed increases, indicating that the dominant lubrication regime within the valvetrain system is mixed lubrication, effectively placing the valvetrain system in the central region of the graph.

2.2   Valvetrain Frictional Losses

The valvetrain system typically contributes about 5-20% of the engine's total frictional losses[14]. The typical valvetrain system is comprised of one or multiple camshafts that spin within journal bearings, and actuate the intake and exhaust valve either indirectly by pushing cam lobes on to rocker arms that open and close the valves, or by pushing cam lobes down on the valves directly.

30

Nose — Lobe Center Line

Lobe Lift

Flank

Clearance
Ramp

Base Circle — Heel
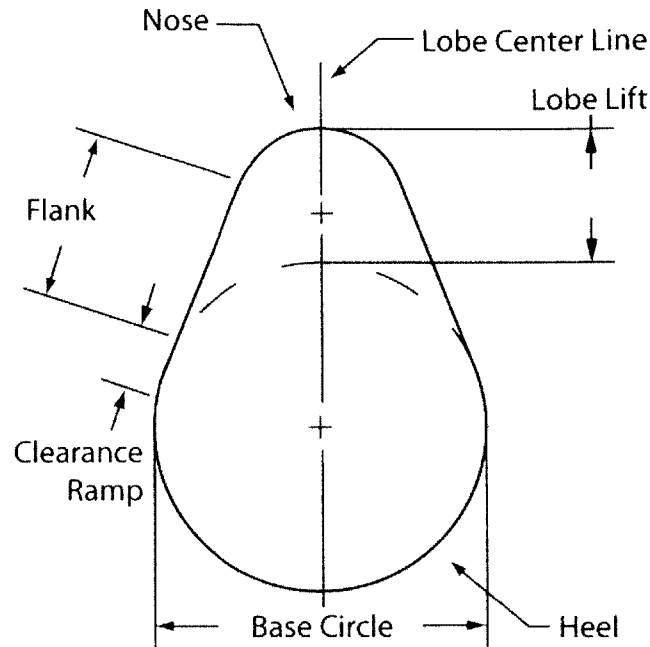
Figure 2-4: Camshaft lob profile.

Figure 2-4 illustrates a typical valve cam profile. The point of the cam lobe, called the nose will experience the highest contact pressures as it translates to the point of highest valve spring deformation. As the flank starts pushing on the cam follower, a larger oil film builds up due to higher sliding speed, but increased pressure shortly thereafter decrease the oil film thickness. The lowest oil film thickness, and full boundary lubrication is experienced at and near the cam nose, as shown in figure 2-5 corresponding to a cam angle of 90°. The blue line in figure 2-5 separates the regions on the cam lobe that are in boundary contact with the follower from those that are experiencing mixed lubrication with both a thin oil film and asperity contact. It is evident that although the cam lobe and follower sliding interface behavior will continuously move along the Stribeck curve, depending on instantaneous and local sliding speeds, pressures and lubricant viscosity.
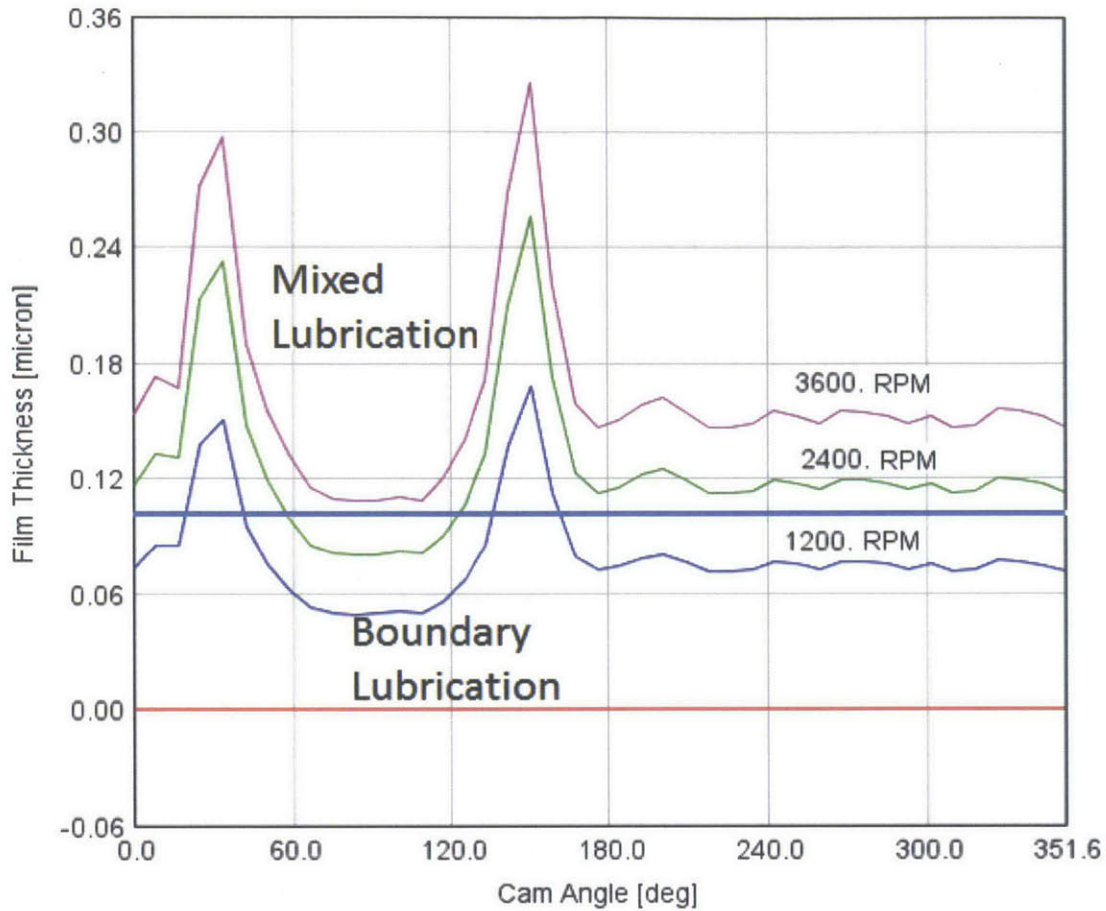
Figure 2-5: Modeled cam lobe oil film thickness. Figure courtesy of Michael Plumley.

In general, the camshaft journal bearings are constantly supplied with pressurized oil and experience predominantly hydrodynamic lubrication. Conversely, the camshaft lobe and follower interface as well as the rocker arm assemble experiences boundary and mixed lubrication, and have larger contributions to overall valvetrain friction than the journal bearings. Therefore, the valvetrain system is effectively dominated by mixed lubrication, and would benefit from higher lubricant viscosity, higher operating speeds, and lower pressures to induced more hydrodynamic behavior, bringing the effective subsystem Stribeck number closer to the transition minimum. Furthermore, the relative overall friction contribution from the valvetrain is higher at low speeds[15].

2.3   Power Cylinder Frictional Losses

The power cylinder system is comprised of the crankshaft, the connecting rods, and the pistons. It is primarily responsible for extracting mechanical work from the combustion charge, but inherently loses some of that energy to friction. The power cylinder frictional losses are distributed among the crankshaft main seals, the crankshaft journal bearings, the sliding action of the piston skirt and piston ring pack on the cylinder liner. Unlike the valvetrain system, the power cylinder is dominated by hydrodynamic lubrication and will experience lower losses at lower speeds and with lower viscosity lubricants[15]. Furthermore, lower lubricant temperatures that yield thicker oil viscosities can result in as much as twice the friction loss at normal operating conditions[16].
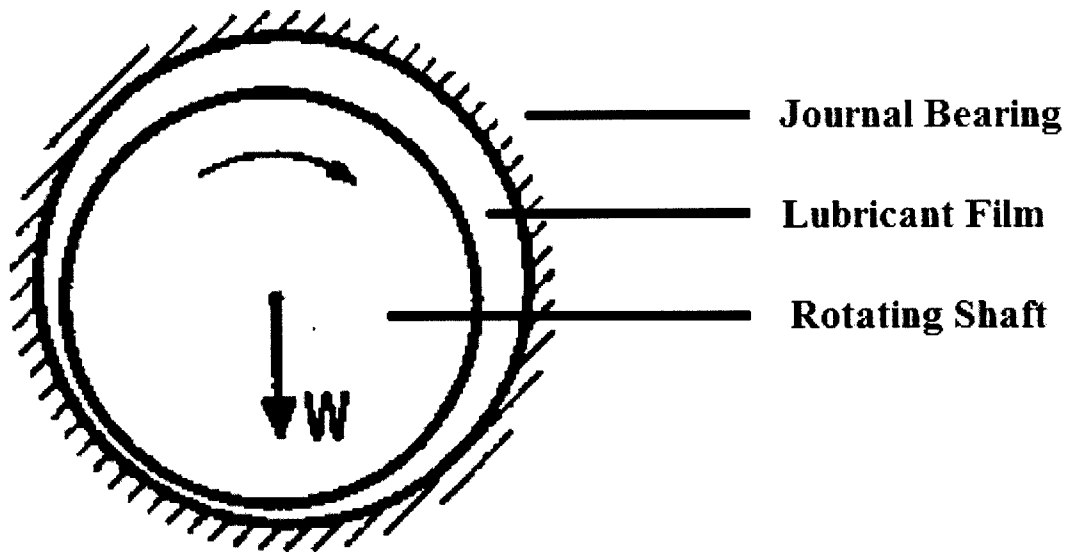
Figure 2-6: Hydrodymically lubricated journal bearing.

Figure 2-6 illustrates the lubrication of a common journal bearing, which is defined as a short, rigid, metal cylinder that surrounds and supports a rotating shaft[14]. Pressurized lubricant is constantly fed to the crankshaft journal bearing through oil passages. The rotational speed and supply pressure of the lubricant ensures pre-

dominantly hydrodynamic lubrication within the engine crankshaft journal bearings, which account for about one third of total engine frictional losses[17].

The piston assembly contributes to frictional losses through various sliding interfaces, accounting for roughly half of the engine's total friction losses[17]. The piston itself is constantly rotating on the piston wrist pin. While this contributes less than a percent of total losses, it is very difficult to supply lubricant to the pin directly and we expect the sliding surfaces to be in the boundary lubrication regime, subject to surface contact and wear. The piston rings and the piston skirt slide along the cylinder liner. The instantaneous linear piston speed is constantly changing as piston reciprocates within the cylinder, experiencing peak velocities that can range from 8 to 15 m/s at midstroke[1]. The changing sliding velocity leads the formation of a large oil film thickness at midstroke when piston speeds are high and little to no film thicknesses at top dead center and bottom dead center where piston speeds are around zero. Consequently, the piston rings and skirt experience predominantly hydrodynamic lubrication at midstroke, but mixed and boundary lubrication at the dead centers. Figure 2-3 illustrates the oil film at midstroke separating one piston compression ring from the cylinder liner.

Chapter 3

Experimental Setup - Engine Rig

Under the proposed project, our group sought to set up a fully instrumented and capable engine testing platform for subsystem specific friction characterization. This platform would be capable of firing and motoring engine tests at a variety of different operating conditions such as speed, load, and temperature. It also needed to reliably measure in-cylinder pressure, brake torque at the flywheel, and torque at the valve-train camshaft. Finally, it should also use a variety of thermocouple sensors placed around the engine to characterize its operating temperature gradients.

This chapter discusses the design, fabrication, and implementation of that testing platform, shown in figure 3-1. It was put together in the Sloan Automotive Laboratory with the aid of fellow graduate students and automotive lab staff.
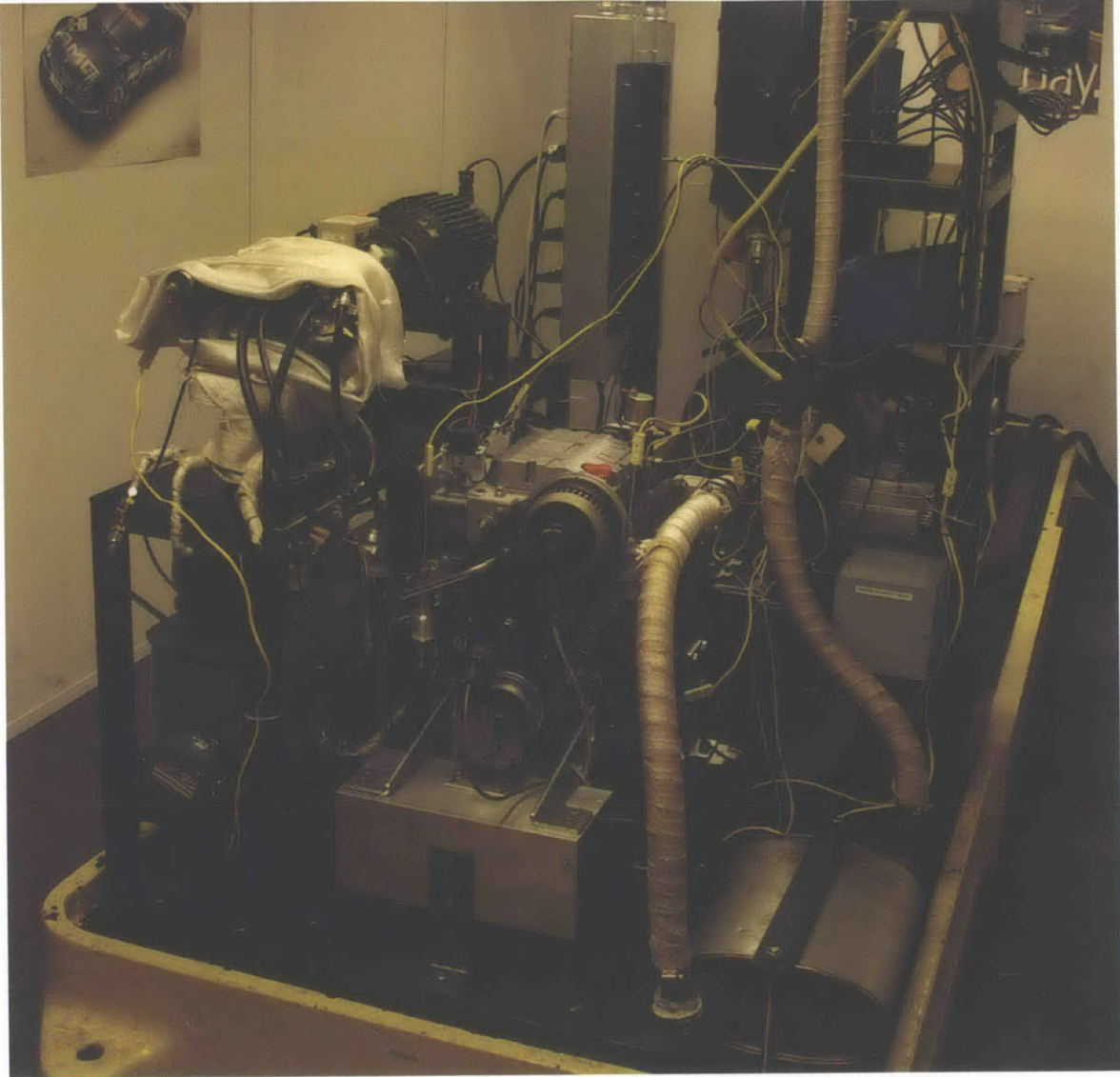
Figure 3-1: Completed set up of engine testing platform.

3.1 Experimental Powertrain Layout

The experimental powertrain is designed to control the engine's operation and enable the acquisition of engine data at desired testing conditions. Our required powertrain capabilities include the ability to operate the engine at any load and speed below its manufacturer specified max torque and speed points as well as reliably measure the output torque and power of the experimental engine. This was accomplished
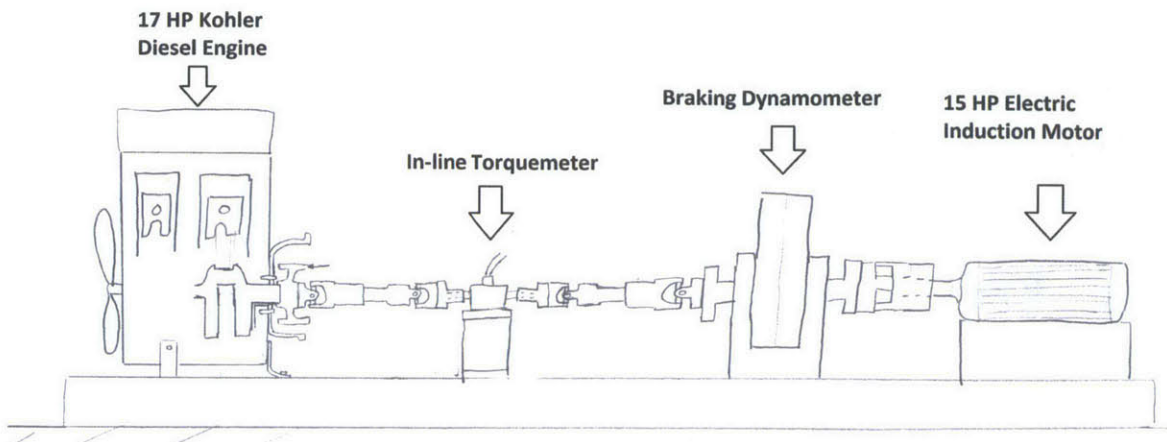
Figure 3-2: Experimental powertrain layout.

by designing and implementing a four component powertrain consisting of the experimental engine, an in-line rotating torquemeter, a braking dynamometer, and an electric motor.

In engine testing, it is common for the candidate engine to be coupled with a motoring or braking dynamometer. A dynamometer generates and applies negative torque to the engine driveshaft so that the engine may operate at different load points. Without it, any testing would be confined to low load operation where engine mechanical work produced was equal to its friction work and no net output work would be produced. Any net positive output work would lead to a engine rotational speed acceleration until either the increased friction balanced the net work or the engine failed. The dynamometer measures both torque and speed and can be configured to control either during operation.

It is also desirable to include some mechanism or electric component that can generate a positive torque, and spin the whole driveline without the combustion of fuel in the engine. When an engine is being spun by such an external component, such as an electric motor, or a motoring dynamometer, it is referred to as being "motored". Advanced testing platforms use dynamometers that can create both negative and positive torque with an internal electric motor and they are referred to as *motored dynamometers*. For our powertrain design, a braking, eddy-current dynamometer was

used for controlling the engine load and a fifteen horsepower alternating current(AC) induction motor was chosen to enable motoring operation. Figure 3-2 illustrates the placement of the engine together with the torquemeter, the braking dynamometer, and the electric motor.

3.2 Engine

In consideration for the primary motivation of subsystem specific lubrication studies, an engine was chosen to satisfy a number of requirements that enable the successful splitting of the lubrication circuit. A two cylinder, indirect injection (IDI), water-cooled diesel engine was chosen and donated by Kohler Company for the research purposes of this project.

The separation of the engine lubrication circuit and the measurement of valvetrain torque would only be achieved if the chosen engine was configured such that valvetrain system oil is located in a separate gallery from the crankcase oil. Overhead cam engines generally exhibit this characteristic, with an oil sump located at the bottom of the engine and a valvetrain region at the top of the engine that houses all valvetrain components, such as the camshaft and the valves. Oil is generally pumped within passages from the lower sump to the upper valvetrain oil gallery. After lubricating valvetrain components, oil falls back down to the main sump through drain passages.

There can be different variants of this configuration - the most notable with single or multiple camshafts, or with a chain-driven or belt-driven camshafts. Chain-driven camshaft designs require that the timing chain is constantly lubricated during operation with engine oil. This is commonly achieved by letting oil drain out of the upper valvetrain oil gallery out directly on to the chain. This is contrasted by a composite timing belt design that does not need lubrication. The separation of the valvetrain lubrication from the rest of the engine is much easier with a non-lubricated timing belt versus a lubricated chain.

Another problem is mitigated with the use of a non-lubricated timing belt config-uration - that is, the ability to install an electrical torque measuring sensor in place

38

of the camshaft pulley. Consequently, the candidate test engine must be have an overhead cam configuration with belt-driven timing.
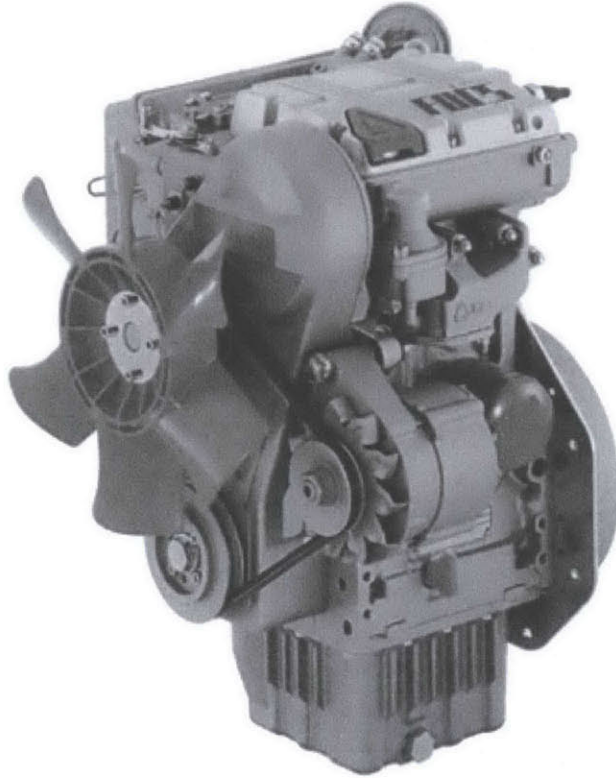
Figure 3-3: Kohler KDW 702 Engine

The engine chosen, shown in figure 3-3, has an overhead cam configuration and a composite rubber timing belt, satisfying the aforementioned requirements. Additionally, it uses a single camshaft for both intake and exhaust valve events, requiring only one camshaft pulley torquesensor to measure valvetrain torque instead of the two that would be needed for dual camshaft designs.

One additional advantage considered in the selection of this engine was the positive working relationship between the MIT Sloan Automotive Laboratory and the Engines division of Kohler Company. Throughout the project, Kohler was extremely active and generous in providing useful advice, insight, and needed parts during fabrication.

A disadvantage to using this engine configuration is the engine's camshaft driven mechanically actuated fuel delivery system. In addition to the intake and exhaust

valve cams, there are additional cams on the camshaft that actuate the mechanical fuel injectors. As a result, the injector timing is fixed and cannot be controlled. The only available fuel control mechanism is the injectors' variable pulsewidth. Their control will be discussed in section 4.7.

The relevant specifications for comparison and analysis pertaining to this engine are detailed in Table 3.1.

Table 3.1: Engine Specifications

Cylinders	2
Bore [mm]	75
Stroke [mm]	77.6
Displacement [cm^3]	686
Compression Ratio	22.8:1
Maximum Speed [RPM]	3600
Maximum Power [kW(HP)]	12.5(17)
Maximum Torque [Nm @ 2000 RPM]	40.5

3.3 Dynamometer Setup and Control

An eighty kilowatt, eddy current, braking dynamometer was selected and used to control the engine speed during testing. The Taylor DE-80 shown in figure 3-4 uses the principle of electromagnetic induction to induce eddy currents within a rotating disk that in turn creates a braking torque on the disk opposite the direction of rotation. The disk is coupled to the rest of the driveline, transmitting the braking torque to the engine and maintaining a particular speed point. This feedback control of speed is accomplished by a Digilog dynamometer controller that senses rotational speed, and excites the dynamometer's internal coils to maintain a particular setpoint.

Thermodynamically, a dynamometer converts mechanical generated by the IC engine into heat that is carried away by cooling water. The induced eddy currents responsible for creating a Lorentz force that slows down the internal rotating disks

generate heat through resistive dissipation.

Figure 3-4: Taylor DE-80 eddy current braking dynamometer.

For proper operation, the dynamometer needs electricity supplied to its coils as well as water to cool the disk and coils. Additionally, two sensors are also wired - a load cell that measures braking torque and a hall effect sensor that measures rotational speed.

Electrically, the dynamometer was connected to its Digilog controller, shown in the figure 3-5 (see relevant wiring diagrams and schematics in Appendix B). EXTREME CAUTION should be exercised when working electrical systems, and only qualified personnel should handle high voltage power above 50V. The system wiring includes providing 230V single phase AC power to the controller, connecting the field coil wires from the controller to the dynamometer terminals, connecting the load cell excitation and signal wires, and connecting the hall effect sensor for RPM. More connections can be made to increase the sophistication and capabilities of the controller, such as

Figure 3-5: Dynamometer controller - Digalog Series 1000A

throttle and load control. For this project, only speed control was configured on the dynamometer controller. Load control is accomplished with the fuel control system discussed later.

Pressurized water was supplied to the dynamometer for active cooling. One inch diameter tubes were run to the inlet and outlet dynamometer cooling ports, providing up to seventy-five pounds (PSI) of pressure to the dynamometer. These water lines come from the two vertical, insulated pipes in the back right corner of the test cell.

The right insulated pipe is the water supply line while the left is the return. Both sides are controlled by ball valves. The drain valve is usually left open, while the supply valve must be opened each day and shut after testing. After the supply valve, there are two pressure gauges with a filter between them. During operation, there should be no more than a 20 PSI drop from the first to the second across the water filter. A large pressure drop indicates that the filter is clogged and should be replaced.

The dynamometer requires a minimum of 14.5 PSI of water pressure to operate and has a maximum water pressure of 60 PSI. When the supply valve is fully open, more than 60 PSI is supply, therefore it is necessary to slowly close the valve until a post filter water pressure of 40-60 PSI is achieved. If the valve is fully open and the pressure is below 40 PSI, this indicates that either laboratory water supply pump is off or other test cells on the east side of the lab are using a lot of water as well. The laboratory water supply pump can be turned on at the switch located outside 31-035D, and it's "on" state is indicated by a red light bulb attached to the power switch on the wall.

After the dynamometer was properly connected, a calibration procedure was performed for proper torque measurements and a tuning procedure was performed to match the feedback controller gains with the dynamic and steady state behavior of the engine.

The dynamometer measures torque by using a load cell, or a tension gauge, to measure the force needed to prevent the dynamometer case from rotating when it puts a torque on its internal rotating disc. The load cell calibration procedure, discussed in section 2-4 of the Digalog Dynamometer Controller manual, is performed using standard "dead" weights to apply controlled known torques on the dynamometer case while adjusting the load cell readings accordingly. Two arms are attached to either side of the dynamometer, and the dead weights are hung from the arms to create a torque on the dynamometer case.

On the controller face, underneath the two large knobs are small knobs that can be used to detach a small cover, revealing an array of numbered potentiometers and numbers post terminals. The potentiometers are numbered R1, R2,... and the post terminals are numbered TP1,TP2,... for future reference. Table 3.2 lists the relevant potentiometers used in the calibration of the load cell as well as the tuning of the controller gains.The dynamometer controller tuning procedure is outlined in chapter 2 of the Digalog Series 1000A Controller manual and was performed to set proper feedback gains for smooth control. Using common PID feedback knowledge and potentiometers R46-R48, it is possible to tune the dynamometer controller to desired

performance.

Table 3.2: Dynamometer Controller Potentiometers

Potentiometer	Significance
R46	Feedback PID control proportional gain
R47	"Reset Time" - Feedback PID control integral gain
R48	"Inertia" - Feedback PID control derivative gain
R52	Load cell span gain
R53	Load cell zero point
R54	Load cell excitation voltage

3.4 Electric Motor and Controller

In consideration for the braking dynamometer's inability to create a positive driving torque, an electric motor was used to turn the driveline. A Marathon Black Max Y549, fifteen horsepower, AC induction motor was installed and controlled by a Durapulse GS3-2015 drive inverter. When coupled to the rest of the driveline, the electric motor is able to drive the engine at speeds up to 3600 RPM. The function of the drive inverter is to take 230V, 3 phase, AC power and convert it to a variable voltage, variable frequency power supply to the motor. During engine startup and motoring tests, we can control the driveline rotational speed with the Durapulse drive inverter. The keypad, shown in figure 3-6, allows us to change not only the driving frequency, but also many other configurations.

Referring to page 4-29 of the inverter manual, the controller is configured with parameter P3.00 set to 03, and parameter P3.01 set to 02. These settings set the instrument panel "crank" button as the only way the motor will turn on. It also disables reverse rotation and enables the keypad "stop" button. Additionally, parameter P3.03 set to 01 and the electric motor's protection thermistors must be wired to terminal DI4, so that the inverter knows to shut down the motor if it ever overheats.

44
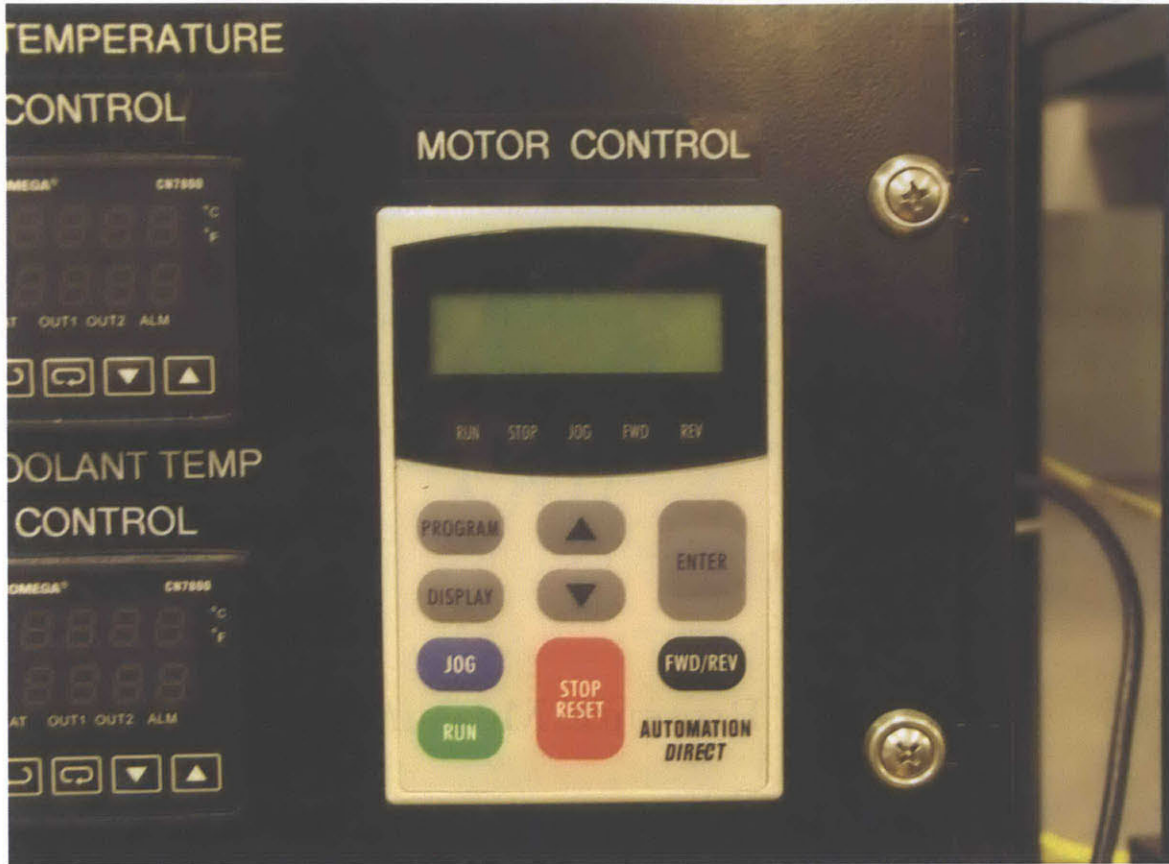
Figure 3-6: Electric motor control keypad used to set drive inverter voltage and frequency.

Initially, the engine's stock starter motor was wired to the crank button as well so that both the starter and the AC 15 HP motor started at the same time. This was intended to alleviate the torque requirement of the large electric motor, but operational tests indicated that the motor can handle the start up, yielding a smoother start-up transient, with lower experienced torque spikes.

The "Motor enable" switch on the engine instrument panel controls a set of contacters within the grey box below the inverter and above the panel. These contacters switch 208V, three phase AC power through a set of fuses and a line reactor (a component intended to dampen supply voltage transients) to the inverter itself.

It was important to achieve a method by which during motoring operation, the user can transition to exclusively firing operation, and vice versa. This would require

the electric motor to free wheel or coast, as well as regain operation at speed. This was accomplished by the external base block function, detailed on page 4-33 of the inverter manual. The "motor coast" switch at the top of the instrument panel is set to enable the external base block function during this transition. Essentially, the external base block function causes the motor to coast, or free wheel at any speed. When external base block is disabled, the inverter will begin a speed search function that re-energizes the motor at its current rotational speed.

3.5   In-Cylinder Pressure Measurements

The measurement of cylinder pressure instantaneously is a common and established method to characterize indicated engine work. The visualization of cylinder pressure and volume can also be a great troubleshooting tool for engine and combustion problems. Two Kistler 6052C pressure transducers were installed in the engine cylinder head. The Kolher engine was designed with a coolant jacket running through the cylider head between the upper oil gallery and the combustion chamber. Therefore, it was necessary to machine a hole through the coolant jacket and install a custom adapter sleeve for each pressure transducer. After successful installation of each transducer, it was necessary to properly calibrate the transducers using a dead weight pressure tester.

The pressure transducers are manufactured with piezoelectric crystals near the pressurized face. When a force is applied to the crystal, which in turn causes crystal deformation, the crystal generates a voltage that is measured by a charge amplifier. The Kistler Type 5010 Dual Mode Charge Amplifier senses the generated charge at the crystal and amplifies the signal to a 0-10V output.

46
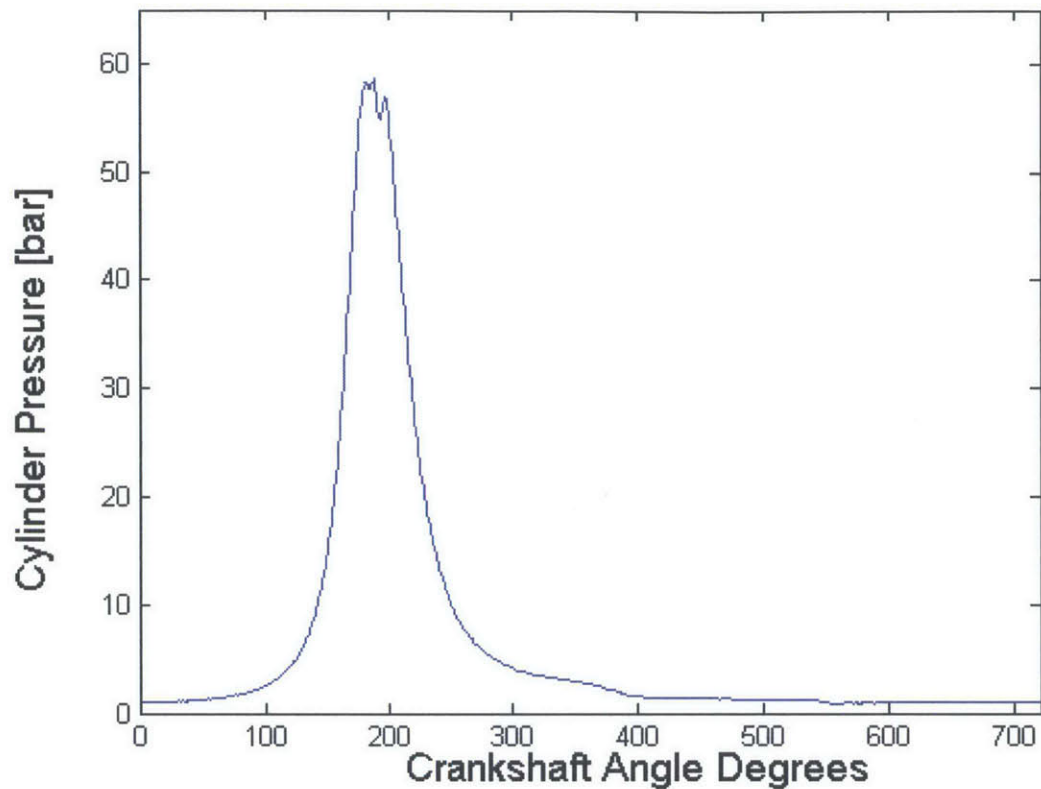
Figure 3-7: Fired engine pressure trace.

Figure 3-7 shows the normal pressure trace for a fired engine cycle. Compression, ignition, expansion, exhaust and intake events can be observed using instantaneous pressure measurements. Net indicated mean effective pressure can be calculated by integrating the pressure trace over the combustion chamber volume throughout one cycle as follows.

$$NIMEP = \frac{\int PdV}{V_d}$$

3.5.1 Cylinder Head Modifications

The installation of pressure transducers requires direct access to a cylinder combustion chamber above the piston's top dead center position. As such, modifications were made on the Kohler engine cylinder head to provide such access to the cylinder clear-

ance volumes. Two holes were machined passing through the cylinder head cooling jacket down to the combustion chamber for the installation of pressure transducer adapter sleeves. Shown in figure 3-8, the sleeves pass through the cooling jackets, sealing on the top and bottom.
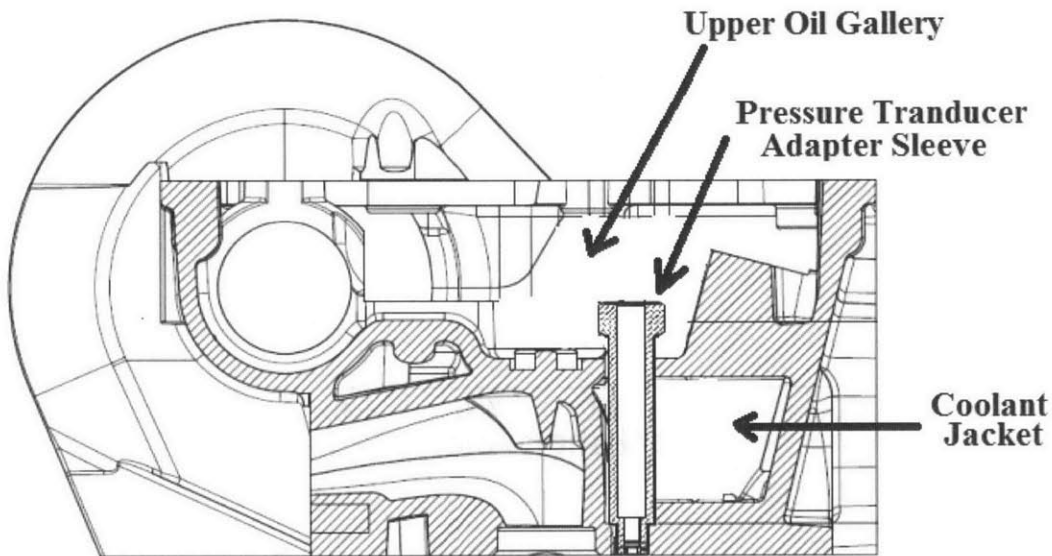
Figure 3-8: Cylinder pressure transducer sleeve installed in engine cylinder head.

The sealing of the adapter sleeve was initially performed using gasket-maker silicon, but this was replaced by JB Weld at the top of the sleeve for better sealing between the upper oil gallery and the coolant jacket.

The installation of the transducers in the sleeves was nontrivial and proper care must be taken when handling the sensors themselves. It is very important to clean every end of the transducer connections with the appropriate Miller-Stevenson solvent and dry it with a heat gun, before installation to remove all contaminants and particles that may change the accuracy of the pressure measurements.

3.5.2 Pressure Transducer Calibration

Each transducer-charge amplifier pair was calibrated using the dead weight pressure tester. It uses standardized weights to exert a known force and pressure on hydraulic fluid, which applies that pressure to an attached pressure transducer. A calibration curve was formed by using a large range of weight sizes.

An adapter was made to fit the Kistler 6052 sensor on the NPT style pipe one the right side of the figure. On the left side of the tester, a crank can be turned to pump hydraulic oil to lift the dead weight place on the center platform. It is important to spin the weight as the pressure measurement is being taken because static friction within the tester can offset the true force of the dead weight. Figure 3-9 below illustrates the linearity of the Kistler pressure transducer's output voltage with respect to pressure.
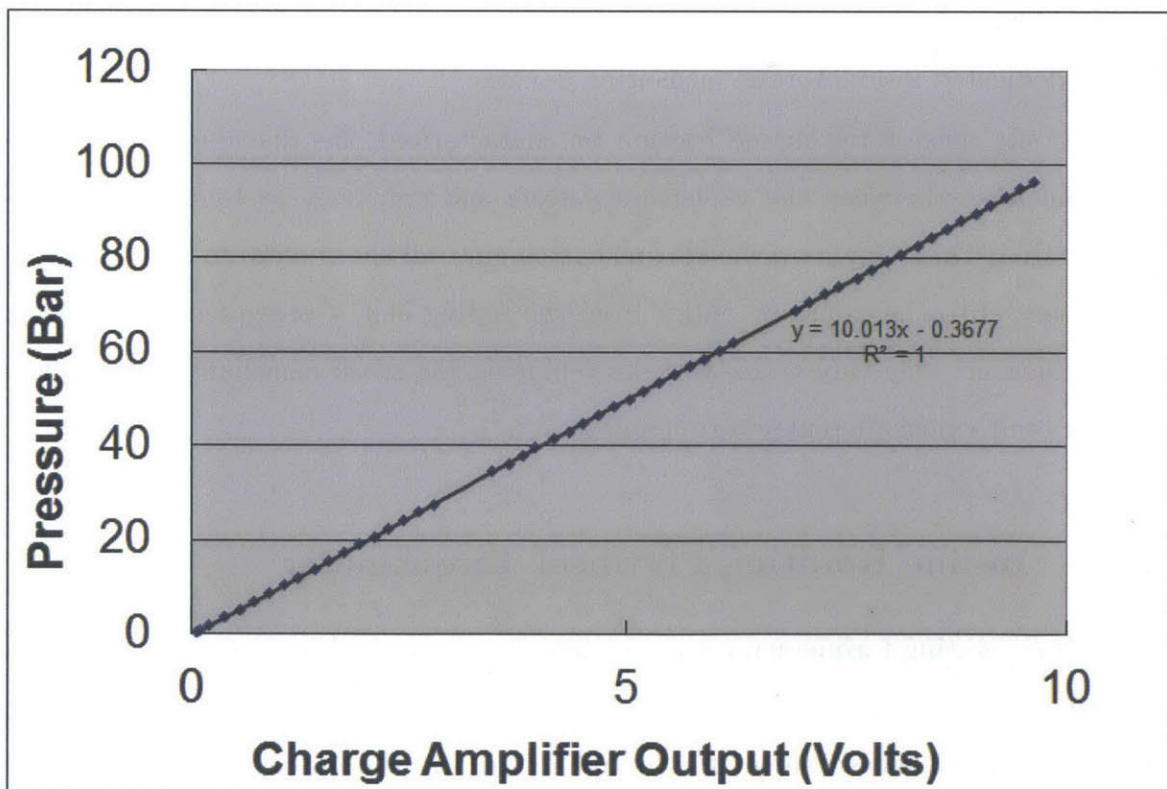
Figure 3-9: Pressure transducer dead weight calibration curve.

3.6 Torque Measuring Equipment

The primary experimental motivation of this experiment is to characterize engine friction with different lubricants. Although it is very difficult to directly measure friction locally at the many individual components and surfaces experiencing frictional losses, we can reliably calculate total friction by measuring the total mechanical work the engine produces as well as the total brake work coming out of the engine and finding the difference, as represented by the equation below.

$$NIMEP = BMEP + FMEP$$

$$FMEP = NIMEP - BMEP$$

where NIMEP, BMEP, and FMEP are defined in section 1.1, and correspond to net indicated work, brake output work, and friction work. Total brake work can be measured with a dynamometer, or a dedicated torque sensor. Although our eddy current dynamometer can measure reaction torque, higher accuracy can be achieved with a dedicated in-line torque measuring device.

Not only must total engine friction be characterized, the distribution of engine frictional losses between the valvetrain system and crankcase system must also be investigated. On a single overhead camshaft engine, all the valvetrain driving torque is transferred to the camshaft pulley from the timing belt. Consequently, we sought out to measure this valvetrain work by replacing the stock camshaft pulley with a custom built camshaft pulley torquesensor.

3.6.1 In-line Rotating Flywheel Torquemeter

An in-line rotating torquemeter was purchased and installed between the engine and dynamometer to measure mechanical work and power that comes out of the engine. This is a critical measurement for the reliable quantification of engine friction and it was important to procure an appropriate sensor with the range, resolution and accuracy to resolve ones of percent changes in engine friction.

The Himmelstein MCRT 49704V torquemeter was purchased and installed in the driveline to measure engine brake work. It has a range of 5,000 lbf-in and a 400% overload specification - that is, it can momentarily experience torque spikes up to 20,000 lbf-in without permanent damage. It has a nonlinearity and hysteresis rating of 0.05% of the 5,000 lbf-in full scale range. This means that our maximum torquemeter uncertainty will be 2.5 lbf-in or 0.28 Nm, which is sufficient to resolve frictional losses that are on the order of 4 Nm or 10% of the Kohler engine's maximum brake torque of 40 Nm.
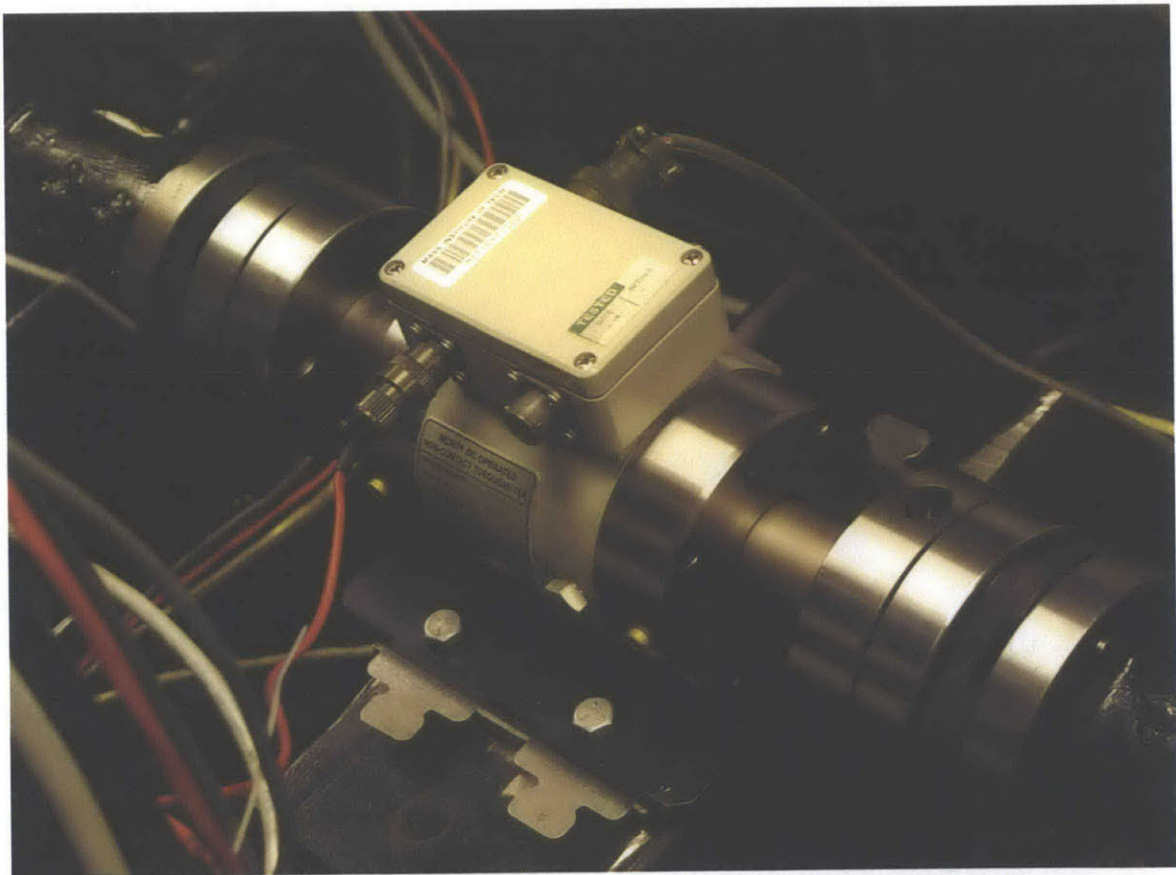
Figure 3-10: Himmelstein MCRT 49704V in-line torquemeter installed at the flywheel.

The Himmelstein torquemeter comes with a serial cable that can be used with a Window computer to interface with the sensors internal programming. Using the provided PDTM software, it is possible to zero and span the sensor programmatically. Figure 3-11 illustrates a single cycle measurement of instantaneous brake torque. We

can calculate the total brake work over a cycle by integrating the instantaneous torque measurement and normalizing by the engine displacement.

$$BMEP = \frac{\int_{0}^{4\pi} \tau_{brake} d\theta}{V_d}$$

where τ_{brake} is the instantaneous brake torque measurement and V_d is the engine displacement volume.
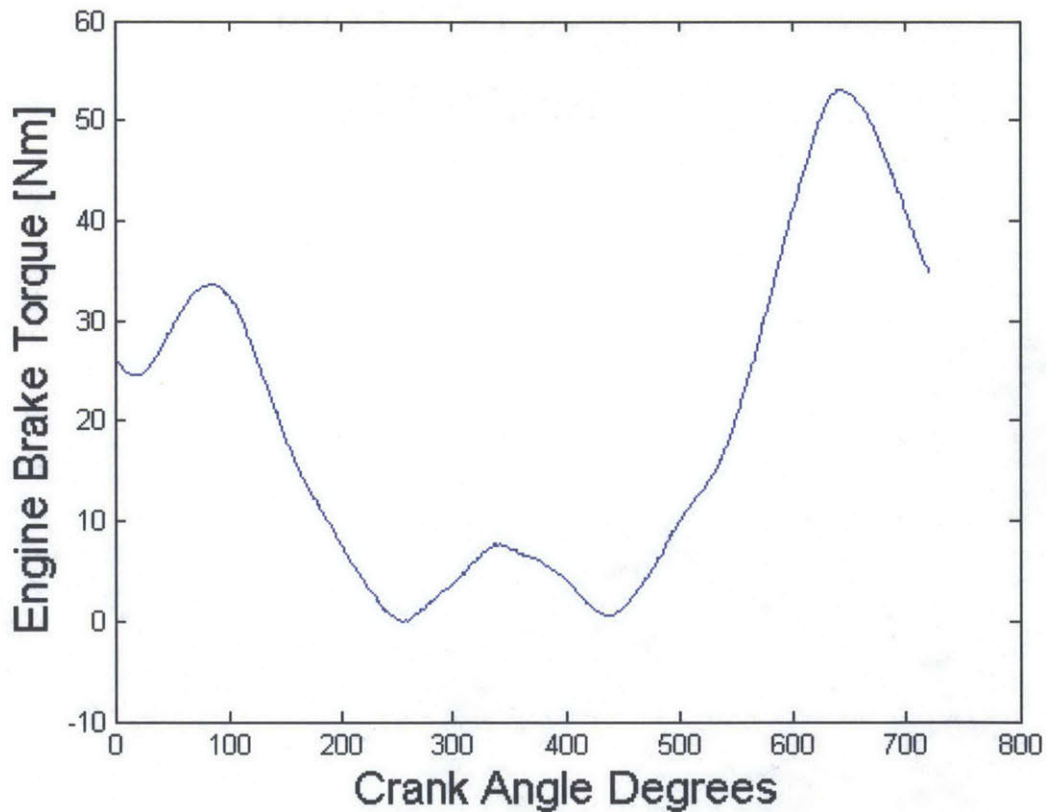
Figure 3-11: Instantaneous brake torque measurement for one cycle.

3.6.2   Camshaft Pulley Torquemeter

The measurement of valvetrain torque is also necessary to separate friction losses of the valvetrain system from friction losses in the crankcase and power cylinder region. The installation of a custom camshaft pulley torquemeter enabled the successful

52

measurement of valvetrain torque.
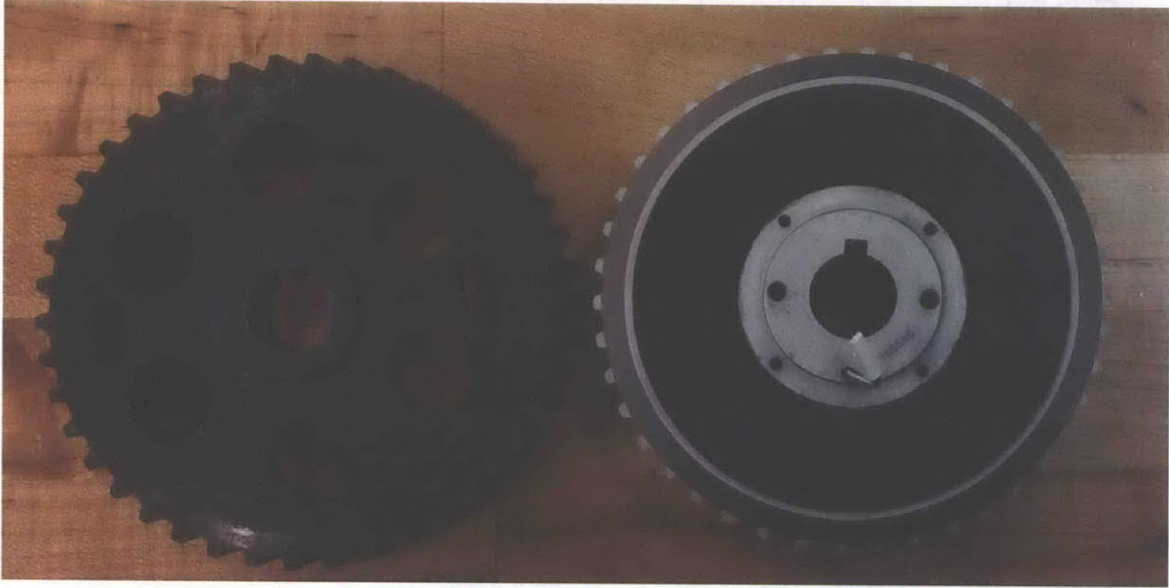
Figure 3-12: Stock camshaft pulley and custom made pulley torquesensor.

Figure 3-12 illustrates a single cycle measurement of instantaneous valvetrain torque. Crankshaft friction and valvetrain work can be calculated using the following relations.

$$FMEP_{valvtrain} = \frac{\int_0^{2\pi} \tau_{valvetrain} d\theta}{V_d}$$

$$FMEP_{total} = FMEP_{crank} + FMEP_{valvetrain}$$

where τ_{brake} is the instantaneous valvetrain torque measurement and V_d is the engine displacement volume.
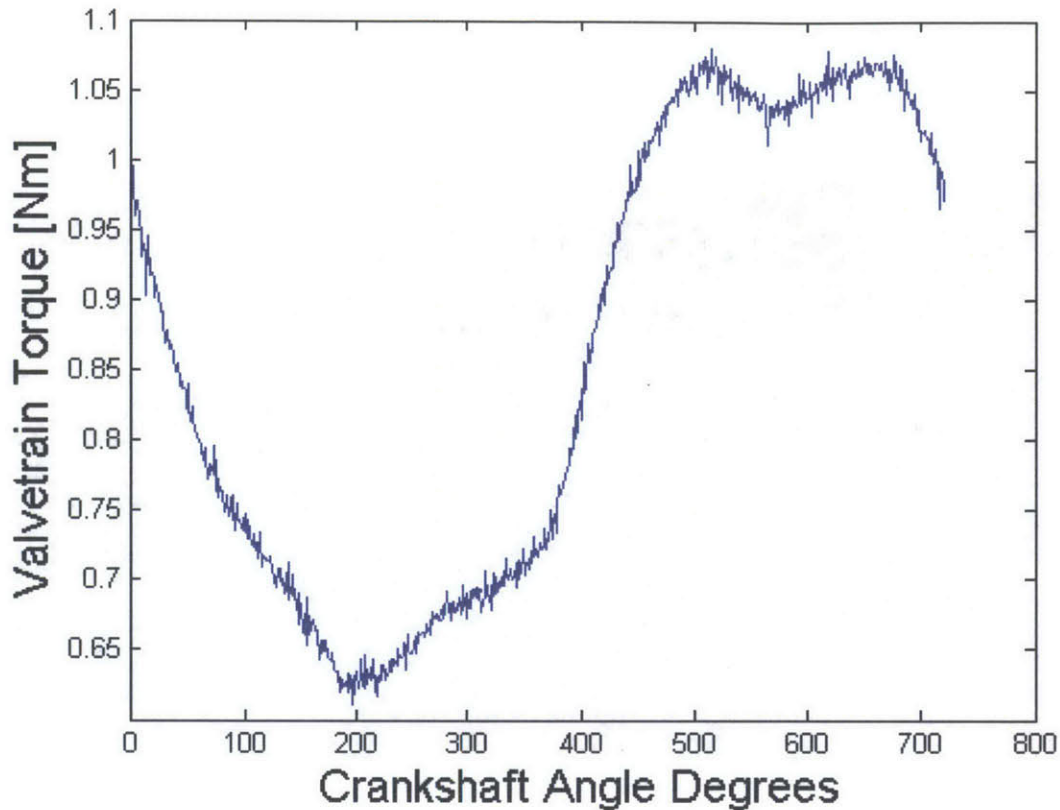
Figure 3-13: Camshaft pulley torque for one cycle of firing engine operation.

3.7 Fuel Injection Control System

In section 3.3, speed control of the engine by the dynamometer controller was discussed. At a particular rotational speed, the engine can be run at any load and the dynamometer controller will mirror that load accordingly to maintain a desired engine speed. A fuel control system was designed and set up to command a particular engine NIMEP, and load point. This was accomplished by disabling the mechanical governor mechanism in the engine, replacing it with a rigid linkage connected to servo motor that actuates the fuel pulsewidth directly, and implementing electronic control of the servo motor that can be commanded from outside the test cell at the instrument panel.
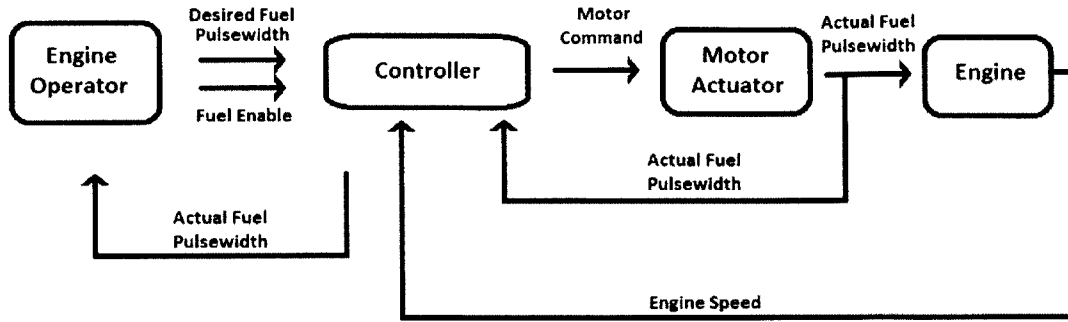
Figure 3-14: Fuel control system architecture.

Figure 3-14 illustrates the feedback control structure of the implemented system. The operator enables the system and commands a fuel pulsewidth servo position setpoint using a toggle switch and a knob potentiometer, respectively. The controller senses the actual servo position as well as the engine speed, actuates the servo motor and displays the servo position to the operator with an LED display.

3.7.1 Mechanical Fuel System

The Kohler KDW engine comes stock with a mechanically actuated, camshaft driven fuel injection system. As shown in figure 3.7.1, a large camshaft lobe pushes on a plunger that pumps high pressure diesel at 140 bar to be injected by a nozzle down into a combustion chamber. While the timing of this fuel injection event is fixed, the pulsewidth can be changed by moving a small lever on top of the fuel injector. This lever actuates a valve within the fuel injection pump that controls the amount of fuel that is pumped in to the injector and subsequently into the cylinder.
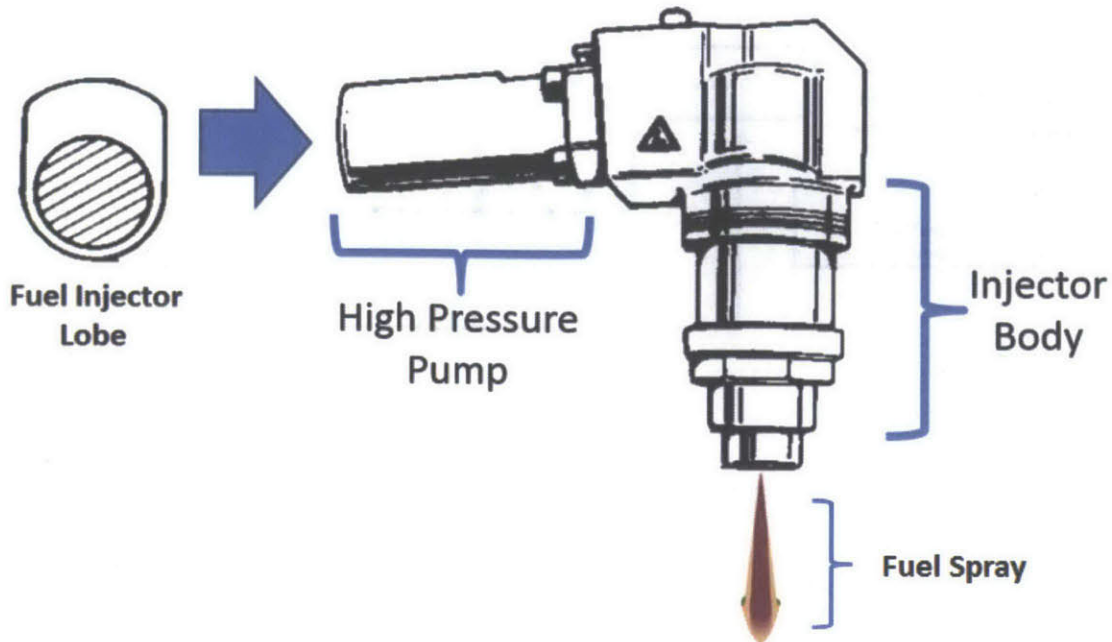
Figure 3-15: Kohler mechanical fuel injector operation.

The two fuel injector levers are connected along a linkage, creating a four bar mechanism controlling both fuel injectors at the same time and at the same lever position, shown in yellow and blue in figure 3-16. This linkage is connected to a governor mechanism intended to control engine speed. The governor accomplishes speed control by balancing spring tension on the fuel linkage with the centrifugal inertial force seen by a set of spinning weights. If the engine goes to fast, the weights spin faster, their centrifugal inertial force increases pushing them out further and putting a larger force on the fuel linkage to close the injector pulsewidth valves. This, in turn, decreases the amount of fuel being injected in to the cylinder and slows down the engine.

3.7.2 Mechanical Modifications and Actuator Installation

The objective of the fuel control system is to use an electromechanical actuator such as a servo motor to control the valvetrain linkage connected to the fuel injector control levers. The first modification in this process was to disable the governor mechanism

and its articulation with the control linkage. A servo motor was then purchased and mounted atop the cylinder head, connected to the governor's speed control lever.
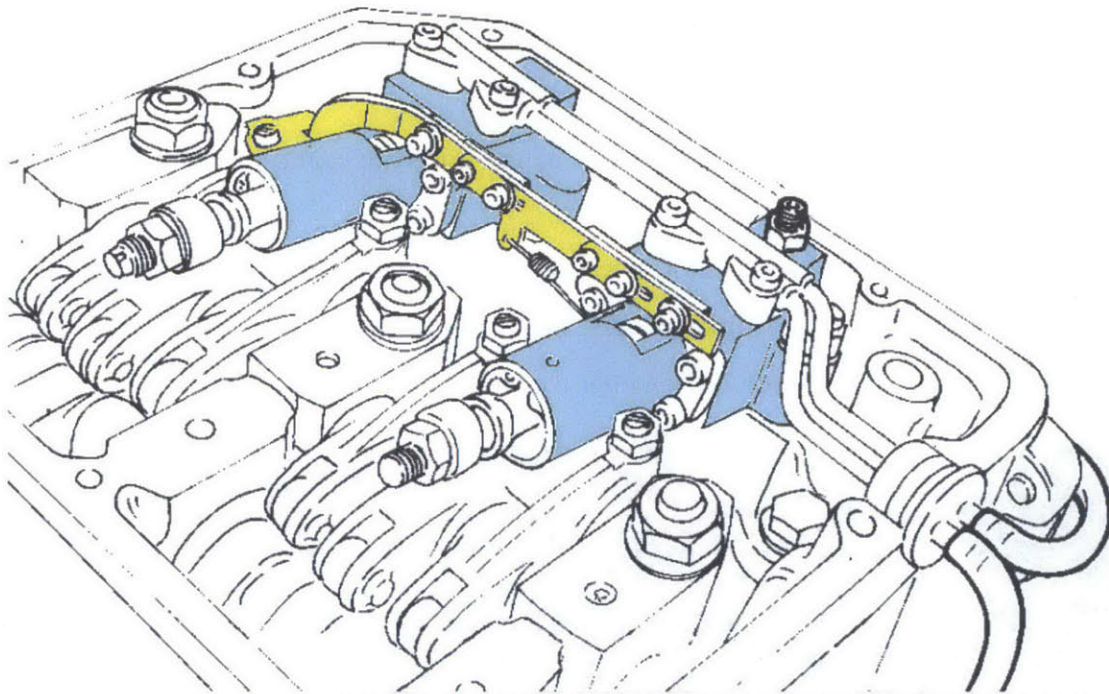
Figure 3-16: Overhead view of the engine valve train system.

Figure 3-17 illustrates an exploded view of the governor components that articulate with the fuel control linkage. As the flyweight assembly spins faster, the individual weights move outward and push on the two small arms of the governor control lever. In order to disable the flyweight control of the fuel completely, these two arms were cut off completely. Instead, an additional link was machined to connect the left side of the governor control lever to an external lever outside the cylinder head.

Speed governor components

Governor control lever

Governor
actuation arms

Flyweight assembly
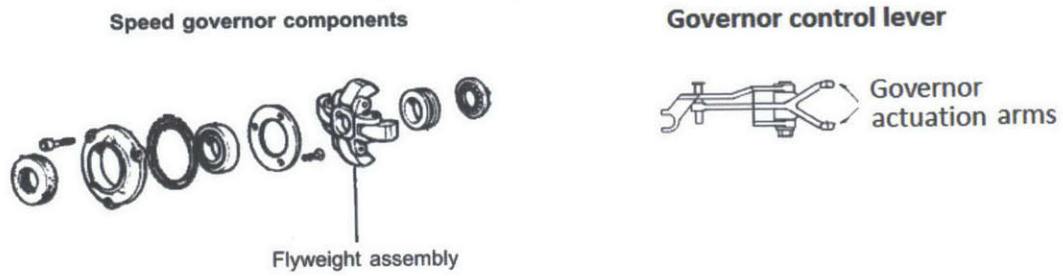
Figure 3-17: Exploded view of the governor components.

A HiTec HS-5645MG servo motor was wired and mounted to the lever connected to the internal fuel control linkage. As this servo motor turns the lever shown in figure 3-18, both fuel injector pulsewidth control levers are actuated.
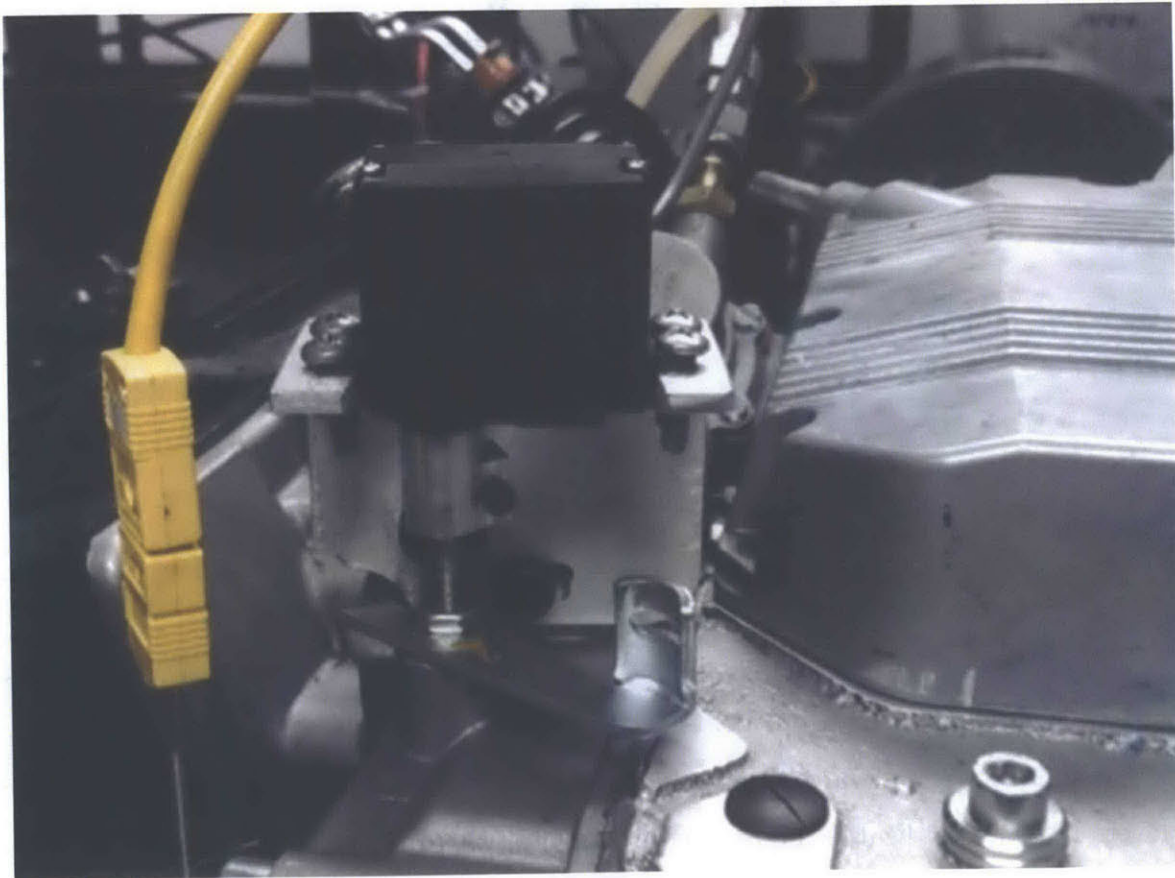
Figure 3-18: Fuel control servo motor mounted on the engine cylinder head.

3.7.3   Electrical and Electronic Setup of Actuator Control

The choice of using an electromechanical actuator to control the mechanical fuel injectors was motivated by the need to control engine load from outside the test cell at our control panel. Signals wires were run from this panel to a microcontroller circuit responsible for powering and commanding the fuel control servo motor. The electrical circuit was designed to sense the operator's fuel setpoint position and command the servo motor accordingly.
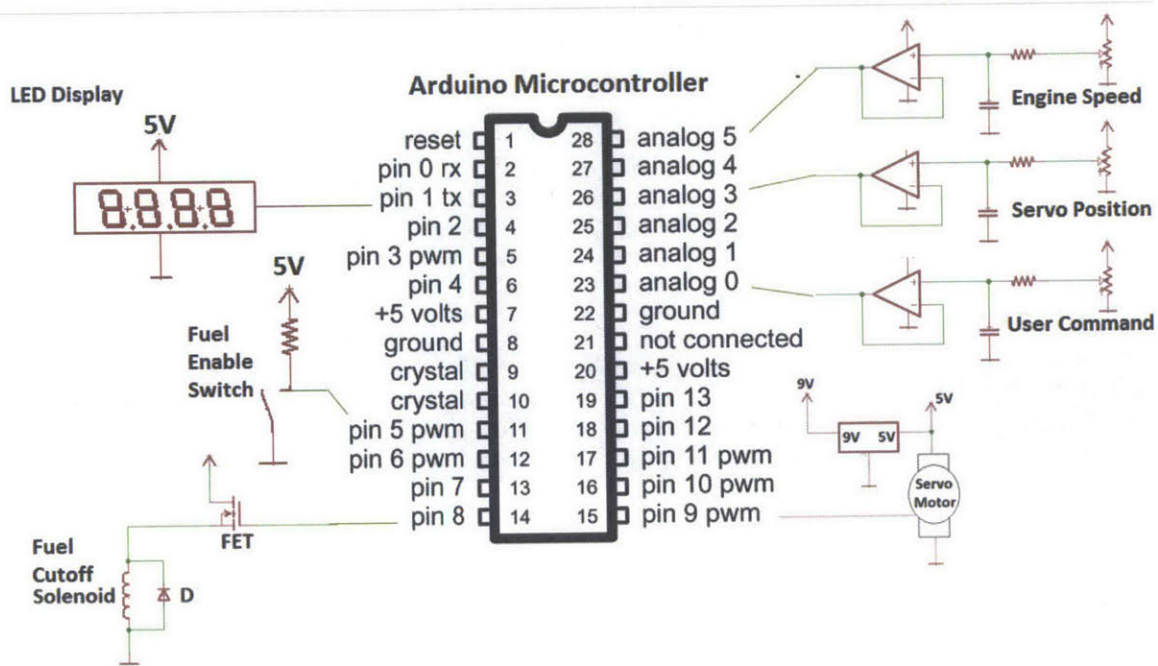
Figure 3-19: Electrical connection for the Arduino microcontroller

At the heart of the servo control electronics is an Arduino Uno microcontroller that reads analog signals, processes them and controls the servo motor. A simplification of the controller and the electronics is shown in figure 3-19. The electric circuit buffers the three analog signals the microcontroller measures - engine speed, present servo position, and commanded servo position. Additionally, a dedicated five volt power supply is connect for the servo motor itself. The controller is enabled or disabled by a switch on the instrument panel and it also displays the current fuel linkage position in percent full on an LED display also on the instrument panel as shown in figure

Figure 3-20: Fuel injection system control panel.

The operator can enable and disable the fuel injection system by switching the "Fuel Enable" toggle switch on the panel. When the system is enabled, the operator can use the large incremented knob to command a linkage position and the microcontroller will comply.

3.7.4 Microcontroller Capabilities

An Arduino Uno microcontroller was installed and programmed to provide the operator with active control of the fuel system as well as protect the engine from harmful runaway conditions. The controller was programmed with four internal states and depending on the position of the operator control knob, the "Fuel Enable" switch, and the engine speed, the controller will switch between the states to ensure smooth

and safe operation.
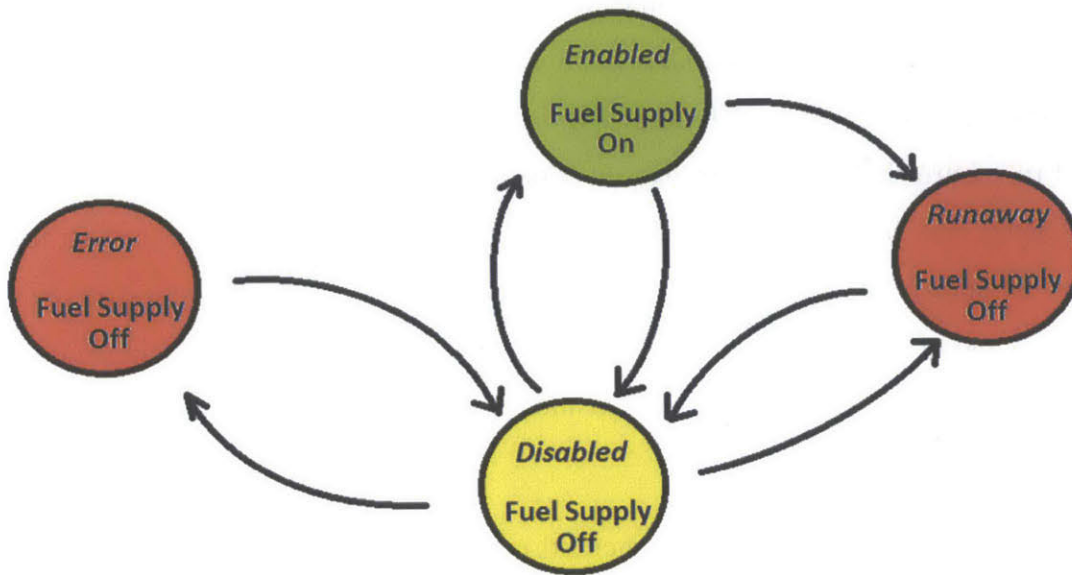
Figure 3-21: Fuel control system state diagram

The state diagram in figure 3-21 illustrates the decision making process programmed in to the controller. The *disabled* state keeps the led display off and the fuel control linkage in the off position. The *enabled* position allows the servo motor to actuate the fuel control linkage through a wide range. These two states are the main operational states with the user either commanding a fuel linkage position or the fuel system is off.

The *enabled* state is the only operational state with the fuel supply on and must be enabled properly. If the control knob is at a position that corresponds to higher than 5% fuel, the controller will enter an *error* state and flash "Er0r" on the LED display. This is done so that an operator does not unknowingly enable the fuel system with a high fuel command, causing the servo to quickly actuate the fuel linkage to a high pulsewidth position, leading to a high torque engine transient that may overload the 15 HP electric motor or stall the engine.

The *runaway* state serves to protect the engine and operators from a overspeed

event. Since the engine is mechanically fuel injected, if the dynamometer malfunctioned or lost power, the engine would experience no load and begin to accelerate. At high load operating conditions, sufficient torque is produced to continuously accelerate the engine past its maximum speed, leading to component failure and explosions. Once the "Fuel Enable" switch is turned on, the microcontroller monitors the engine speed to ensure that it does not exceed 3500 RPM. No testing was performed at this high speed and it was assumed that any moment the engine accelerated to higher than this speed, it would most likely not be commanded by the operator and the safest course of action would be to shut the fuel system off. In this *runaway* state, the microcontroller actuates the servo motor to a full off closed fuel position and flashs "rUnn" on the LED display.

See appendix B for the full commented microcontroller code.

3.8   Lubrication Circuit Separation

In order to optimize lubricants on a subsystem basis, separation of the valvetrain oil gallery is necessary so that two unmixed lubricants may be used within the engine. The split lubrication system, shown completed in figure 3-22, currently supplies the engine valvetrain components with pressurized lubricant, while the main engine oil pump continues supplies the crankshaft and cylinder liner with a different oil.

This was accomplished on the experimental engine by physically blocking oil passages that pumped lubricant from the crankcase to the valvetrain. An external lubricant circuit was then plumbed to supply the valvetrain with a separate oil from that in the crankcase. The valvetrain lubrication circuit possesses its own sump, oil filter, and pump. Additionally, the lubricant temperature within the valvetrain sump is controlled with a dedicated oil heater and temperature controller.
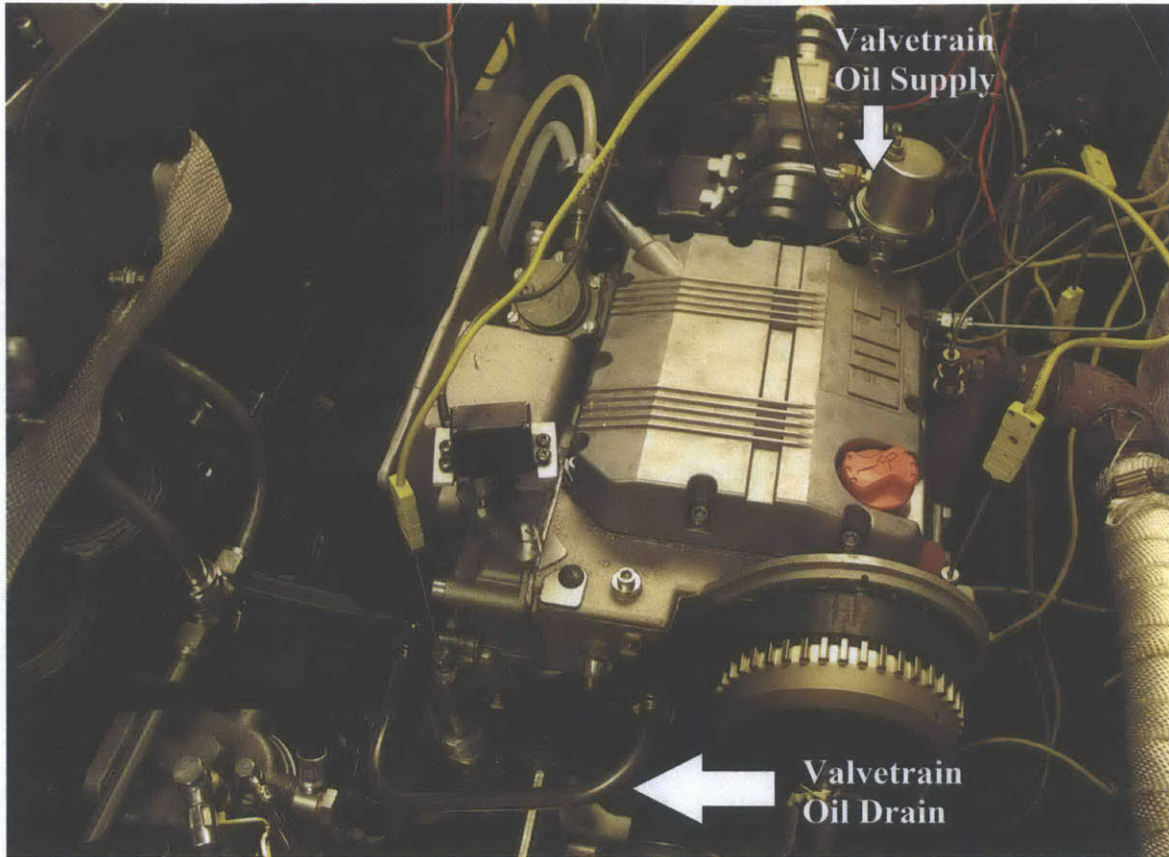
Figure 3-22: Completed external cylinder head lubrication circuit.

3.8.1 Interference Fit Oil Passage Plugs

The engine cylinder head has five passages that communicate with the crankcase. During stock operation, the crankcase oil pump pressurizes the oil passages that carry lubricant up to the valvetrain system through a single supply channel. Pressurized lubricant is supplied to the camshaft bearings and the rocker arm assembly. It lubricates the components and squeezes out the small bearing clearances, pooling within the upper oil gallery. There are three large drain holes within which the lubricant will fall back down to the crankcase and the main oil sump. The fifth oil passage connecting the crankcase and the cylinder head carries no oil, but rather lubricant vapors up to a positive crankcase breather. All five holes were characterized, measured and plugged with precision machined aluminum interference plugs.

Figure 3-23: Installation of stock lubrication passage interference plugs to separate the lubrication circuit.

Figure 3-23 shows the use of an arbor press to insert the interference plugs into the cylinder head. The plugs were machined to diameters that are 5 ten-thousands larger than the internal diameters of the holes they would plug. They were each turned on a machine lathe using an outside micrometer accurate to within one ten-thousandth of an inch to verify the appropriate outside diameter.
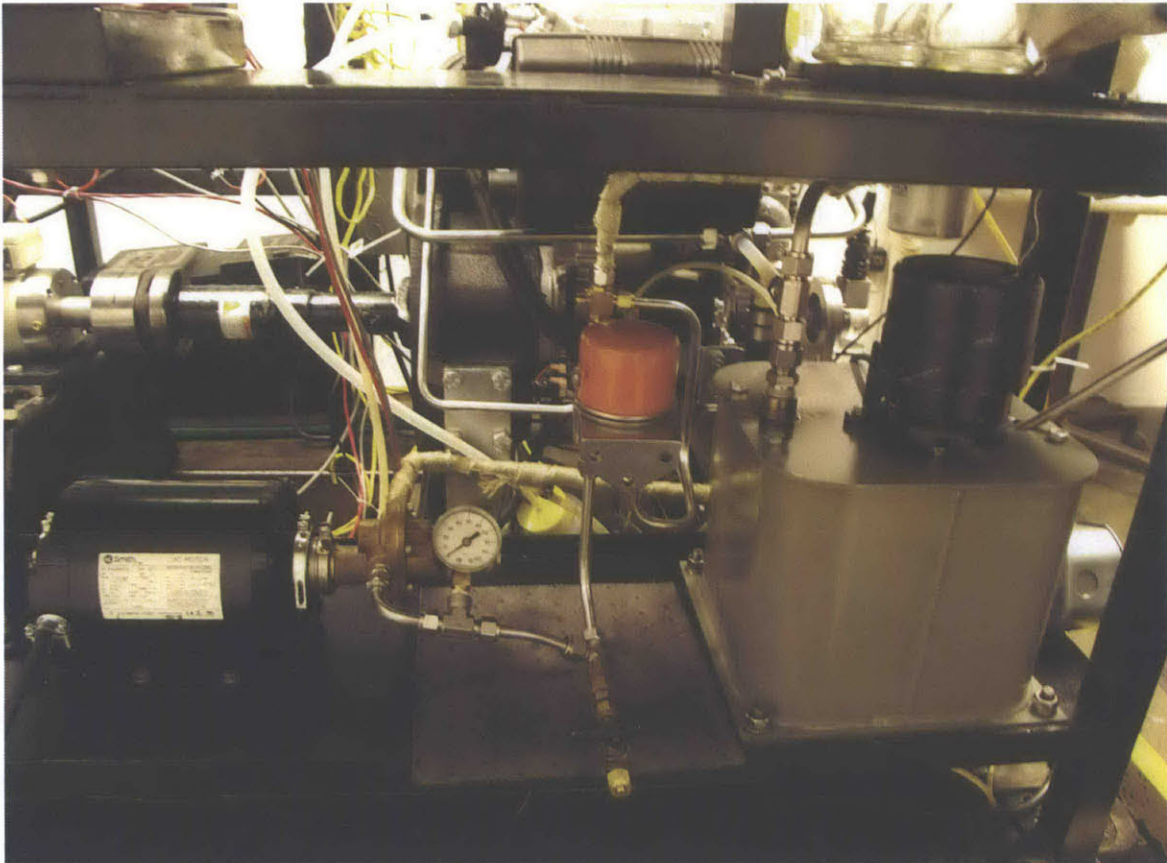
Figure 3-24: External lubrication circuit pump, filter and temperature controlled sump.

3.8.2 External Oil Sump, Filter, and Pump

Oil lines were plumbed so as to supply the valvetrain components with pressurized lubricant during operation. This system is shared with the second cylinder head bench experiment, with the ability to supply oil to the main engine cylinder head or the cylinder head bench test rig by simply turning a valve. This system is comprised

of a positive displacement bronze gear pump, an original equipment oil filter, and a temperature controlled sump.

A 0.5 HP electric motor drives the bronze gear type oil pump, shown on the left of figure 3-24. The pump possesses an internal bypass circuit allowing the control of output oil pressure up to 100 pounds. Oil travels from the pump to the remote cylinder head oil filter and then to the engine valvetrain system. The oil sump, shown on the right of figure 3-24, is filled with 4500 ml of oil for testing. This quantity is used so that the electric oil heater within the sump is always covered by oil, or else it will get excessively hot and burn the oil it is in contact with.

3.8.3   Lubricant Temperature Control

A one and a half kilowatt electric heater was installed within the oil sump to achieve active heating and temperature control. Since the heat losses from the oil lines and off the engine are larger than the heat absorbed from combustion and friction, no cooling mechanism is needed to achieve desired temperatures. The heater is controlled by an Omega CN7800 temperature controller, shown in figure 3-25. An electric motor stirrer was also installed in the sump to induce a flow with the sump and prevent lubricant from locally burning at the heater element surface.

The Omega CN7800 controller outputs a DC pulse signal, using modulation to control the heater effort. At lubricant temperatures close to the setpoint temperature, the controller will briefly excite the heater while longer pulses are seen at temperatures farther away from the setpoint.

Figure 3-25: Omega CN7800 temperature controller.

3.9 Engine Speed and Position Measurement

Since the pressure and combustion events of an IC engine are timed according to the position of the piston as it travels up and down the cylinder, engine data is often sampled on a crank angle basis, not at a fixed frequency. To accomplish this, both incremental and absolute crankshaft position must be know. An optical encoder was installed at the crankshaft pulley to track its rotational position. Additionally, the encoder's crank angle signal can be used to calculate instantaneous speed and supplement the dynamometer's speed measurement. The encoder outputs two distict signals - a crank angle resolved squarewave with each rising edge representing a crank angle travelled, and a reset signal with only one pulse every revolution of the crankshaft. These two signals allow us to track the absolute position of the crankshaft as well as the engine speed.

3.10 Cooling System

Figure 3-26: Engine cooling reservoir, heat exchanger, and pump.

A custom cooling system was setup to replace the stock belt-driven water pump and radiator combination that was responsible for cooling the engine. Instead, an electric pump and temperature controlled cooling reservoir was installed to provide a stable, continuous supply of engine coolant. The coolant system, shown in figure 3-26, pumps coolant from the central coolant reservoir to the engine, out the engine to a cooling heat exchanger and back to the coolant reservoir. An electric heater was installed in the coolant reservoir to heat the coolant to a user specified temperature. A solenoid valve was installed in the city water supply line of the heat exchanger to control coolant heat rejection. The Omega CN7800 temperature controller installed in the main panel controls both the electric heater and the heat exchanger's solenoid valve

to heat or cool the engine coolant to a fixed temperature.

3.11   Thermocouple Installation and Distribution

As discussed in chapter 2, engine hydrodynamic friction is highly dependent on lubricant viscosity and viscosity is strongly a function of temperature. Therefore, it is important to characterize the thermal conditions within an engine when performing friction tests. Without knowing lubricant temperature in key areas of the engine, differences in friction due to lubricant formulation cannot be decoupled from those due to changes in temperature. Consequently, the Kohler engine was equipped with five thermocouples in key locations to monitor testing conditions and preserve experimental repeatability.
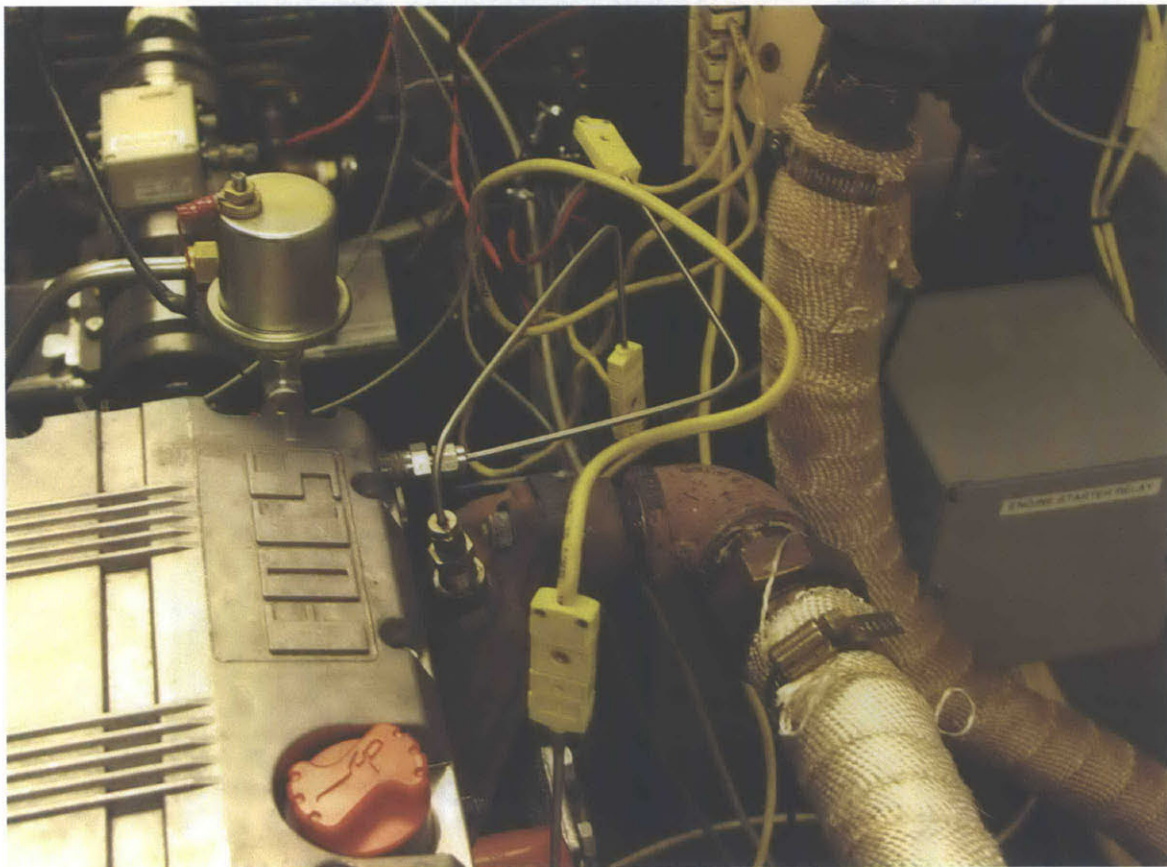
Figure 3-27: Coolant outlet, valvetrain oil inlet, and exhaust thermocouples.

K-type thermocouples were installed in the following key locations - the coolant inlet, the coolant oulet, the valvetrain oil inlet, the main engine oil sump, and the exhaust. Figure 3-27 shows the exhaust and valvetrain oil inlet thermocouples installed and connected back to the data acquisition system through the thermocouple panel on the right.

3.12 Instrument Control Panel

Figure 3-28: Operator instrument control panel.

The instrument panel, shown in figure 3-28, was designed and fabricated to allow the engine operator to control almost all test equipment from outside the test cell. Nearly every electrical component within the testing platform can be quickly turned on and controlled from the instrument panel using the installed switches, knobs, or controllers. The entire panel is split into three subpanels atop of the dynamometer controller. The bottom section of the instrument panel controls the engine platform specific components. The middle section controls the cylinder head bench components and the upper panel provided extra room for more controls, now housing the fuel injection system controls and additional oil pressure gaugues.

The panel was designed with safety and security in mind. The master key controls the supply power to all controls, allowing the operator to lock out the system from operation by simply removing the key. The terminal blocks and wiring are easily accessible but shielded by a plastic cover.

Each switch on the panel is part of a carefully thought out and implemented circuit that controls its specific component. For example, the engine coolant pump control switch supplies 12V power to a solid state relay that switches the 120V AC outlet the pump is plugged into. A cluster of solid state relays and control outlets within the test cell provide power to many components. The relevant wiring diagrams for the control of all test cell components can be found in Appendix B.

3.13 Data Acquisition System

The data acquisition (DAQ) system is comprised of extremely capable National Instruments (NI) measurement hardware controlled by Labview virtual instruments. Both the engine and cylinder head bench testing platforms utilize the NI hardware and have their own dedicated virtual instruments to visualize and capture testing data. The signal wires were routed to easily modifiable BNC panels, shown in figure 3-29. By connecting a short BNC cable from a measurement port on the NI BNC-2090 module to any of the incoming voltage signals, we can quickly choose what to measure and what to visualize on the computer.
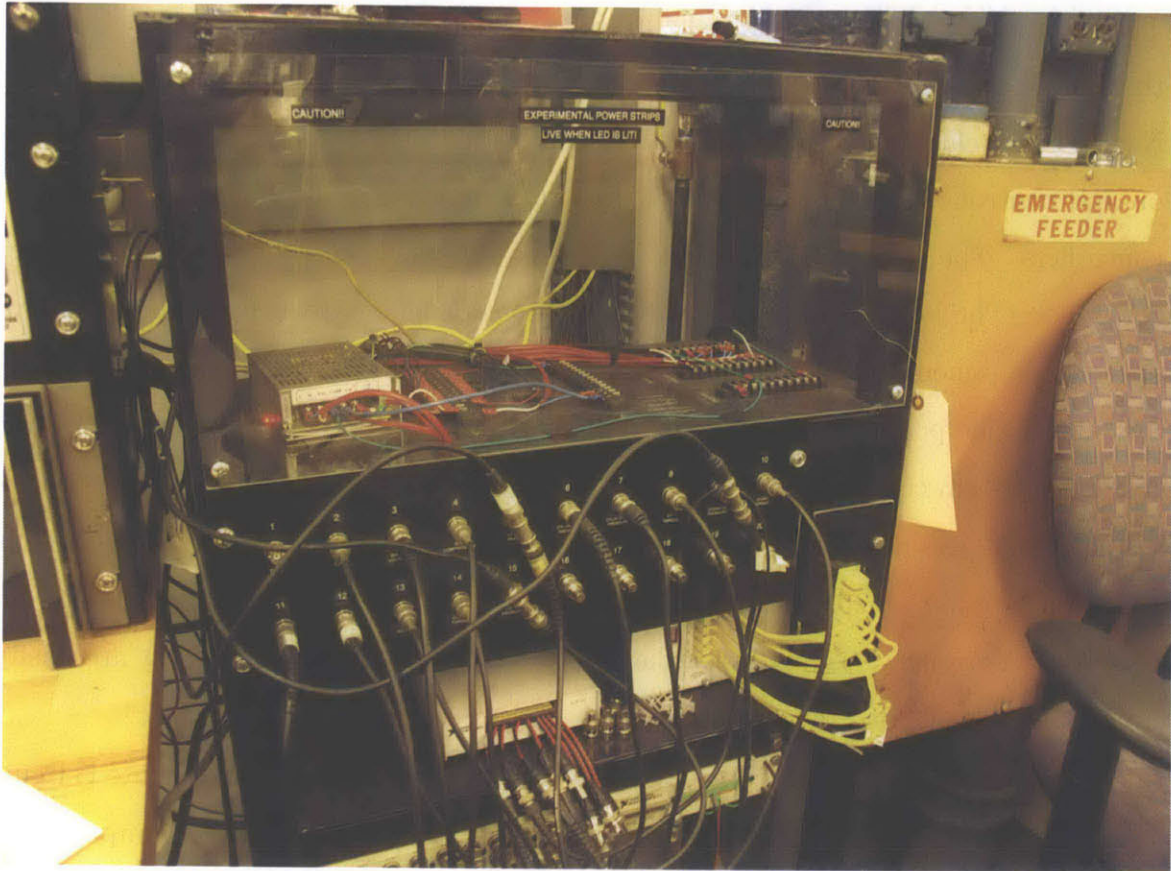
Figure 3-29: Sensor signal routing and data acquisition hardware.

3.13.1 National Instruments Hardware

Five data acquisition components were used for the high speed measurement of engine sensor data. Two analog-to-digital sampling cards, an NI PCI-6251 and an NI PCI-6259 were installed into our computer. Each is capable of sampling speeds of one million samples a second, enabling crank angle resolved data acquisition for up to 40 channels at 3600 RPM. The PCI cards must connect to receiver modules with either bnc ports or terminal blocks to plug in the relevant signals for the cards to measure. As such, three modules were used to interface with sensor signals. The BNC-2090 has eight BNC ports capable of making differential voltage measurements. As shown in figure 3-29, the BNC-2090 is sampling from various signals that connect to sensors within the test cell. Additionally, a SCB-68 provides a terminal block to accept eight more signals. Lastly, the SCXI-1100 signal conditioning module is used

for the sampling of thermocouple temperature measurements.

3.13.2 Labview Virtual Instrument

The coding of a Labview virtual instrument (VI) was done in collaboration with my project colleague, Michael Plumley. Michael oversaw a large majority of the architectural design and functional implementation of the virtual instrument's components. The virtual instrument is extremely capable, allowing the operator to visualize crankangle resolved and time varying data. The main pane, shown in figure 3-30, shows the pressure trace of both cylinders, the pressure-volume diagram of cylinder one, as well as torque, temperature and calculated mean effective pressure data, effectively characterizing the current operating state of the engine.

The virtual instrument configures the NI hardware to use the engine encoder's crank angle pulses to trigger sampling events, yielding crank angle resolved pressure and torque data needed for NIMEP, BMEP and FMEP calculations. The VI is also configured to record all sensor data as well as testing conditions for post-processing and analysis.
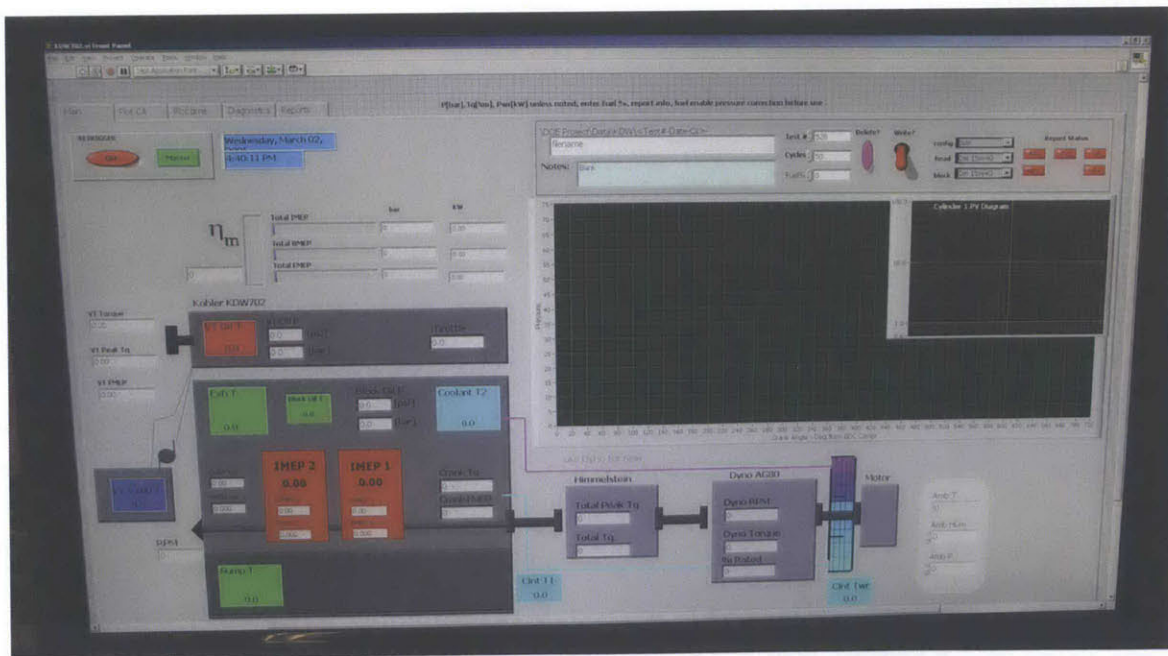
Figure 3-30: Engine test virtual instrument.

Chapter 4

Experimental Setup- Cylinder Head Bench

A second experimental rig was set up for dedicated valvetrain friction investigations. This cylinder head bench (CHB) testing platform serves multiple functions and has been instrumental in our characterization of valvetrain specific lubrication. The CHB test rig is primarily comprised of a cylinder head of the same model as the main engine - a Kohler KDW 702, driven by an electric motor through an in-line torquemeter. The testing platform is currently capable of performing comprehensive motored valvetrain tests at speeds up to 1800 RPM.

The challenge of modeling the average and maximum torque experienced by the Kohler engine camshaft pulley was presented to us when first contracting a company to build a custom camshaft pulley torquesensor. While there is significant literature detailing the friction and torque characteristics of the components actuating the intake and exhaust valves, such as the cam lobes, rocker arms, and valve springs, the modeling of the mechanical fuel injection system proved difficult. Considering the high cost and three month lead time of the custom pulley torquesensor, we decided to set up an independent motored cylinder head experiment to empirically determine the average and peak torque experienced by the camshaft pulley during operation. Not only would this testing platform ensure that the right sensor would be procured for the engine, but it would continue on to serve as a dedicated experimental test

setup capable of more involve valvetrain friction studies.
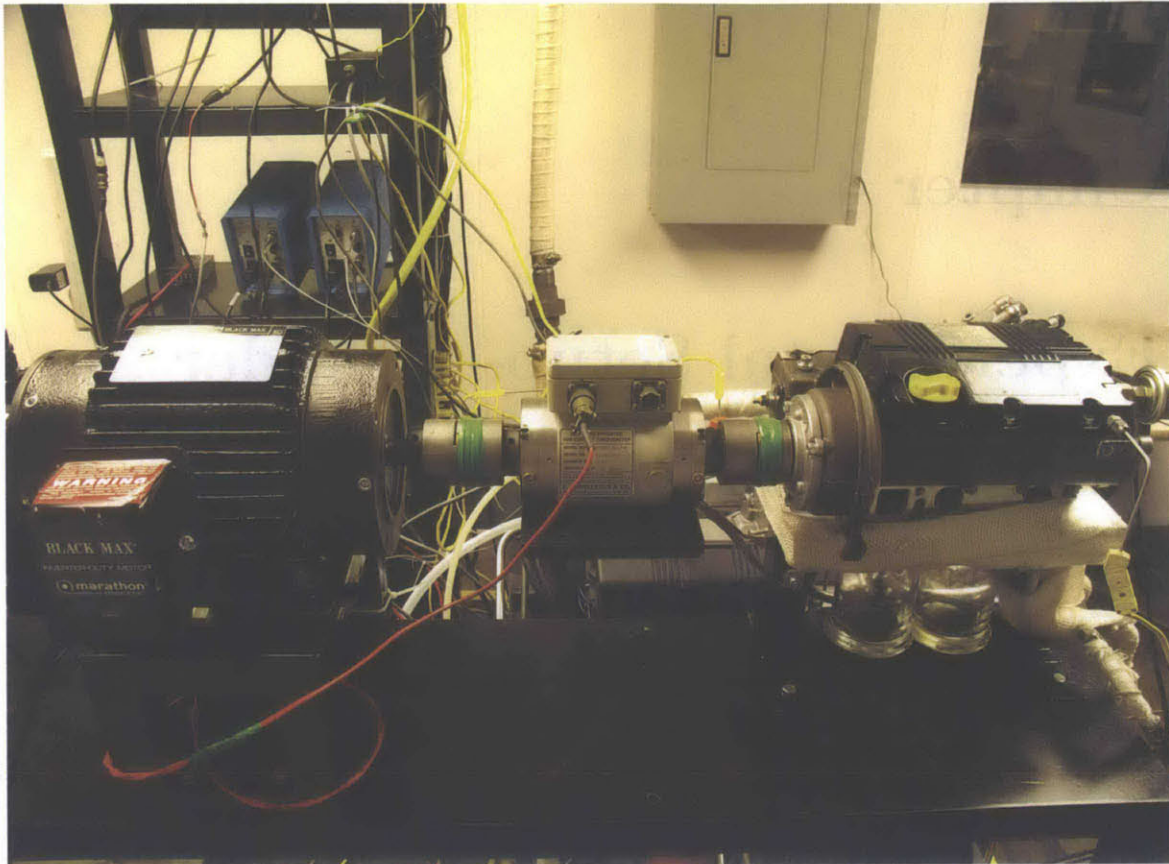
Figure 4-1: Completed cylinder head bench driveline.

4.1 Driveline Layout

The cylinder head bench was set up to fully operate a standalone Kohler engine cylinder head. The cylinder head was installed on a machine mounting plate, with appropriate supply and drain oil passages for proper lubrication. The camshaft pulley was replaced with a coupling connecting the camshaft through a torquemeter to a two horsepower, AC induction electric motor.

An aluminum plate was machined to mimic the top surface of the crankcase for cylinder head mounting. The plate was designed to have two large holes, in place of cylinders, that glass vials can be placed under and contain any fuel that is being sprayed from the injectors during motored operation. The plate was plumbed with

lubricant inlets and drains to supply the cylinder head with a constant source of lubrication as it is driven.

4.2 Electric Motor and Controller

A Marathon Black Max Y551-A772, two horsepower, AC induction motor was installed and controlled by a Durapulse GS3-22P0 drive inverter. The motor rotational speed is controlled by the "Motor Control" keypad on the "Cylinder Head" instrument panel. By changing the inverter drive frequency, the cylinder head camshaft rotational speed can be set up to 1800 RPM.

The "Motor enable" switch on the cylinder head bench instrument panel controls a set of contacters within the grey box below the inverter and above the panel. These contacters switch 208V, three phase AC power through a set of fuses and a line reactor (a component intended to dampen supply voltage transients) to the inverter itself.

Unlike the main engine motor, the cyinder head electric motor has an integrated optical encoder to track shaft position and rotational speed. The encoder also has two distinct pulse signals that are used to track absolute position. One signal is a pulse that rises only once per cycle, the other pulses every one thousandth of a cycle. Therefore, the data acquisition system uses the single pulse to begin its sampling, and the thousandth resolved pulses to trigger each sampling event.

4.3 Himmelstein In-line Torquemeter

An in-line rotating torquemeter was purchased and installed between the cylinder head and the electric motor to measure the mechanical work and power that is needed to drive the valvetrain system. The sensor is connected between the cylinder head camshaft pulley and the electric motor drive shaft by two spider-type jaw couplings.

The Himmelstein MCRT 49702V torquemeter was purchased and installed on the cylinder head bench to measure motored valvetrain friction. It has a range of 500 lbf-in and a 400% overload specification - that is, it can momentarily experience

torque spikes up to 2,000 lbf-in without permanent damage. It has a nonlinearity and hysteresis rating of 0.05% of the 500 lbf-in full scale range.

The Himmelstein torquemeter comes with a serial cable that can be used with a Window computer to interface with the sensors internal programming. Using the provided PDTM software, it is possible to zero and span the sensor programmatically. Figure 4-2 illustrates a single cycle's measurement of instantaneous motored valvetrain torque.
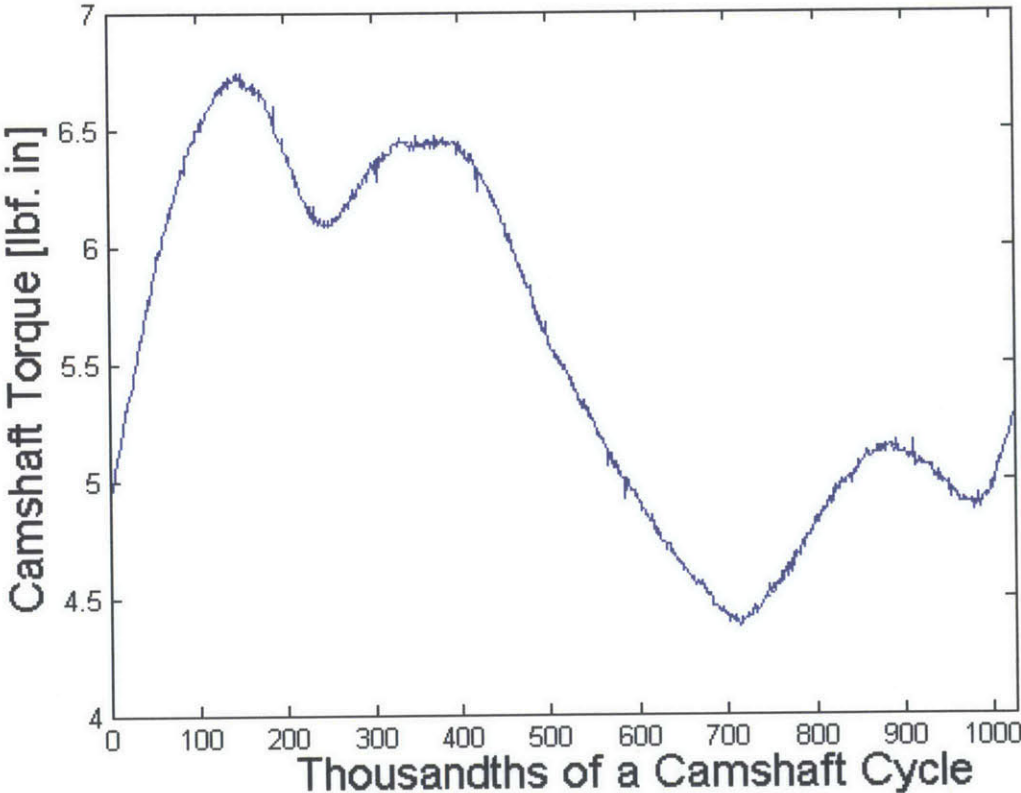
Figure 4-2: Cyinder head bench instantaneous camshaft torque.

4.4 External Oil Sump, Filter, and Pump

The same external lubrication lines used to supply the main engine's valvetrain system was configured to also supply the cylinder head bench with oil during operation. By turning a ball valve, the operator can either supply lubricant from the external sump

to the engine cylinder head or the standalone cylinder head.

The cylinder head bench was plumbed to supply the valvetrain with lubricant for motored tests. The sump, fitted with an electric oil heater, allows for the active control of inlet valvetrain oil temperature while the oil pump pressurizes the lubricant and supplies it to the cylinder head valvetrain through the oil filter. All oil lines were plumbed using stainless steel tubing and swagelok compression fittings.

4.5 Instrument Control Panel

A dedicated instrument control panel was designed and wired to allow the operator to control the cylinder head bench test rig from the safety of outside the engine test cell. Relevant wiring diagrams can be found in appendix A.

The toggle switches on the panel give the operator the ability to toggle power to the oil temperature controller, the external oil supply pump, the CHB torquemeter, the CHB fuel cutoff solenoid, and the CHB electic motor drive. Above the switches, a tachometer uses the electric motor's integrated encoder pulses to display rotational speed. On the right are the electric motor controller keypad and the temperature controller where the camshaft speed and oil temperature can be commanded, respectively.

4.6 Labview Virtual Instrument

The central data acquisition system discussed in section 3.13 is also used for the cylinder head bench tests. A Labview virtual instrument, shown in figure 4-3, was designed to display and record important valvetrain test data, such as instantaneous and average valvetrain torque, oil temperature, oil pressure, and camshaft speed. The virtual instrument was also programmed to calculate the average and peak camshaft torque during operation.

The virtual instrument also enables the user to write the valvetrain test data for later processing and analysis. The data files include instantaneous sensor readings

sampled at every thousandth of a camshaft cycle, cycle averages, and other important

meta data such as sensor calibration constants.
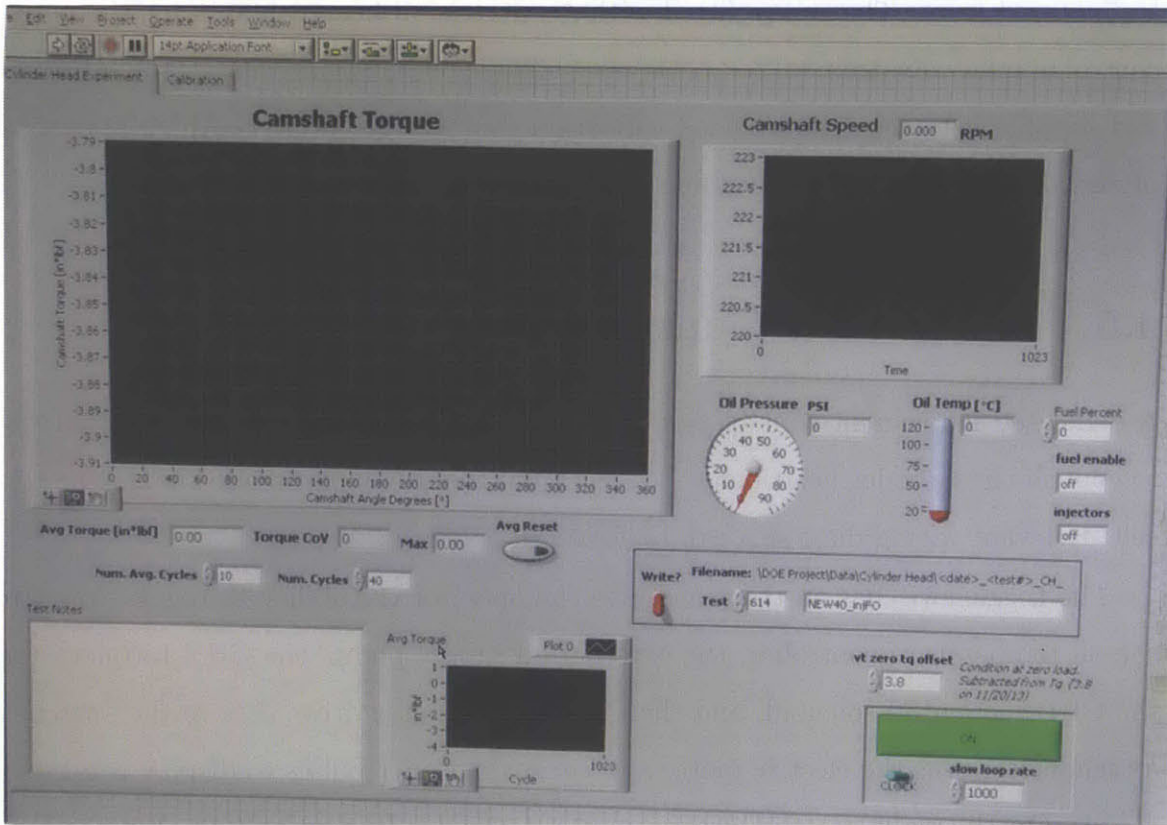
Figure 4-3: The cylinder head bench testing virtual instrument.

Chapter 5

Experimental Plan

This study seeks to experimentally initiate our group's investigation of lubricant formulations on engine friction by looking exclusively at base oil viscosity as a compelling optimization parameter. To this end, we were provided with a set of four candidate lubricants from our industry collaborator, Infineum, USA. The four oils were formulated with the same additive package and only differed by viscosity classification. The lubricants were then subjected to comprehensive experimental tests using the two testing platforms discussed in chapters 4 and 5.

The experimental test matrix and tests seek to isolate changes in engine friction from lubricant viscosity alone. Therefore, careful consideration for engine speed, temperature, load and other testing variables was taken to ensure accuracy and repeatability. The majority of the engine friction tests were performed at a constant speed with varying engine load, while the cylinder head bench tested the lubricants at both varying speeds and oil temperatures.

5.1   Experimental Lubricants

Four candidate lubricants were provided by Infineum, USA. Mixed with the same additive package, the lubricants only differed by viscosity classification. As engine oil heats up, its viscosity will decrease and change the lubrication behavior around the engine. Table 5.1 below presents the five lubricants tested within this phase of the

project - four experiment Infineum oils and one commercially available oil.

Table 5.1: Experimental Lubricants

Lubricant	Viscosity Classification	Kinematic Viscosity @ 40°C [cSt]	Kinematic Viscosity KV @ 100°C [cSt]	High Temp-High Shear [cP]
Infineum IM1300207	sub 0W-20	31.2	6.18	2.14
Infineum IM1300208	5W-20	45.3	8.24	2.67
Infineum IM1300209	10W-30	71.6	10.72	3.23
Infineum IM1300210	15W-40	115.1	15.07	4.07
Chevron Delo-400	15W-40	125	15.7	4.3

The high temperature high shear value represents the dynamic viscosity measurement of the lubricant at 150°C and a shear rate of 10^{-6} second^{-1}. Figure 5-1 illustrates the temperature dependent viscosity behavior that all five lubricants experience. The dark line represents the Chevron lubricant, while the light lines represent the four Infineum supplied oils.

Using the high and low values for the lubricant kinematic viscosity, we can apply fit the Vogel equation to obtain individual temperature versus viscosity curves for all five experimental lubricants. The Vogel equation states that an oil kinematic viscosity will vary exponentially with the lubricant temperature, such that:

$$\nu = ke^{\left(\frac{\theta_1}{\theta_2 + T}\right)}$$

Figure 5-1 illustrates the lubricant viscosity response to temperature. It is important to note that we experience an entire order of magnitude decrease in kinematic viscosity heating an oil to operating engine temperatures from ambient conditions.
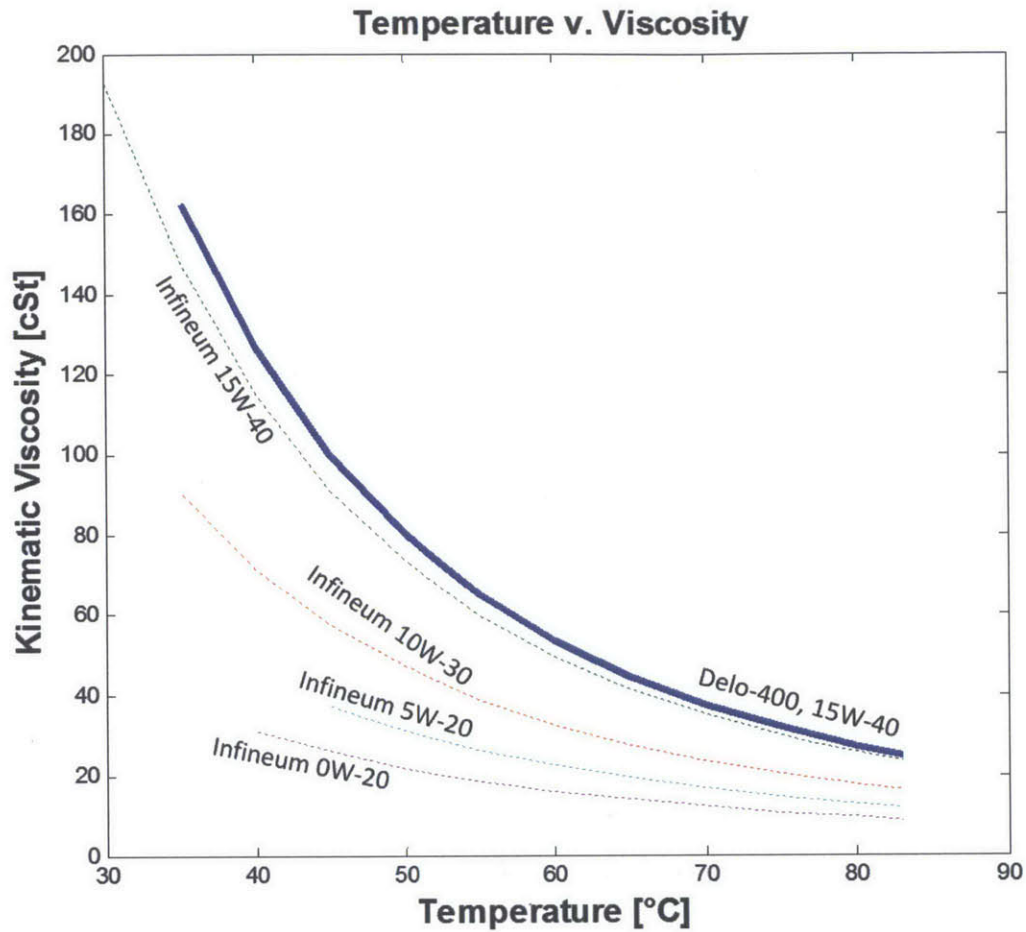
Figure 5-1: Experimental lubricant viscosity versus temperature curves.

5.2 Experimental Test Matrix

An individual test matrix was created for both the main engine as well as the cylinder head bench testing platforms. The objective for tests conducted on the CHB is to identify the dominant lubricant regime that governs valvetrain friction and propose an optimal viscosity classification for a valvetrain system specific lubricant. Likewise, the engine testing aims to characterize the effective lubrication regime dominant in the power cylinder and subsequently identify the optimal viscosity classification for the crankcase.

5.2.1 Cylinder Head Bench Testing Conditions

The cylinder head bench rig underwent tests under a variety of oil pressures, oil temperatures, and rotational speeds. For repeatable friction testing, the oil temperature was controlled to 100°C and the oil pressure to 45 psi. Data was taken at speeds that range from 450 RPM to 1800 RPM. Since the camshaft is timed to a full engine cycle, the rotational speed of the camshaft is half that of the crankshaft and these speeds correspond to engine speeds of 900 RPM to 3600 RPM.

Table 5.2: Cylinder Head Bench Test Matrix

Test Number	Test Conditions	Test Type	Lubricant
1	Constant Speed @1200 RPM	Temperature Sweep	Chevron 15W-40
2	Constant Temperature @80°C	Speed Sweep	Chevron 15W-40
3	Constant Speed @1200 RPM	Temperature Sweep	Infineum 15W-40
4	Constant Temperature @80°C	Speed Sweep	Infineum 15W-40
5	Constant Speed @1200 RPM	Temperature Sweep	Infineum 10W-30
6	Constant Temperature @80°C	Speed Sweep	Infineum 10W-30
7	Constant Speed @1200 RPM	Temperature Sweep	Infineum 5W-20
8	Constant Temperature @80°C	Speed Sweep	Infineum 5W-20
9	Constant Speed @1200 RPM	Temperature Sweep	Infineum sub 0W-20
10	Constant Temperature @80°C	Speed Sweep	Infineum sub 0W-20

5.2.2 Engine Testing Conditions

The necessary engine operating conditions should be dialed in and a warm up transient period must pass for all systems to stabilize. The engine is said to be in steady state operation when thermal transients have ended and measured temperatures do not vary more than a degree Celcius. Warm up can be accomplished running at about 25% full load for 30 minutes. The candidate lubricant friction testing was performed under the following operating engine conditions.

The 2400 RPM operating speed was chosen in light of the engine's relative vibrational stability. At speeds below 2000 RPM, large torque spikes up to 500 Nm would be experienced at the in-line torquemeter. Above 3000 RPM, the engine inherently also has higher noise and vibration. Furthermore, 2400 RPM is near the maximum torque specified speed of 2200 RPM, giving us a full range of engine load to study without the excessive pumping losses seen at high speeds.

- Rotational speed of 2400 RPM.

- Valvetrain oil pressure of 45 psi.

- Crankcase oil pressure of 70 psi.

- Valvetrain oil temperature of 100°C.

- Crankcase oil temperature of 110°C.

- Engine coolant inlet temperature of 80°C.

The test matrix for this platform is comprised of running the Infineum 15W-40 and the Infineum 10W-30 lubricants within both the valvetrain system and the crankcase. Engine friction was characterized using the following split lubrication configurations. Since diesel engines do not normally run lower than 10W-30 weight lubricant, only the 15W-40 and 10W-30 lubricants were tested on the engine so as to prevent any permanent damage from wear. Furthermore, all lubricants were fully tested on the cylinder head bench, which allows for fast replacement of the test cylinder head should

any damage occur. Table 5.3 lists the primary engine tests conducted on the engine testing platform for this study.

Table 5.3: Engine Test Matrix

Test Number	Test Condition	Valvetrain Oil	Crankcase Oil
1	Constant Speed @ 2400 RPM	Infineum 10W-30	Infineum 10W-30
2	Constant Speed @ 2400 RPM	Infineum 10W-30	Infineum 15W-40
3	Constant Speed @ 2400 RPM	Infineum 15W-40	Infineum 15W-40
4	Constant Speed @ 2400 RPM	Infineum 15W-40	Infineum 10W-30
5	Constant Speed @ 2400 RPM	Infineum 10W-30	Infineum 10W-30

Chapter 6

Experimental Results

Over fourteen sets of tests were conducted on two separate experimental testing platforms to investigate the effect lubricant viscosity has on subsystem friction. The dedicated cylinder head bench was used to comprehensively characterize valvetrain lubrication regimes. The main engine testing platform was used to test split lubrication configurations and demonstrate friction benefits of subsystem lubricant optimization.

Chapter 2 discusses the different lubrication regimes present in the engine, referring to the literature to assert that most engine valvetrain systems are dominated by mixed and boundary lubrication, while most engine power cylinder systems are dominated by hydrodynamic lubrication. Recognizing that higher viscosity oils reduce friction on boundary lubricated surfaces by increasing the oil film thickness, while lower viscosity oils reduce friction on hydrodynamically lubricated surfaces by decreasing viscous shear, we hypothesized that the optimal split lubricant configuration would use a more viscous oil in the valvetrain system, and a less viscous oil in the power cylinder system. The following sections present empirical evidence to demonstrate and support this claim. The presented results correspond to cylinder head bench operation with a disabled fuel system, and all friction contributions come from the camshaft journal bearings, the lobe and follower interfaces, the rocker arms, and the camshaft main seal.

6.1 Valvetrain Investigations

Although the literature reports that the valvetrain system is dominated by mixed lubrication, discussion with industry sponsors do not corroborate this claim. They indicate that valvetrain systems are becoming more efficient and operating in the hydrodynamic lubrication regime. Valvetrain friction tests were performed on the cylinder head bench to empirically determine with regime is dominant in our Kohler KDW-702 engine's cylinder head, so that we may recommend the optimal lubricant for friction minimization. All five candidate lubricants were run on the cylinder head bench, performing temperature sweeps and speed sweeps. The lubricants themselves, and the testing operating conditions are discussed in chapter 5.
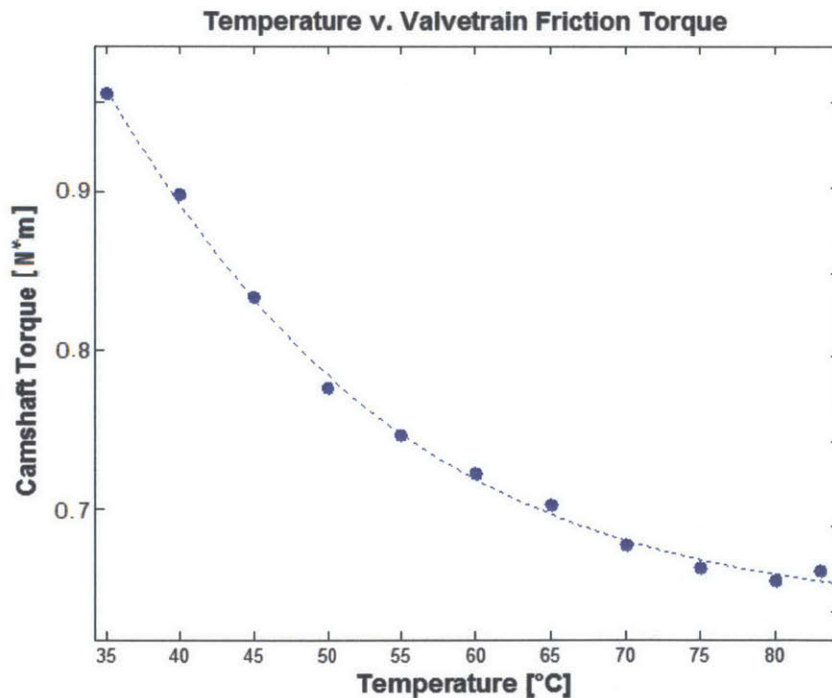
Figure 6-1: Valvetrain friction response to changing inlet oil temperature. Camshaft speed is held constant at 1200 RPM, and the lubricant used is the Delo-400 15W-40.

6.1.1 Cylinder Head Bench Friction - Temperature Dependence

The cylinder head bench camshaft was motored at 1200RPM continuously while the lubricant and cylinder head was heated to approximately 80°C. Figure 6-1 below shows the valvetrain frictional losses using the Delo-400 15W-40 weight viscosity classification at different oil temperatures. We see roughly a 33% decrease in friction when the oil temperature increases from 35°C to 80°C. Engine oil viscosity is highly sensitive to changes in temperature, and this decrease in friction can be explained by the decrease in lubricant viscosity from about 170 centistokes to 25 centistokes. This behavior is characteristic of hydrodynamic lubrication, where frictional losses come from viscous shear.

Acknowledging that each data point represents a different lubricant viscosity at that temperature, we can plot the same data against the Delo-400 kinematic viscosity, using the viscosity versus temperature curves presented in section 5.1. Figure 6-2 shows this same data, illustrating the strong relationship between viscosity and friction within the hydrodynamic regime.

The temperature response of valvetrain was similarly tested with the Infinuem 10W-30 lubricant, and the same behavior was observed. Like the Delo-400 lubricant, the Infincum 10W-30 oil caused the valvetrain friction to decrease with temperature, as lubricant viscosity decreased as well. However, at 65°C the friction stopped decreasing and began rising with temperature. Figure 6-3 plots the friction data against the lubricant viscosity. Like the friction response with the Delo-400, valvetrain friction is here seen decreasing until a lubricant kinematic viscosity of 25 centistokes, characteristic of hydrodynamic lubrication behavior. Below 25 centistoke lubricant viscosity, we begin to observe mixed lubrication behavior with friction increasing with decreasing viscosity. This minimum represents the minimum seen in the Stribeck curve at the transition between the mixed lubrication regime and the hydrodynamic regime.
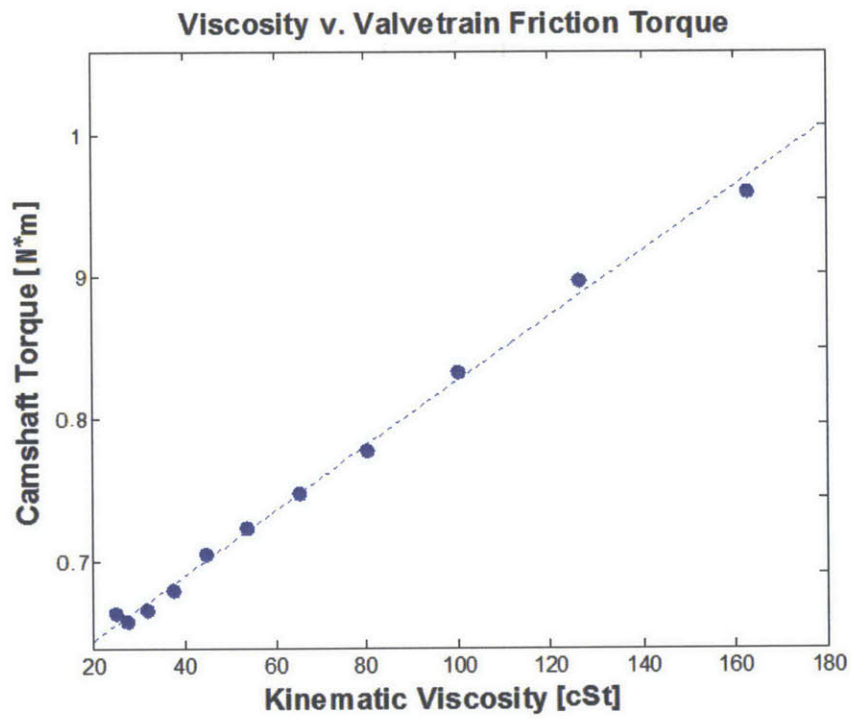
Figure 6-2: Valvetrain friction response to viscosity change from increasing inlet oil temperature. Camshaft speed is held constant at 1200 RPM, and the lubricant used is the Delo-400 15W-40 oil.
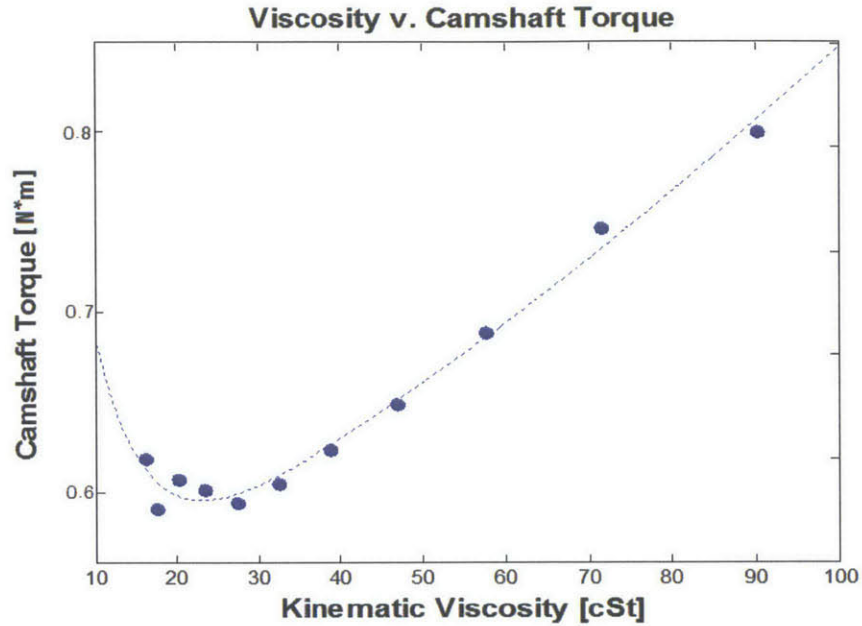
Figure 6-3: Valvetrain friction response to viscosity change from increasing inlet oil temperature. Camshaft speed is held constant at 1200 RPM, and the lubricant used is the Infineum 10W-30 oil.

Temperature sweeps were performed used all five candidate lubricants - the results shown in figure 6-4. The five curves roughly reproduce the Stribeck curve, with a minimum experienced for lubricant viscosities between 20 and 25 centistokes. At a constant speed of 1200 RPM, we also expect the camshaft load to be constant, however as the cylinder head heats up, its thermal expansion slightly increases contact pressure the sliding components are putting on one another. Therefore, we see different magnitudes of minimum friction for the five lubricants because they exhibit the 20-25 centistoke viscosity at different temperatures, and consequently different degrees of cylinder head thermal expansion.

At the minimum shown around 20 centistokes, where hydrodynamic lubrication becomes dominant, we can observe valvetrain friction increasing with lubricant viscosity. The lower viscosity oils, like the Infineum sub 0W-20 and the 5W-20 experience about 10% less friction than the thicker 15W-40 weight oils.

Viscosity v. Camshaft Torque
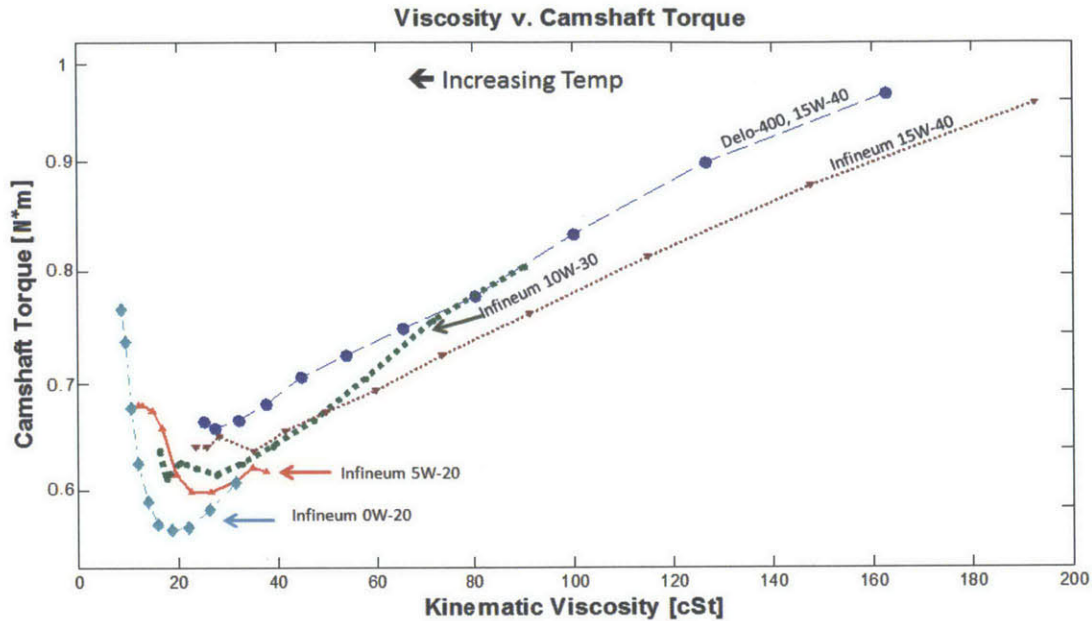
Figure 6-4: Valvetrain friction response to viscosity change from increasing inlet oil temperature. Camshaft speed is held constant at 1200 RPM, and all candidate lubricants are shown.

6.1.2 Cylinder Head Bench Friction - Speed Dependence

While at an operating temperature of 80°C, all five test oils were tested at various speeds to investigate how friction is affected by camshaft rotational speed. As discussed in section 2.1, sliding speed is important in determining the lubrication Stribeck number and characteristic oil film thickness. The following results provide more insight to the frictional behavior of the valvetrain, illustrating that at camshaft speeds lower than 1200 RPM, the valvetrain operates in mixed lubrication.

Figure 6-5 shows the valvetrain friction response to changing camshaft speed using the Delo-400 lubricant at 80°C. As the camshaft speed increases, we first experience a decrease in friction, indicating dominance of valvetrain mixed lubrication. Increases in the camshaft rotational speed increase viscous velocity gradients and viscous pressure, effectively pushing surfaces apart and increasing oil film thicknesses. After 1200 RPM, we observe friction increasing again as hydrodynamic viscous shear becomes dominant. We can clearly assert that this speed sweep transitions the effective val-

vetrain Stribeck number from the mixed lubrication regime to the hydrodynamic regime.
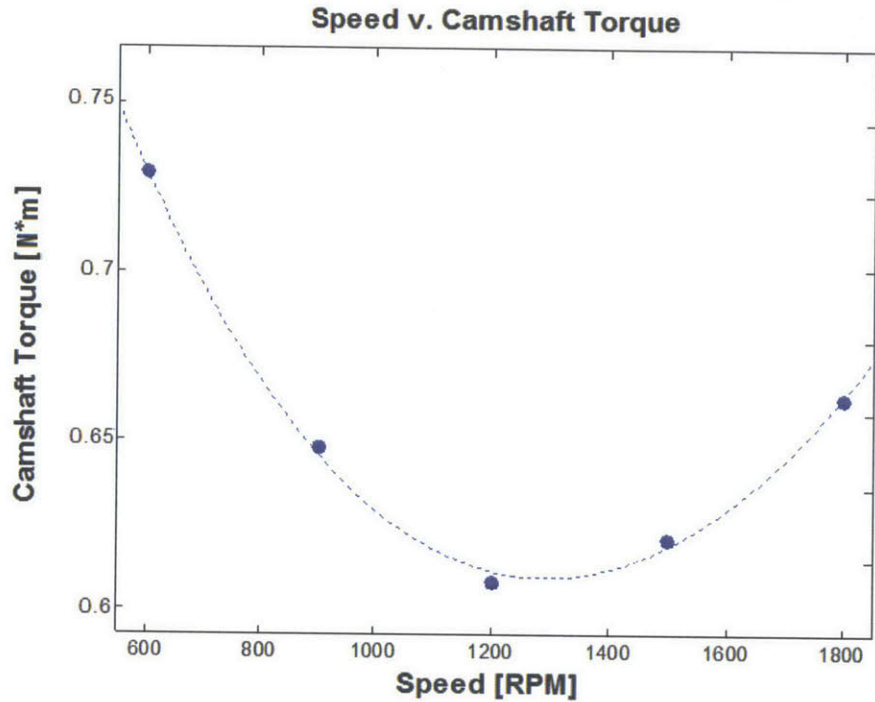
Figure 6-5: Valvetrain friction response to camshaft speed. Oil inlet temperature is held at 80°C, and the lubricant used is the Delo-400 15W-40.

A lower viscosity lubricant will decrease the effective Stribeck number, and therefore we expect the transition to overall hydrodynamic dominance to happen at higher speeds with a lighter oil. Figure 6-6 validates this claim, showing the frictional valvetrain response using a lighter 5W-20 oil. We observe the friction torque minimum occuring at about 1500 RPM versus 1200 RPM, indicating that higher speeds are necessary to induce the same oil film thicknesses that the Delo-400 lubricant test would experience at 1200 RPM.

Speed v. Camshaft Torque
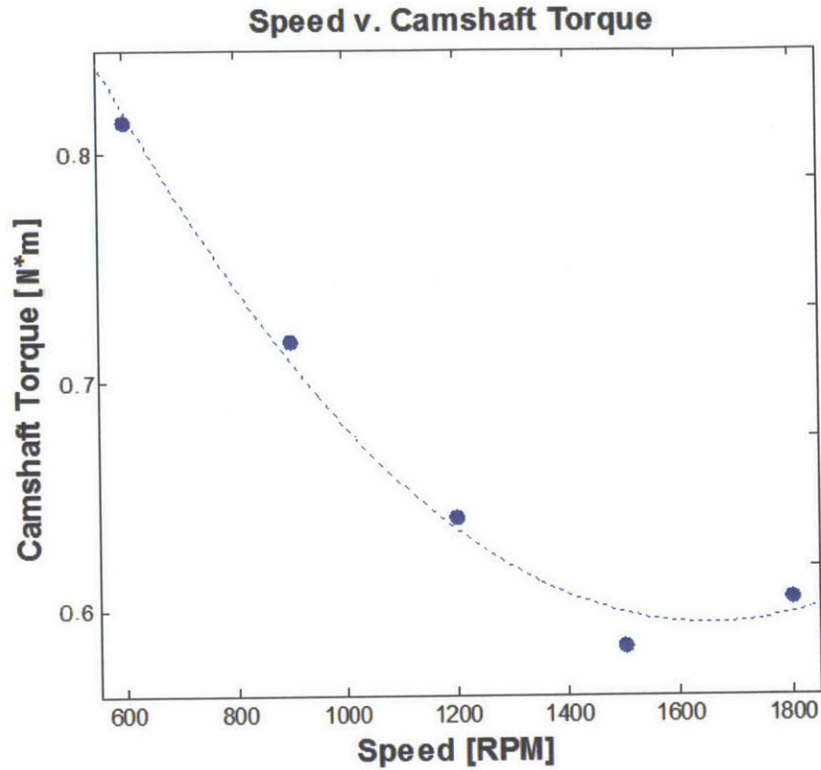
Figure 6-6: Valvetrain friction response to camshaft speed. Oil inlet temperature is held at 80°C, and the lubricant used is the Infineum 5W-20.

Speed sweeps were repeated at the same conditions for all five candidate lubricants. Figure 6-7 shows the predominantly downward friction response the valvetrain exhibits with increasing camshaft speed. In between 1200 and 1500 RPM, we observe a friction minimum present for all candidate lubricants. Below these speeds, lubricants of higher viscosity yield lower frictional losses, and above these speeds, lubricants of lower viscosity yield lower frictional losses. This is explained by the overall mixed lubrication behavior the valvetrain exhibits at low speeds. By utilizing a high viscosity oil, lubricated components will experience thicker oil films and the local Stribeck number will move closer to the minimum experienced at the transition between mixed and hydrodynamic lubrication.
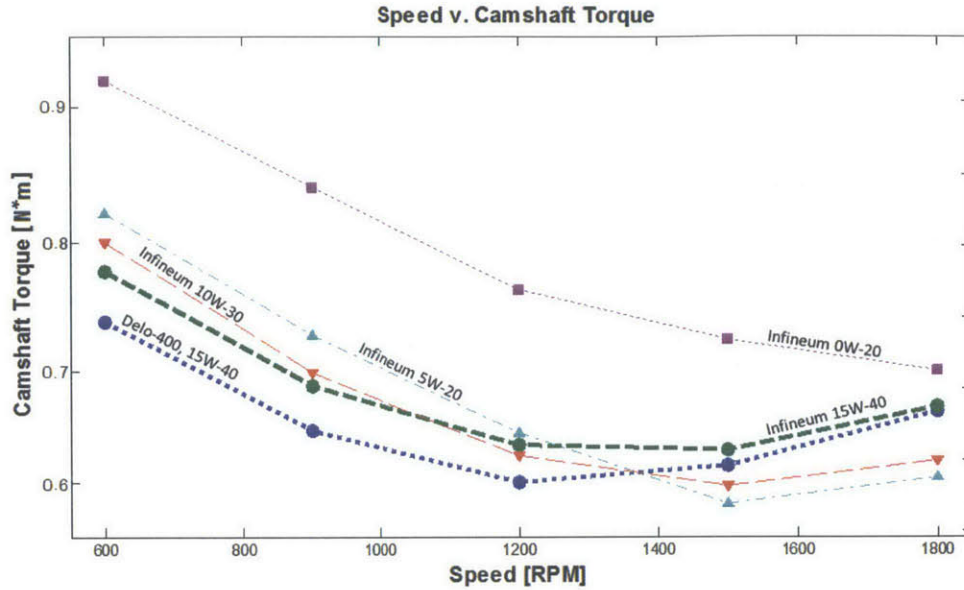
Figure 6-7: Valvetrain frictional response to camshaft speed for all experimental lubricants. Tests were run at a constant 80°C.

Based on the temperature and speed variant valvetrain data, we can characterize the valvetrain system as being dominated by predominantly mixed lubrication. Although the main engine tests and the literature place normal valvetrain oil operating temperatures higher at around 100°C, the cylinder head bench results show any increase in lubricant temperature would only decrease the lubricant viscosity further and push the effective valvetrain Stribeck number further into the mixed lubrication regime. Furthermore, since the camshaft spins once per two revolutions of the crankshaft, the camshaft transition speed of 1200 RPM corresponds to a engine crankshaft speed of 2400 RPM, indicating that for the majority of the engine's speed range, including the speed where it produces maximum torque, the valvetrain system is dominated by mixed lubrication. Consequently, the use of a thicker, higher viscosity lubricant is recommended within the valvetrain to both decrease valvetrain frictional losses and reduce component wear by increasing oil film thicknesses.

95

6.2 Overall Engine Friction

As discussed in chapter 2, the literature claims that the valvetrain system components predominantly operate within the mixed lubrication regime and the power cylinder components predominantly operate within the hydrodynamic lubrication regime. The valvetrain studies presented in the previous section validate that claim for our experimental engine. The engine studies discussed here will both confirm the hydrodynamic behavior of the power cylinder components as well as demonstrate the friction benefits achieved with the use of two separate lubricants of different viscosity classifications.
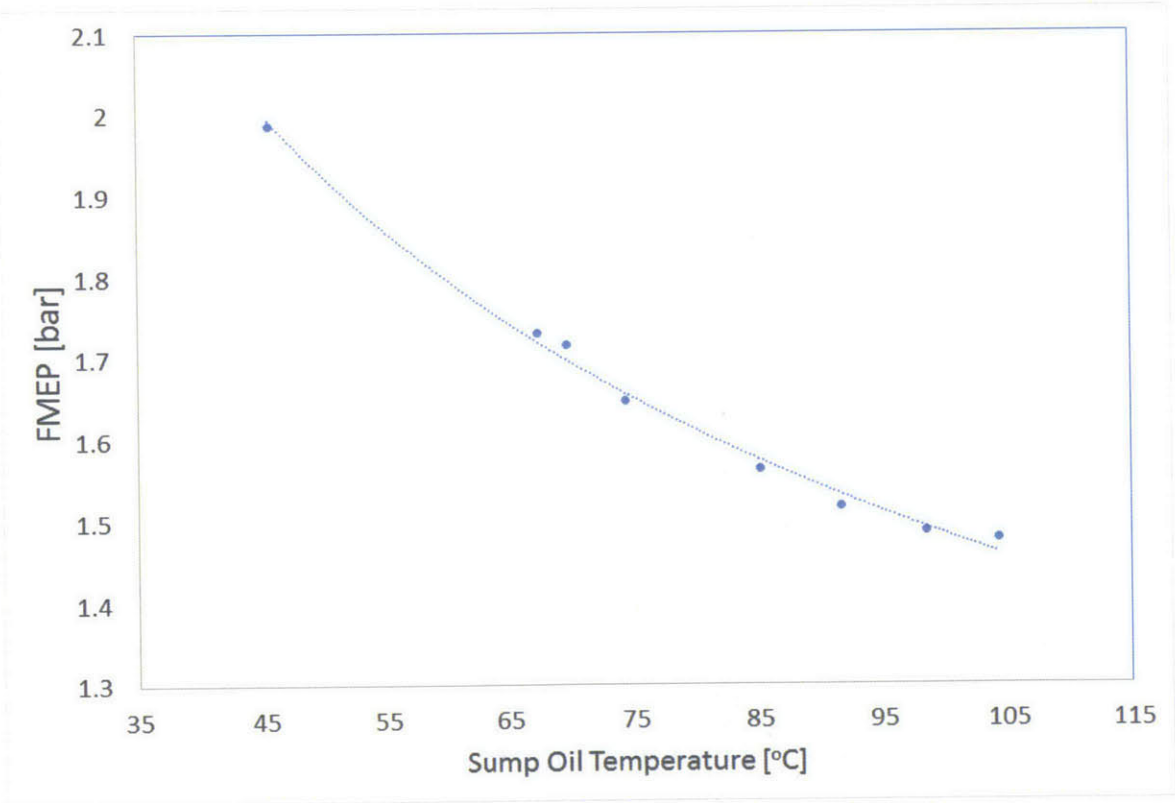
Figure 6-8: Engine friction response during warm-up. The engine is held at 2400 RPM, using the Infineum 10W-30 oil in the valvetrain system, and the Infineum 15W-40 in the crankcase.

6.2.1 Temperature Dependence

While temperature response characterization is important, it is difficult to achieve on the primary engine setup due to large temperature gradients around the engine. The engine coolant, the valvetrain oil, and the crankcase oil can all experience different thermal transients during warm-up. Consequently, warm-up temperature sweeps do not as much reliability and repeatability in data measurements as with the cylinder head bench testing. Figure 6-8 shows the typical temperature response of the engine friction work during warm-up. Much like the cylinder head test results, we see an overall friction benefit of 25% from increasing engine temperatures. When the engine is cold, the lubricant viscosity in each system is an order of magnitude higher than when the engine is at normal operating temperature, resulting in hydrodynamic lubrication almost everywhere in the engine. As the engine heats up and the lubricant viscosity decreases, we experience lower local viscous shear losses as represented by the reduction of friction in figure 6-8.

6.2.2 Load and Viscosity Dependence

Four main tests were conducted to test the engine's friction response to changes in engine load and lubricant viscosity. In order to prevent excessive component wear and damage, the sub 0W-20 and 5W-20 were not run in the main engine. Therefore, split configurations using the Infineum 15W-40 and the Infineum 10W-30 lubricants were tested. All tests were performed at 2400 RPM after thermal transients have stabilized to ensure data goodness and repeatability.

Table 5.3 presents the four split configurations tested with the two Infineum oils-two tests used the same lubricant throughout the engine, one test placed the 15W-40 in the crankcase with the 10W-30 in the cylinder head, and one test used the 15W-40 in the cylinder head with the 10W-40 in the crankcase. Considering the discussed lubrication regimes in the valvetrain and the crankcase, we hypothesized that the most efficient combination uses the thicker 15W-40 lubricant in the head and the thinner 10W-30 lubricant in the crankcase. This decreases valvetrain friction

by reducing asperity contact and wear, and decreases crankcase friction by reducing viscous shear in the hydrodynamic regime.

Figure 6-9 shows the friction losses for the power cylinder components under different engine loads. It is clear to see two main groups have separated and clustered. The two curves toward the top of the graph represent tests that used the thicker 15W-40 lubricant in the crankcase. The three curves below correspond to tests that used the thinner 10W-30 lubricant in the crankcase.
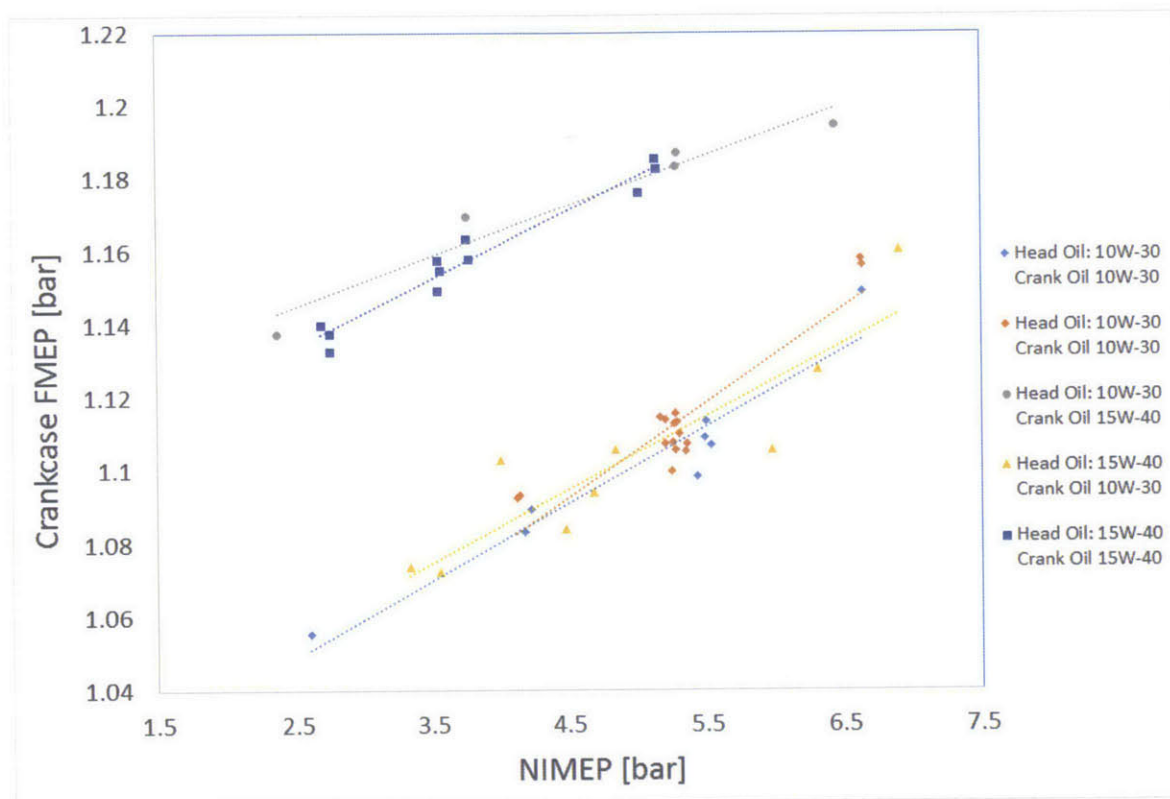
Figure 6-9: Power cylinder system friction response to engine load. The engine is running at thermal steady state and kept at 2400 RPM.

We can clearly observe a constant 0.08 bar friction improvement within the crankcase from using the lighter 10W-30 lubricant versus the heavier 15W-40. This translates to a 6.5-7.5% improvement in crankcase frictional losses. The lower viscosity lubricant decreases the viscous shear experienced by the crankcase sliding components.

The friction losses for the valvetrain system are shown in figure 6-10. For this graph, two less distinct groups form to illustrate the frictional response to lubricant

viscosity. The top three lines and sets of data represent tests that used the lighter 10W-30 lubricant within the valvetrain system. The bottom two lines represent tests that used the heavier 15W-40 lubricant within the valvetrain system.
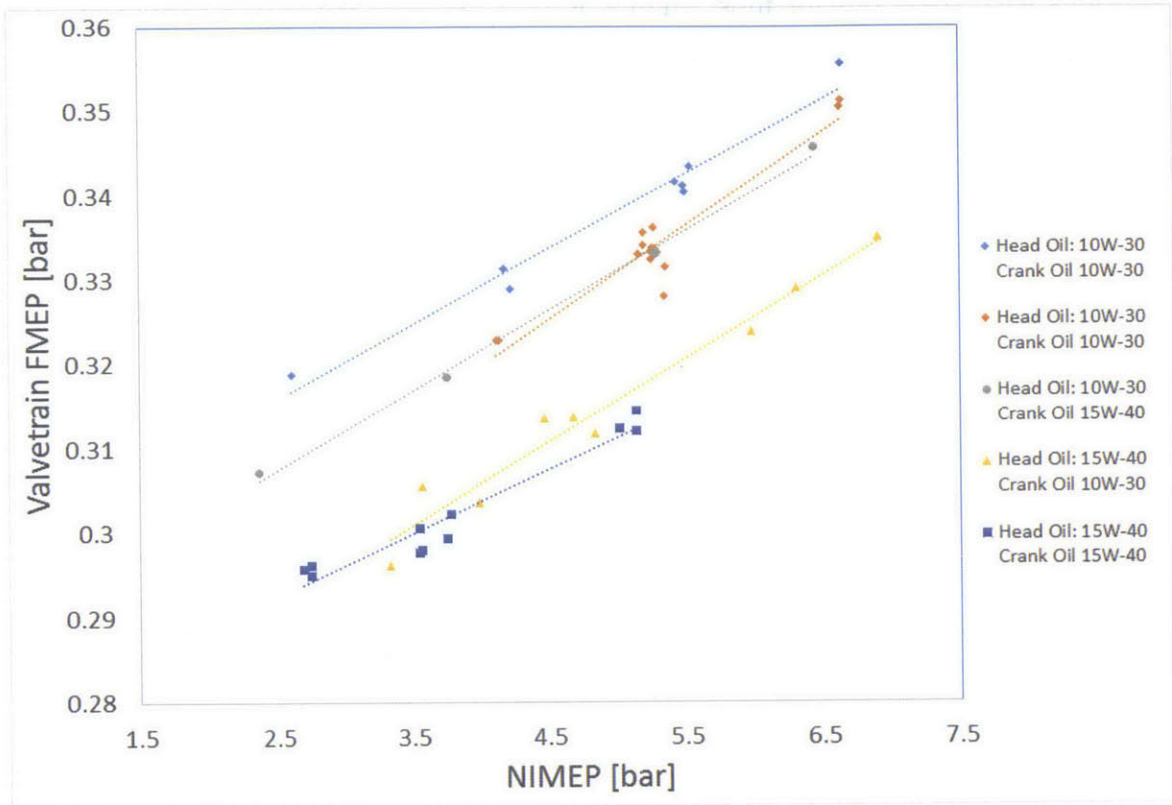
Figure 6-10: Valvetrain system friction response to engine load. The engine is running at thermal steady state and kept at 2400 RPM.

A valvetrain friction benefit of 0.025 bar can be observed by using the more viscous 15W-40 lubricant over the less viscous 10W-30. Not only does this yield a 7-8.5% improvement in valvetrain losses, but the more viscous 15W-40 also reduces wear by increasing oil film thicknesses in the valvetrain system.

The crankcase and valvetrain behavior can be looked at together as overall engine friction. Figure 6-11 shows how total engine friction changes with engine load and lubricant configuration. Again, like in the figure 6-9, two main groups appear at the top and bottom according to the type of lubricant used in the crankcase. Within each of these groups, however, are two sub-groups that depend on the type of lubricant

used in the valvetrain system.

The two middle curves represent common lubricant systems, where the same oil is used in both the valvetrain and crankcase. These are the only two possible configurations with these oils for most engine designs. We can see here a benefit of 0.055 bar, yielding a 4% improvement in overall friction.
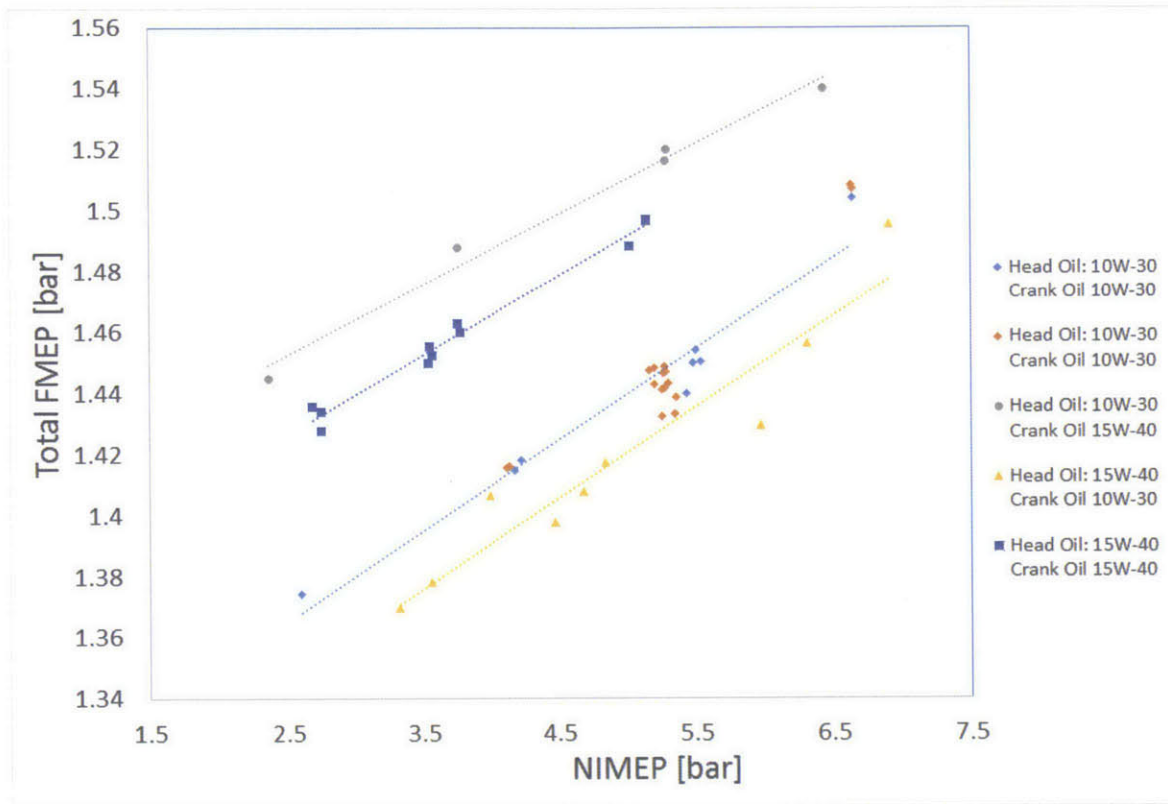
Figure 6-11: Total engine friction response to load. The engine is running at thermal steady state and kept at 2400 RPM.

By separating the lubrication circuit, and segregating the valvetrain lubricant from the crankcase lubricant, we can mix the lubricants used. The topmost and bottom most data sets correspond to mixed lubrication configurations. The top curve corresponds to using the lighter 10W-30 oil in the valvetrain and the heavier 15W-40 oil in the crankcase. This is the worst lubrication configuration for the engine, yielding the greatest amount of friction.

The bottom curve represents the optimal lubricant configuration, with the more

viscous 15W-40 oil lubricating the valvetrain and the less viscous 10W-30 oil lubricating the crankcase. This configuration yields a frictional benefit of 0.08 bar and translates to 5.5-6% lower friction than the full 15W-40 configuration. In other words, we have achieved almost 2% lower overall engine friction than fully switching to a 10W-30 oil in the engine, while still maintaining the wear protection of a 15W-40 in the valvetrain system. This improvement translates to a 3-3.5% overall mechanical efficiency benefit, as shown in 6-12.
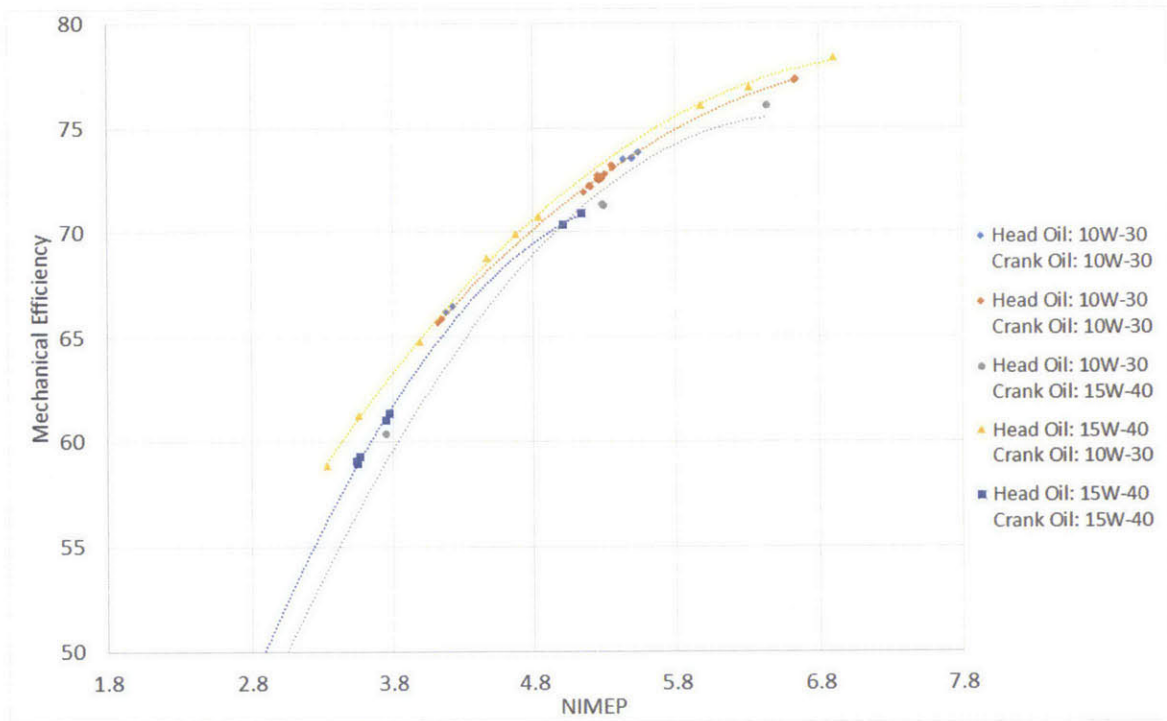
Figure 6-12: Total engine mechanical efficiency response to load. The engine is running at thermal steady state and kept at 2400 RPM.

Chapter 7

Discussion and Conclusions

The optimization of subsystem lubricant formulations can have profound benefits on engine friction, emissions, and durability. By eliminating common trade-offs that lubricant formulators and engine manufacturers frequently consider, more advanced engines can be produced and run, potentially yielding lower emissions, higher fuel economy, and longer lifespans. This study identifies the first steps toward this goal - the set up of a split lubrication system, the identification of two ideal viscosity classifications in our engine's split configuration, and the demonstration of its potential benefits in friction reduction. We successfully showed that 6% friction reduction is possible by simply using a lower viscosity lubricant in an engine crankcase, and keeping a higher viscosity lubricant in its cylinder head. Furthermore, we expect this configuration to exhibit better efficiency gains over switching fully over to a lighter lubricant, while still maintaining the valvetrain wear protection of the thicker lubricant. There are still many steps this project can take toward achieving advanced lubricant formulations and I am optimistic that significant gains in efficiency, emissions, and durability are yet to be seen.

7.1   Temperature Effect on Viscosity

Acknowledging the effect temperature has on a lubricant base stock viscosity is paramount when formulating an optimized lubricant for subsystem friction reduc-

tion. From room temperature to normal operating engine temperatures, a lubricant's viscosity can decrease over two orders in magnitude. Consequently, achieving a desired local lubricant viscosity within an engine may be considered not only by a lubricant formulator, but also by an engine manufacturer. While the formulator can mix different base stocks and additives to achieve a particular lubricant behavior, with a desired viscosity at a specified temperature, engine manufacturer's can use also use basic heat transfer principles to manipulate the local lubricant temperature, and therefore viscosity to reduce friction.

Figures 6-1 and 6-8 illustrate this concept by presenting engine and valvetrain friction behavior as lubricant temperature changes. In this manner, an engine manufacturer can significantly reduce engine friction by actively controlling oil temperatures, with either oil coolers or indirectly by controlling coolant temperature.

7.2 Efficiency Gains from Viscosity Optimization

While the reduction of engine friction through the use of lower viscosity lubricants is not novel, the selection of lubricant viscosity classification on a subsystem basis is. Through split lubrication engine tests, 7% subsystem and 6% overall friction reductions were demonstrated. The characterization of subsystem lubrication using a simplified Stribeck curve analysis allowed the intelligent selection of subsystem lubricant viscosity classifications in order to achieve such gains. While a full engine oil change from a 15W-40 oil to a 10W-30 would result in a 4% improvement in engine friction, this comes at the cost of higher friction and most likely higher wear within the valvetrain system.

The friction reductions demonstrated using the split configuration yield a 3-3.5% increase in mechanical energy conversion efficiency when compared to the stock unmixed 15W-40 operation, and a 0.5-1.5% increase in mechanical efficiency when compared to using 10W-30 in the entire engine.

104

7.3 Recommendations for Industry Formulations

This study aims to illustrate the importance of lubricant viscosity to engine friction and how different subsystems within an engine have different requirements within an engine that may not be satisfied by only one common lubricant. We successfully showed that a split lubrication system aids in the formulation of individually optimized lubricants and how those lubricants further reduce engine frictional losses compared to a stock configuration.

Although the integration of a split lubrication system into engine designs may still be in consideration, other technologies may be implemented to address the individual needs of different engine subsystems. For example, if a particular engine manufacturer identifies the dominant lubrication regime within their engine valvetrain to be mixed, an oil cooler may be installed before the cylinder head lubricant supply to keep the valvetrain oil temperature locally at a cooler temperature than within the crankcase. This will result in higher lubricant viscosities within the valvetrain system and reduced friction.

7.4 Future Work

This project continues on to expand the lubricant formulation investigations to study potential efficiency gains and improvements in emissions from additive selection as well as lubricant longevity benefits from the unmixed nature of the split lubrication system. To complement the main engine and the cylinder head bench testing platforms, an additional split configuration engine is being implemented to study the long term degradation effects from segregating the clean valvetrain system from the dirty crankcase. This work is being carried out predominantly by my colleague Michael Plumley and I am optimistic of the results.

Additionally, the engine testing platform is capable of further friction characterization and emissions testing that can complement this study well. Parametric engine tests using lubricant formulations with varying concentrations of anti-wear, friction

105

modifying, detergent, and dispersant additives can provide additional insight to individual needs of each engine subsystem. The installation of a diesel particulate filter on the exhaust of the engine would also provide insight to how the split system affects engine out emissions. In a split lubrication configuration, there is no mechanism for valvetrain oil to be consumed by the combustion process, inherently allowing lubricant formulators to create valvetrain system oils without consideration for its impact on emissions.

7.5 Conclusions

Two experimental testing platforms were set up to enable independent subsystem friction investigations. Testing was carried out the successfully characterize the dominant lubrication regimes with the valvetrain and power cylinder of a Kohler KDW-702 engine. Furthermore, friction tests were performed to demonstrate the frictional benefits of segregating the engine lubrication circuit and tailoring each subsystem's lubricant viscosity accordingly.

This study demonstrated the profound impact lubricant viscosity has on engine friction, increasing frictional losses during cold operation up to 100% compared to normal, warm operation. It also showed that the control of lubricant operating temperature as well as the formulation of lubricant base stocks to have a particular viscosity behavior, are two very effective ways of manipulating lubricant viscosity during operation for the reduction of friction. To this end, an overall friction reduction of 6%, corresponding to a 3-3.5% increase in mechanical efficiency within this particular engine, was empirically demonstrated, using a split 15W-40(head oil)/10W-30(crank oil) lubrication strategy over full 15W-40 operation.

Furthermore, this study begins to address the many potential benefits attainable using a split lubrication strategy within an engine. While primary friction benefits are extremely important to fuel efficiency and fuel economy, improvements in engine emissions, engine durability, and lubricant longevity may soon make the case for a segregated oil system compelling for engine manufacturers.

Appendix A

Schematics and Wiring Diagrams

A.1 Dynamometer Wiring Schematic

This figure comes from the taylor dyanamometer manual[18].
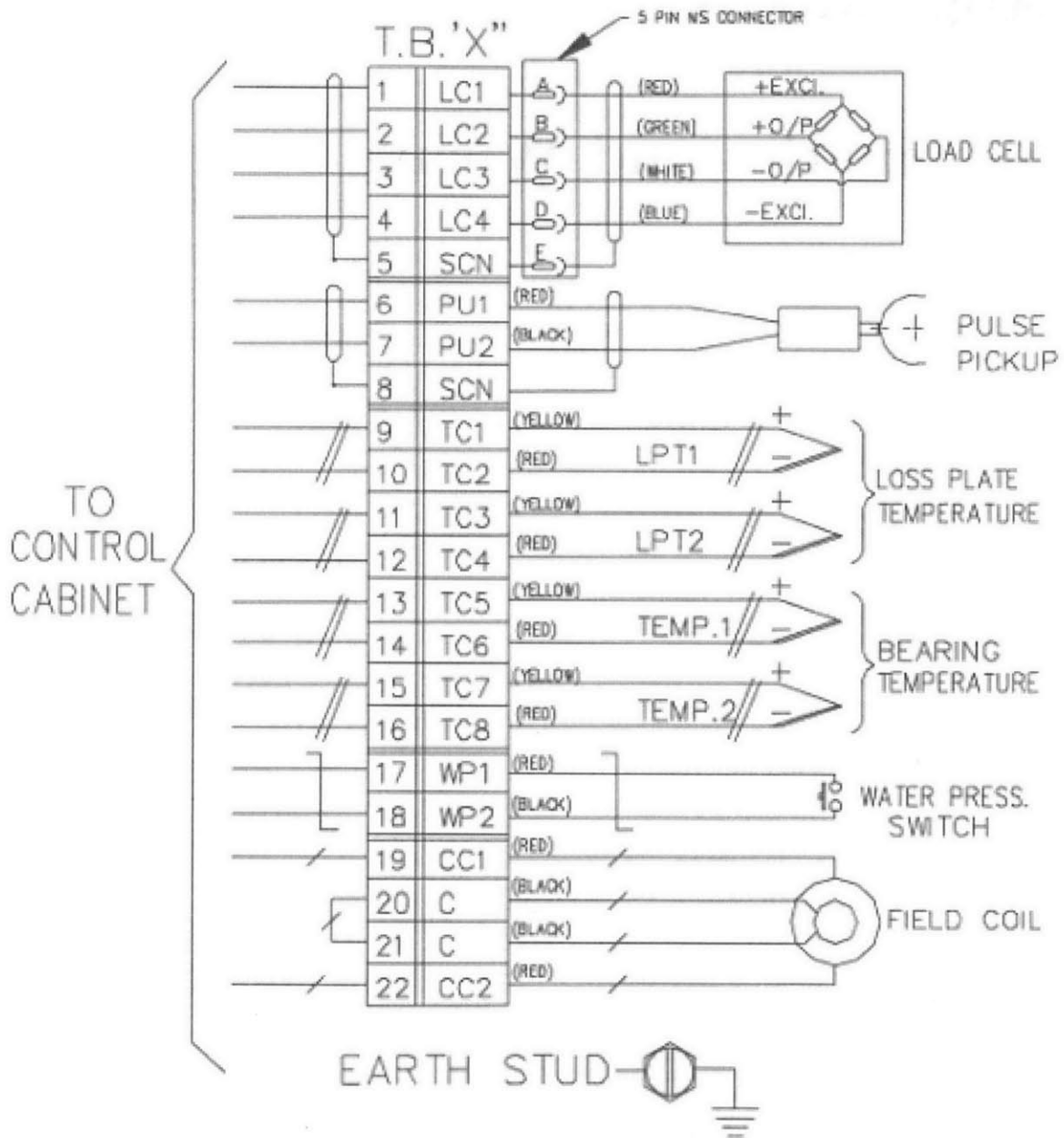
Figure A-1: Taylor dynamometer electrical connections.

A.2 Dynamometer Controller Wiring Schematic

FIGURE 2-2

CONTROLLER-DYNAMOMETER INTERCONNECTIONS

Page 14

Series 1000A Dynamometer Controller
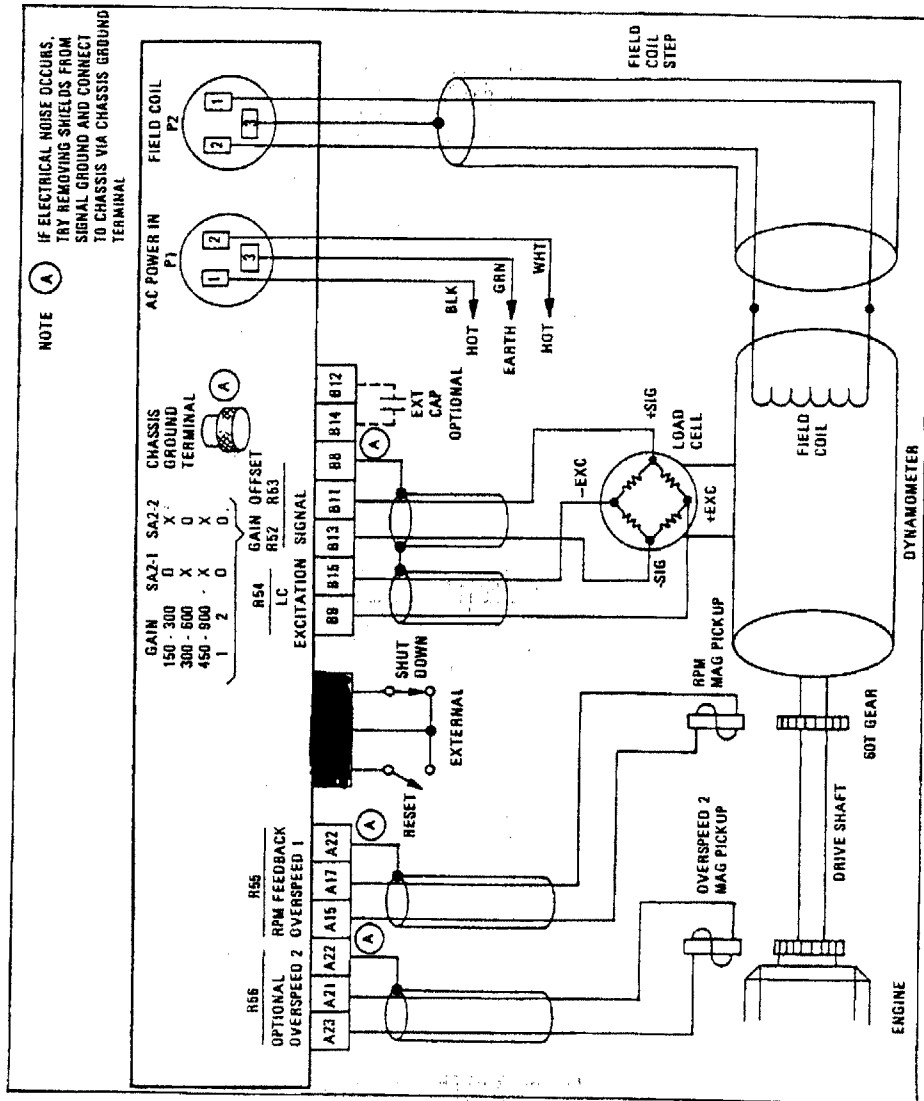
Figure A-2: Digilog Dynamometer Controller Wiring

A.3 Instrument Panel Wiring Diagrams
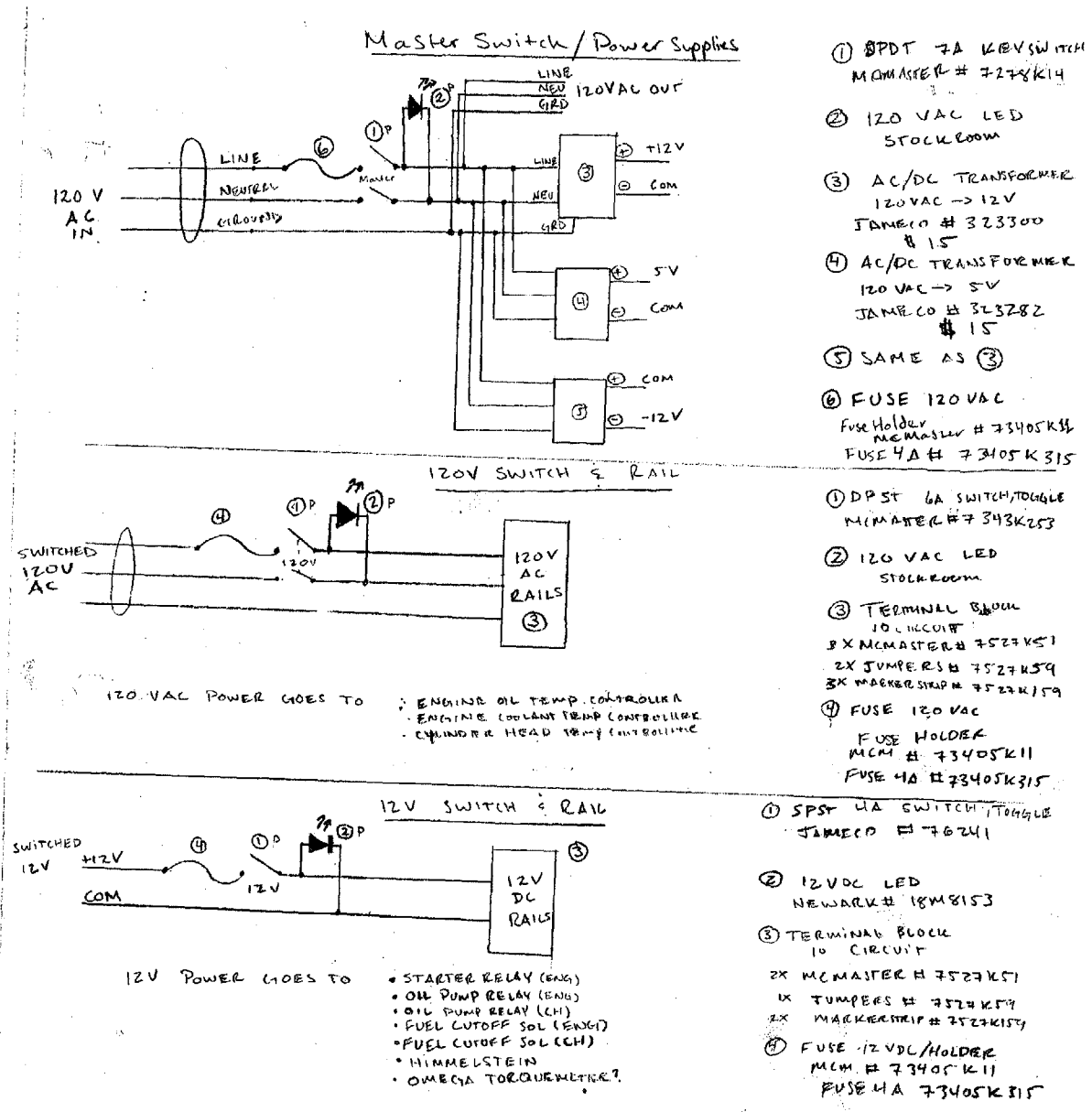
Figure A-3: Panel wiring diagrams #1

ENGINE MOTOR CONTROL

① SPST 4A SWITCH, TOGGLE
   JAMECO # 76241
② 12VDC LED
   NEWARK # 18M8153
③ 3 PHASE AC RELAY
   STOCKROOM
④ LINE REACTOR
   AUTOMATION DIRECT
⑤ DRIVE INVERTER
   AUTOMATION DIRECT
⑥ BLACKMAX MOTOR
   AUTOMATION DIRECT
⑦ 3 POLE FUSE BLOCK
   DURAPULSE
   2HP: GS-22P0-FKIT-3PH
   15HP GS-2015-FKIT
   REPLACEMENT FUSES:
   CHANGE "FKIT" TO "FUSE"

Cylinder Head MOTOR CONTROL SAME CIRCUIT

ENGINE STARTER CONTROL

① SPST 6A SWITCH, BUTTON
   MCMASTER # 8382K212
② KOHLER ENGINE STARTER
③ STARTER RELAY
   MCMASTER # 7995K31
④ 12V BATTERY
⑤ FUSE 125A - MCMASTER
   7447K344

TORQUE METER ENABLE

① SPST 4A SWITCH, TOGGLE
   JAMECO # 76241
② 12VDC LED
   NEWARK # 18M8153
③ SOLID STATE RELAY 7AMP
   MCMASTER # 7456K21
④ AC/DC POWER SUPPLY
   120VAC - 12V
   JAMECO # 323300
⑤ TORQUE METER
   HIMMELSTEIN

Figure A-4: Panel wiring diagrams #2

111
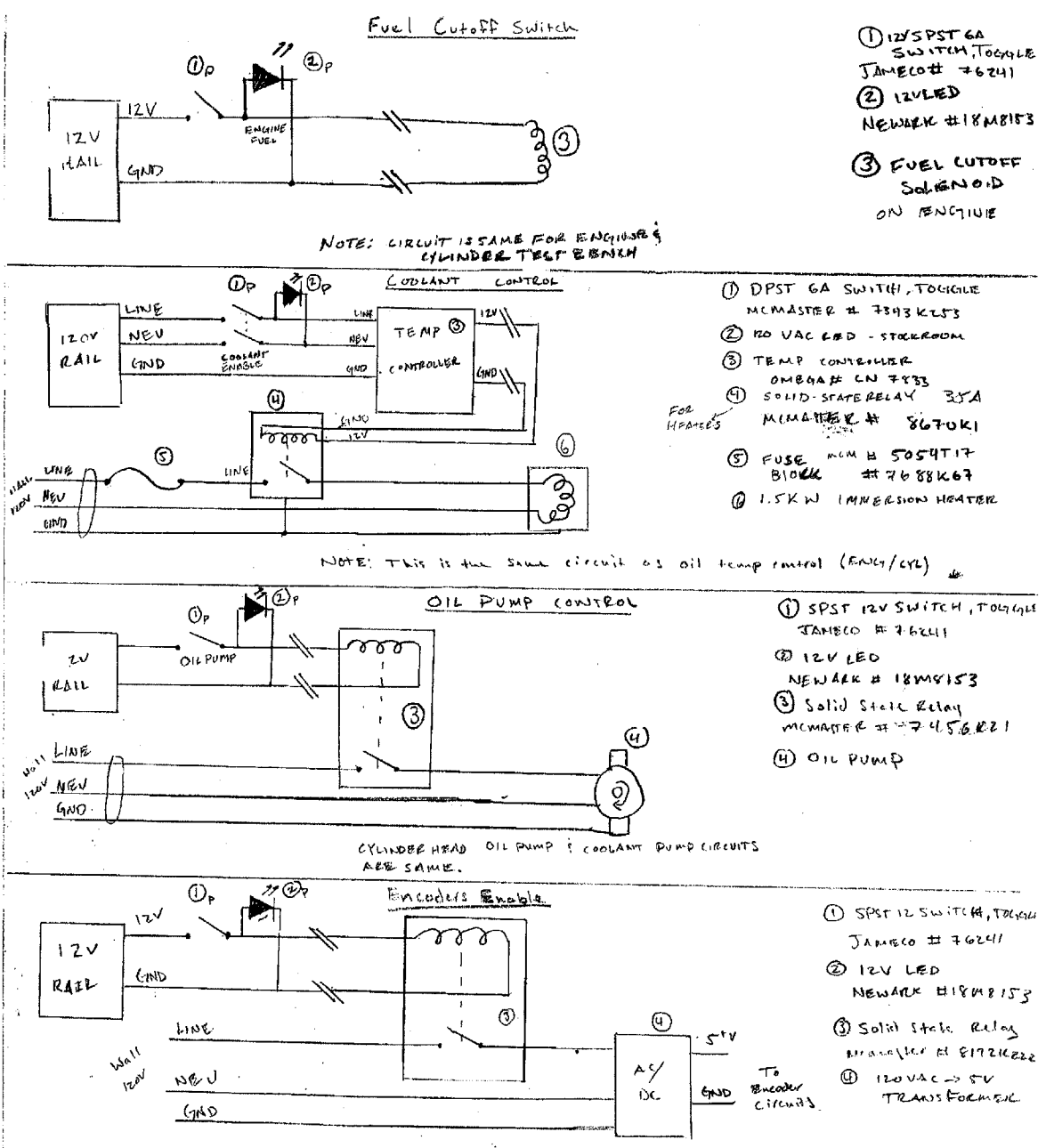
Figure A-5: Panel wiring diagrams #3

Appendix B

Arduino Microcontroller Code

```
//DOE Project Injector Servo Controller Code
//Written by Tomas Vianna Martins
//February 5, 2013


//Revision 3 - September 3, 2013


//Include Packages
#include <SoftwareSerial.h> //Imports Arduino Library to convert a digital pin to a
#include <PWMServo.h> //Imports Arduino Library to generate the proper pulse wavefo


//Define analog pin assignments- Note: the define command merely replaces the first
//For example, #define cat dog - would search through the script for any instance o
#define speedPin 0
#define presentValuePin 1
#define setPointPin 2


//Define digital pin assignments
#define rxPin 2
#define servoSigPin 9
#define panelEnablePin 5 //blue , brn - gnd
```

113

```
#define txPin 6 // yellow , red - +5v, grn - gnd


PWMServo myservo;  // create servo object to control a servo
SoftwareSerial ledDisplay(rxPin, txPin);


//Initialize analog values
float presentValue;  //wht, org - +5v, blk - gnd  // variable to read the value fr
float presentPercent;  // pot value from 0-100% 0-1000 in tenths of a percent
float setPoint;
float setPointPercent;
float speedVal;
char ledString [4];
float servoCommand;
int ledCount = 0;
boolean potReady = false;
boolean runAway = false;


void setup()
{
  //Set digital pin I/O configs
  ledDisplay.begin(9600);
  Serial.begin(9600);
  pinMode(panelEnablePin,INPUT);

  //Analog Pins
  //A0 - Speed Signal
  //A1 - Servo Pot
  //A2 - Setpoint Pot


  myservo.attach(servoSigPin);  // attaches the servo on pin 9 to the servo object
```

```
    ledDisplay.write(0x76); //Clears the LED display

    ledDisplay.write(0x7A);

    ledDisplay.write(0xFF); //Turns on the LED Decimal Point


    setPoint = analogRead(2);

    if (setPoint < 100) //Checks for the Error condition during setup

    {

      potReady = true;

    }

    else

    {

      potReady = false;

    }

    servoCommand = 82;

}


void loop()

{

    //First we see if the panel enable pin is low. If it is high, we continue on.

    //The loop first reads the value of the potentiometer. This value will be between

    //Then it scales it to a percentage. That value will be between 0 and 1000 in tent

    //Then it will scale that to the servo range (will be from full open to full close

    //It will then iuliujh

    //Then it will repeat.


    speedVal = analogRead(speedPin); //Monitors Engine Speed


    if(speedVal > 700) //checks for the Runaway condition

    {
```

```
  runAway = true;

  ledDisplay.write(0x76);

  ledDisplay.print("rUnn");

}


if (runAway)

{

  if (digitalRead(panelEnablePin) == LOW){

    runAway = false;

  }

  //Bring the Servo back to zero

  if (servoCommand > 83)

  {

    servoCommand -= 2;

    delay(15);

  }


  myservo.write(servoCommand);

}

else

{

  if (digitalRead(panelEnablePin) == HIGH)

  {

    if (potReady)

    {

      //Read the Setpoint Pot value (0-775)

      setPoint = analogRead(setPointPin);


      //Constrain setPoint to the operating range (90 - 775)

      setPoint = constrain(setPoint,90,775);
```

```
//Convert setPoint to a percentage
setPointPercent = map(setPoint,90,775,0,1000);


//Convert setPoint to a servo command
servoCommand = map(setPoint, 90, 775, 9700, 10800);
servoCommand = servoCommand/100;
//      servoCommand = map(setPoint, 90, 775, 1560, 1680);


//Read the Servo Pot value ()
presentValue = analogRead(presentValuePin);


//Constrain presentValue to the operating range ()
presentValue = constrain(presentValue,0,1023);


//Convert presentValue to a percentage
presentPercent = map(presentValue,350,221,0,1000);


//Use setPointPercent instead of presentPercent
presentPercent = setPointPercent;



//      Read Serials for Calibration
//        Serial.print(setPoint);
//        Serial.print(" ");
//        Serial.print(presentValue);
//        Serial.print(" ");
//        Serial.println(servoCommand);


//Calibration
```

```
//Fully Closed
//setPoint:407
//presentValue:350
//servoCommand:82
//Fully Open
//setPoint:587
//presentValue:221
//servoCommand:130 (106 for Usable Range)


//Control the Servo
myservo.write(servoCommand);


if (ledCount == 10)
{
  //Turn on the decimal point
  ledDisplay.write(0x76);
  ledDisplay.write(0x77);
  ledDisplay.write(0x04);


  //Convert presentPercent to a string
  if (presentPercent < 4)
  {
    itoa(presentPercent,ledString,10); //integer to ascii command
    ledDisplay.print("0000");
  }
  else if (presentPercent < 10)
  {
    itoa(presentPercent,ledString,10);
    ledDisplay.print("000");
    ledDisplay.print(ledString);
```

```
      }
      else if (presentPercent < 100)
      {
        itoa(presentPercent,ledString,10);

        ledDisplay.print("00");

        ledDisplay.print(ledString);

      }
      else if (presentPercent < 1000)
      {
        itoa(presentPercent,ledString,10);

        ledDisplay.print("0");

        ledDisplay.print(ledString);

      }
      else
      {
        ledDisplay.print("1000");


      }
      ledCount = 0;
    }
    ledCount += 1;
    delay(50);
  }
  else
  {
    //Flash Error
    ledDisplay.write(0x76);
    delay(500);
    ledDisplay.print("Er0r");
    delay(500);
```

```
      }
    }
    else //The Enable Switch is off
    {
      ledDisplay.write(0x76);
      //Bring the Servo back to zero
      if (servoCommand > 83)
      {
        servoCommand -= 1;
        delay(15);
      }

      myservo.write(servoCommand);

      //Read the SetPoint Pot value
      setPoint = analogRead(setPointPin);

      //Check to see if the SetPoint Pot value is at a safe one
      if (setPoint < 100)
      {
        potReady = true;
      }
      else
      {
        potReady = false;
      }
    }
  }
}
```

Appendix C

Experimental Operating Procedures

C.1 Engine Operation

The experimental engine setup discussed in chapter 4 is capable of performing both motoring and firing engine tests. It is actively used for friction characterization with different kinds of test lubricants for the valvetrain and power cylinder systems. It is paramount that the proper start up procedure and operational considerations be followed so as to ensure the acquisition of repeatable data and prevent component damage or operator injury. The following sections detail the proper start up, motoring, firing, and shut down procedures for the main engine testing platform.

C.1.1 Engine Start Up Procedure and Motoring

The following is the start up procedure that must be followed whenever starting up the main engine experiment.

1. Turn on the desktop computer.

2. Turn on the laboratory city water pump. The switch can be found on the wall outside 31-035D CHECK. When the pump is on, the red lightbulb will also turn on.

3. Open the city water supply ball valve at the back right corner of the test cell. Only open such that the post filter water pressure is around 50 psi. Do not open fully. If you open the valve fully, and the pressure does not rise above 30-40 psi, it is because either the lab city water pump is not on, or other engines on the east side of the laboratory are using a significant amount of water.

4. Turn on the power strip on the accessory tower within the test cell to supply power to the fuel control system.

5. Ensure that the oil diversion valve underneath the cylinder head bench setup is turned to supply lubricant to the main engine valvetrain. THIS IS EXTREMELY IMPORTANT.

6. Turn the master key to the right to energize the power supplies and all switches.

7. Toggle the following switches on the "Engine" Panel:

120V AC - Energizes all 120V AC power.

12V DC - Energizes all 12V DC power.

Battery Charger - Turns on the 12V battery charger. This may be done infrequently, as it is only to make sure the 12V battery, which goes unused, does not completely discharge.

Encoders Enable - Energizes the encoder circuit power supplies.

Motor Enable - Toggles the 15 HP AC motor inverter drive power.

Coolant & Oil Pump - Energizes the engine coolant pump. No oil pump is controlled with this switch. Originally it was thought that it would control both the coolant pump and the separate valvetrain pump.

Temperature Control - Energizes the Omega CN7800 temperature controller that controls the engine coolant temperature.

Torquemeter Enable - Energizes the dedicated 12V power supply that powers the large Himmelstein torquemeter as well as the camshaft pulley torquemeter.

Charge Amplifiers - Energizes the cylinder pressure transducer charge amplifiers.

8. Toggle the following switches on the "Cylinder Head" Panel:

Temperature Control - Turns on the Omega CN7800 temperature controller that controls the secondary oil sump that supplies the valvetrain.

Oil Pump - Energizes the external valvetrain oil pump, supplying lubricant to the engine cylinder head.

9. Press the "Controller" button on the dynamometer controller to power the system. It needs about five minutes to warm up.

10. Toggle the "operate" button on the cylinder pressure transducer charge amplifiers inside the test cell.

11. Set the rotational speed of the electric motor. The standard setting is 40.2 Hz, corresponding to 1200 RPM.

12. Verify that there is a nonzero oil pressure in the engine cylinder head. This gauge is located on the top instrument panel next to the fuel control system. THIS IS EXTREMELY IMPORTANT.

13. Verify that the following switches are in the "off" position:

The main engine "Fuel Enable" - No fuel should flow during start up.

The "Servo Enable" switch of the instrument panel. - The fuel control servo motor should be in its off position and the LED display should be clear.

The "Motor Coast" switch right next to the "Servo Enable" switch CHECK - This switch allows the motor to free wheel. The motor wont provide a torque if it is on.

14. Press the "Crank" button. The whole driveline should start spinning. If it does not, and the electric motor keypad display reads "ground fault", press the "stop/reset" button and try again.

15. Verify that both oil pressure gauges show an oil pressure above 20 psi, indicating that both engine subsystems are being properly lubricated.

16. Open the "KDW 702.vi" file on the desktop and click run.

At this point, the engine is spinning without the combustion of fuel, or motoring. Two pressure traces should show up in the center virtual instrument graph. Engine speed can be controlled with the electric motor keypad by changing the driving frequency, valvetrain oil and coolant temperatures can be controlled by their respective Omega controllers, and data can be recorded using the Labview virtual instrument.

C.1.2 Transition to Firing

The testing platform was designed to allow for smooth transitions to firing operation while running, making it possible to perform both motoring and firing tests on the fly. The transition procedure to firing operation from motoring is detailed below and should be read and understood before being attempted. Failure to properly control the engine dynamometer or electric motor settings can result in engine stalls and possibly component damage.

1. Make sure the valvetrain oil temperature and coolant temperature have increased to at least 50°C through initial warmup before transitioning to firing operation.

2. Bring the driveline motoring speed to 1200 RPM. This is a suitable speed to perform the transition. This speed will be displayed on the "RPM" display of the dynamometer controller.

3. Bring the dynamometer setpoint speed to 2000 RPM by turning the "RPM" knob to the right while the "Performance Monitor" knob is set to "Man RSP" (MANual Rpm SetPoint).

4. Press the yellow "Dynamometer" button on the top of the dynamometer controller to energize the dynamometer field coils. The dynamometer only functions

124

as a braking device, therefore it will only apply an excitation when RPM set-point, displayed on the "Monitor" display, is less than the speed shown on the "RPM" display. Energizing the field coils with a setpoint speed much higher than the current rotational speed should ensure that no sudden torques are applied to the driveline.

5. Slowly decrease the speed setpoint to 1200 RPM by turning the "RPM" knob to the left.

6. Toggle the main panel "Fuel Enable" and the fuel control system "Servo Enable" switches. The servo position LED display should turn on, showing all zeros. If the display blinks "Er0r", toggle the "Servo Enable" switch off, turn the servo position knob all the way to zero, and toggle the switch back on.

7. Turn the servo control knob to about 55% servo position and quickly flip the "Motor Coast" switch on. The engine is now driving the driveline and the electric motor is freewheeling. If the engine begins to slow down, incrementally increase the servo position control knob, until the speed stabilizes. Important: During the time between turning the fuel position to 55% and toggling the "Motor Coast" switch, both the electric motor and the engine are providing torque to turn the driveline, while the electric motor and dynamometer are trying to maintain the 1200 RPM rotational speed. Consequently, the control mechanisms of the engine, motor, and dynamometer inherently fight each other, and if too much time passes before flipping the "Motor Coast" switch, the electric motor may experience an over-voltage fault and shut itself off. This prevents returning from firing operation back to motoring while running.

8. Verify that the mean effective pressure readings on the virtual instrument are reasonable and begin the warm up procedure for testing.

C.1.3 Engine Cool Down and Shut Down

In order to cool the engine down, it is necessary to return it to motoring operation so that the lubrication and cooling system can decrease its fluid temperatures before completely shutting down the driveline. This ensures that there are hot spots in the engine while sitting that may lead to deformation or engine damage. The procedure to shut down the engine is essentially the reverse of the transition and start up procedures and is detailed below.

1. Decrease the engine speed to 1200 RPM by turning the "RPM" knob of the dynamometer controller to the left and decreasing its RPM setpoint. This will match the rotational speed of the driveline to the driving frequency of the electric motor, once it comes back on.

2. Set the fuel position to about 54% to achieve a low engine load condition.

3. Turn off the "Motor Coast" switch, commanding the drive inverter to search for the current driveline rotational speed and turn on the motor.

4. About a second after enabling the electric motor drive, the "Servo Enable" switch can be turned off, cutting the supply of fuel to the combustion chambers from the fuel injectors.

5. Turn the main "Fuel Enable" switch off to ensure no fuel flow to the engine's fuel system.

6. Bring the valvetrain oil temperature down to 50°C using the cylinder head Omega temperature controller.

7. Bring the engine coolant temperature down to 50°C using the main panel coolant temperature controller.

8. After a cool down period where the oil and coolant temperatures decrease to about 50°C, press the red "Stop/Reset" button on the main motor control keypad to shut down the drive line.

9. Turn off all toggle switches on the all panels.

10. Press the yellow "Controller" button to shut down the dynamometer controller.

11. Turn the master key to the left to cut all power to control circuits and power supplies.

12. Turn off the power strip in the test cell attached to the instrumentation tower to cut power to the fuel control system.

13. Close the supply side ball valve on the city water inlet pipe in the back right corner of the test cell.

C.2 Cylinder Head Bench Operation

The cylinder head bench testing platform allows for the independent study of valvetrain friction under a variety of operating conditions not possible on the main engine. Although the exact pressure and thermal enviromnent experienced by the gas exchange valves is not reproduced, variables like lubricant pressure, lubricant temperature, and camshaft speed can be finely controlled. Additionally, it is possible to operate the valvetrain system with specific components removed or disabled, to perform "break-down" tests, where the relative contribution of each component to friction is characterized. The following sections detail the proper start up, testing, and shut down procedures for the cylinder head bench testing platform.

C.2.1 CHB Start Up Procedure

The following procedure should be followed when starting the cylinder head bench testing platform.

1. Turn on the desktop computer.

2. Ensure that the oil diversion valve underneath the cylinder head bench setup is turned to supply lubricant to the cylinder head bench system. THIS IS EXTREMELY IMPORTANT.

3. Turn the master key to the right to energize the power supplies and all switches.

4. Toggle the following switches on the "Engine" Panel:

    120V AC - Energizes all 120V AC power.

    12V DC - Energizes all 12V DC power.

    Encoders Enable - Energizes the encoder circuit power supplies.

5. Toggle the following switches on the "Cylinder Head" Panel:

    Motor Enable - Toggles the 2 HP AC motor inverter drive power.

    Temperature Control - Energizes the Omega CN7800 temperature controller that controls the valvetrain oil temperature.

    Oil Pump - Energizes the external oil pump.

    Torquemeter Enable - Energizes the dedicated 12V power supply that powers the small Himmelstein torquemeter between the cylinder head camshaft and the electric motor.

6. Verify that the valvetrain oil passages have oil pressure, indicated on the cylinder head panel oil pressure gauge.

7. Set the desired oil pressure by adjusting the bypass valve on the bronze gear pump. This looks like a threaded rod coming out of the center of the pump.

8. Set the desired camshaft speed by adjusting the driving frequency on the cylinder head panel motor control keypad. A frequency of 30 Hz corresponds to 900 RPM, while 60 Hz corresponds to 1800 RPM.

9. Open the Cylinder Head virtual instrument to visualize and record instantaneous test data.

10. Push the green "Run" button on the motor control keypad to begin driving the valvetrain.

11. The rotational speed can be actively changed by using the up and down arrows on the keypad to change the driving frequency.

C.2.2 CHB Shut Down

The shut down procedure for the cylinder head test bench is as follows.

1. Press the "Stop/Reset" button on the motor control keypad.

2. Shut down all toggle switches on both panels.

3. Turn the master key to the off position, cutting power to all instrumentation and power supplies.

Bibliography

[1] Heywood, J. *Internal Combustion Engine Fundamentals*. McGraw-Hill Science/Engineering/Math, 1st edition edition, 1988.

[2] Sousanis, J. *World Vehicle Population Tops 1 Billion Units | News & Analysis content from WardsAuto*, January 2014.

[3] dePaula, M. *Diesel Boom? Ownership Of Diesel Cars Way Up, But Still A Fraction Of U.S. Market*.

[4] Flynn, P.F., Durrett, R.P., Hunter, G.L., zur Loye, A.O., Akinyemi, O.C., Dec, J.E., and Westbrook, C.K. *Diesel combustion: an integrated view combining laser diagnostics, chemical kinetics, and empirical validation*. 1999.

[5] Sappok, A. *Emissions and In-Cylinder Combustion Characteristics of Fischer-Tropsch and Conventional Diesel Fuels in a Modern CI Engine*. Ph.D. thesis, Massachusetts Institute of Technology, February 2006.

[6] Khair, M. *The Case for the Diesel Engine*.

[7] EPA. *Total U.S. Greenhouse Gas Emissions by Economic Sector in 2011*, January 2014. Sources of greenhouse gas emissions, inculding electricity production, tranportation, industry, agriculture, and forestry.

[8] EPA. *Global Greenhouse Gas Emissions Data*, January 2014. Sources of greenhouse gas emissions, inculding electricity production, tranportation, industry, agriculture, and forestry.

[9] EPA. *EPA Proposes Tier 3 Motor Vehicle Emission and Fuel Standards*.

[10] EPA. *Control of Air Pollution From Motor Vehicles: Tier 3 Motor Vehicle Emission and Fuel Standards*, May 2013.

[11] *Obama Administration Finalizes Historic 54.5 MPG Fuel Efficiency Standards | The White House*, August 2012.

[12] Tian, T. *Modeling the performance of the piston ring-pack in internal combustion engines*. Ph.D. thesis, Massachusetts Institute of Technology, 1997.

[13] Staron, J.T. and Willermet, P.A. *An Analysis of Valve Train Friction in Terms of Lubrication Principles.* Technical Report 830165, SAE International, Warrendale, PA, February 1983.

[14] Wang, Y. *Introduction to engine valvetrains.* SAE International, Warrendale, PA, 2007. ISBN 0768010799 9780768010794.

[15] Patton, K.J., Nitschke, R.C., and Heywood, J.B. *Development and Evaluation of a Friction Model for Spark-Ignition Engines.* Technical Report 890836, SAE International, Warrendale, PA, February 1989.

[16] Sandoval, D. and Heywood, J.B. *An Improved Friction Model for Spark-Ignition Engines.* Technical Report 2003-01-0725, SAE International, Warrendale, PA, March 2003.

[17] Livanos, G. and Kyrtatos, N.P. *A Model of the Friction Losses in Diesel Engines.* Technical Report 2006-01-0888, SAE International, Warrendale, PA, April 2006.

[18] Dynamometers, T. *Taylor Dyno Manual.pdf.*